12-1-1983

A comparison study of atmospheric radiometric calibration methods for aerial thermograms

A. E. Byrnes

A COMPARISON STUDY

OF ATMOSPHERIC RADIOMETRIC CALIBRATION METHODS

FOR AERIAL THERMOGRAMS

by

A.E. Byrnes
B.Sc. Laurentian University
(1975)

A thesis submitted in partial fulfillment
of the requirements for the degree of Master of Science
in the School of Photographic Arts and Sciences
in the College of Graphics Arts and Photography
of the Rochester Institute of Technology

December, 1983

Signature of the Author A. E. Byrnes
Photographic Science and
Instrumentation Department

Accepted by Ronald Francis
Coordinator, M.S. Degree Program

A COMPARISON STUDY

OF ATMOSPHERIC RADIOMETRIC CALIBRATION METHODS

FOR AERIAL THERMOGRAMS

by

A.E. Byrnes
B.Sc. Laurentian University
(1975)

930041

College of Graphic Arts and Photography
Rochester Institute of Technology
Rochester, New York

CERTIFICATE OF APPROVAL

M.S. DEGREE THESIS

The M.S. Degree Thesis of Arthur E. Byrnes
has been examined and approved
by the Thesis Committee as satisfactory
for the thesis requirement of the
Master of Science degree.

Dr. John Schott, Thesis Advisor

Dr. Willem Brouwer

Dr. Edward M. Granger

12/3/84
Date

THESIS RELEASE PERMISSION FORM

ROCHESTER INSTITUTE OF TECHNOLOGY
COLLEGE OF GRAPHIC ARTS AND PHOTOGRAPHY

Title of Thesis: A COMPARISON STUDY OF ATMOSPHERIC RADIOMETRIC CALIBRATION METHODS FOR AERIAL THERMOGRAMS

I, Captain Arthur Edward Byrnes, prefer to be contacted each time a request for reproduction is made. I can be reached at the following address:

signature: ____________________
A.E. BYRNES

date: ____________________
JULY 1984

A COMPARISON STUDY

OF ATMOSPHERIC RADIOMETRIC CALIBRATION METHODS

FOR AERIAL THERMOGRAMS

by

A.E. Byrnes

Submitted to the
Photographic Science and Instrumentation Department
in partial fulfillment of the requirements
for the Master of Science degree
at the Rochester Institute of Technology

ABSTRACT

A comparison study was conducted to evaluate limitations of several atmospheric calibration techniques, including: Angular, Profile, and spectrally corrected and uncorrected LOWTRAN. To accomplish this, a thermal mapper was flown over a shoreline where water surface temperatures were measured coincidentally by a ground crew. The thermogram-derived observed radiances were corrected using each of the atmospheric calibration methods so that ground surface temperatures could be predicted. The R.M.S. errors of these ground temperature predictions indicated that all calibration techniques yielded similar results at 1000-foot altitude. The error remained constant for the Profile and LOWTRAN calibration techniques to 6000-foot altitude, but the Angular results singularly indicated a pronounced altitude dependence in ground temperature prediction errors to 6000-foot altitude.

ACKNOWLEDGEMENTS

Successful completion of this thesis owes recognition to support from many sources. Valuable and timely assistance and advice was particularly appreciated from the following:

Dr. John Schott of the R.I.T. Photo-Science Department who kindly consented to act as thesis advisor for the proposal, and gave much of his time and encouragement in its supervision;

Mr. Joseph Biegel, an associate of the above, for his sound advice on matters of statistical analysis, and the practicalities of the science;

Dr. E.M. Granger, of Kodak Research Laboratories, who provided insight and direction in resolving some of the more perplexing aspects of this study;

Dr. W. Brouwer, Visiting Professor to R.I.T., whose wealth of practical experience helped keep the work in its proper perspective;

Captain Joe Szydlik, of 1 CF Photo Unit, Ottawa, for his support in the early phases of the study;

Mr. Tim Gallagher, also of R.I.T., who operated the thermal mapper in-flight and in the laboratory, and, through some technical wizardry, was able to pull the thesis data set out of the bag;

Mr. Norman of R.I.T. workshops who, with skill and patience, modified the necessary equipment;

Mr. Jim Turpin who forfeited numerous weekends to ferry the ground crew and their equipment on Lake Ontario;

Mr. Ian Ross of the Ontario Centre for Remote Sensing for his experiences in the realm of this study;

Mr. Bud McKibbon of the Canadian Centre for Remote Sensing, also, for his experiential advice;

Dr. Bev Young of the Defence Research Establishment, Ottawa for his encouragement, and loan of the Visicorder oscillograph;

Calspan Corporation for the loan of their Bendix LN-3 thermal mapper;

The New York State Energy Research and Development Authority for the loan of their 14-channel tape recorder;

The crew of the Rochester Detachment of the United States Coast Guard;

The Monroe County Planning Board; and

The Coordinator of Graduate Studies for the Photographic Science and Instrumentation Department, Dr. R. Francis, whose motivation and support were most invaluable.

The support of the Canadian Forces Educational Grant Program is also acknowledged with sincere appreciation.

DEDICATION

This thesis is dedicated to three very special ladies, Donna, Tracey, and Ashley, who enthusiastically, and lovingly, supported this ambition and graciously accepted my absence on uncountable occasions, time which was rightfully theirs.

TABLE OF CONTENTS

LIST OF FIGURES

FIGURE PAGE

LIST OF TABLES

LIST OF SYMBOLS AND ABBREVIATIONS

AGL	above ground level
ASTM	American Society for Testing and Materials
b	slope intercept of linear relation
c	velocity of light
cm	centimetre
°C	degree Celcius
CO_x	carbon oxide compound
CO_2	carbon dioxide
CRT	cathode ray tube
D	film density
E	exposure
$E_{subscript}$	error
EMR	electro-magnetic radiation
FOV	field of view
ft	feet
G	thermal mapper gain
GMT	Greenwich Mean Time
h	Planck's constant
H	altitude
hr	hour
H_2O	water
IR	infrared
k	Boltzmann's constant
km	kilometre
kohm	kilo-ohm
°K	degree Kelvin
L	observed radiance
L_{bb}	thermal mapper blackbody radiance

L_d	sky, or down-welled, radiance
L_g	apparent radiance emitted and reflected from target surface
L_T	target surface radiance due to surface temperature
L_u	atmospheric-path upwelled radiance
m	slope of linear relation
M	meter
NO_x	nitrous oxide compound
N.Y.	New York State
OH	hydroxide
O/P	output
O_2	oxygen
O_3	ozone
P	flux remaining after traversing path length X in absorbing layer
P_0	flux entering absorbing layer
PRT	portable radiometric thermometer
R	surface reflectivity
R.I.T.	Rochester Institute of Technology
R.M.S.	root mean square
$R_{\Delta\lambda}$	relative spectral response of thermal mapper optics
SR	steradian
T	thermal mapper output (observed) temperature
T_{bb}	thermal mapper blackbody temperature
T_{sky}	sky, or albedo, temperature
TIR	thermal infrared
U.S.	United States
V	thermal mapper output voltage
V_{bb}	thermal mapper blackbody voltage
V_0	intercept of thermal mapper response curve
V-D	voltage-density
W	watts
Z	path length

α	absorptance
β	thermal mapper field of view
ε	emissivity
θ	view angle
λ	wavelength
$\Delta\lambda$	bandwidth increment
μm	micro-metre
π	3.14159
ρ	reflectance
σ	Stefan-Boltzmann constant
τ	(atmospheric-path) transmittance
τ'_i	extinction coefficient
ϕ	Angular-calibration offset angle
Ω	solid angle
w^*	equivalent absorber amount

INTRODUCTION

The growth of remote sensing research has seen concomitant applications of this versatile and effective information gathering technique to problems of forest management, geologic survey, sea surface temperature determinations, residential heat loss detection, military reconnaissance, and impact studies of power plant thermal discharges on the aquatic environment, to name just a few examples.[10]

Airborne thermal infrared imaging instruments have been used to study some of these problems. These systems are ideal for these studies as they generate a thermal infrared (TIR) image, or thermogram,[53] (similar to a photograph) of the heat energy radiated from earth.[17] For example, the brighter the ground feature appears on the image, the higher the temperature of the ground.[37] This approach facilitates the temporal, spatial, and shape analyses of a ground target area.

The upwelling electromagnetic radiation (EMR) from earth is a function of the physical and chemical states of the surface and the atmosphere.[10] Thus, in principle, it should be possible to recover information about the physical and chemical structure of the surface and the atmosphere from analysis of the upwelling EMR. However, the problem in analysing such data lies in finding ways to uncouple the interactions of the surface radiation from the atmospheric-path radiance and transmittance factor in order to retrieve the true values of each unknown parameter separately. This is the essence of atmospheric calibration of thermograms, and is essential for successful quantitative remote sensing.[24,28]

The accounting for atmospheric effects in the analysis of aerial thermograms has been addressed through the development of atmospheric calibration techniques by several workers. The atmospheric calibration methods to be reviewed in this work include the Profile, Angular, and LOWTRAN techniques.

The Profile calibration technique[34] involves overflying a target at multiple altitudes, preferably at least four,[48] as illustrated in figure 1. The IR scanner output, which can be converted to temperature or radiance, is plotted against altitude for a specific target. This curve is extrapolated to ground altitude enabling the apparent ground temperature to be found. If the overflights include targets of a wide range of temperatures, then the atmospheric parameters necessary for calibration can be found. This technique was developed by Schott and Tourin (1975) and has been employed in many of their subsequent studies.[35,36,37,38,39]

The Angular calibration technique[20,37] also involves overflights of the target, but instead of multiple altitude flight paths, the target is imaged at a single altitude from directly overhead and from an offset angle as depicted in figure 2. Large angles reportedly result in the most precise results. Similar analysis to that of the Profile method will yield the atmospheric parameters. The development of the technique is the work of MacLeod (1983), in which archival imagery was employed to test the concept. The technique was not field tested prior to the study reported here.

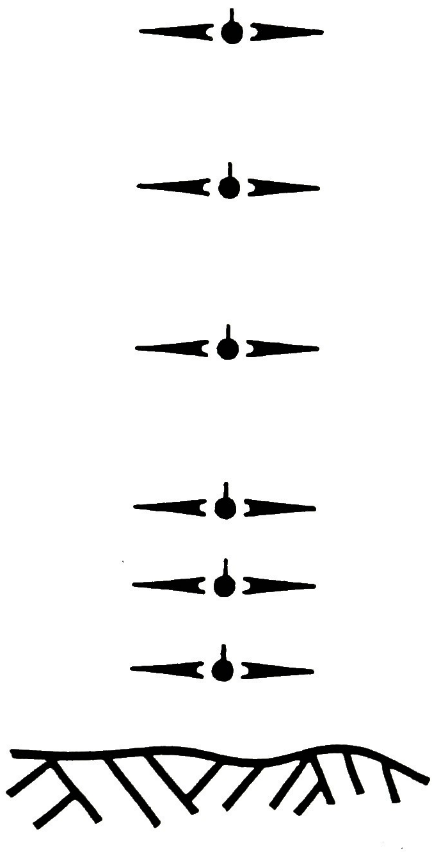

Figure 1. Profile Calibration Flight Format. Repetitive Data Acquisition Over a Site is Employed to Empirically Determine Ground Surface Temperatures. The Process Entails Analyzing the Change in Radiometer Output as a Function of Altitude.

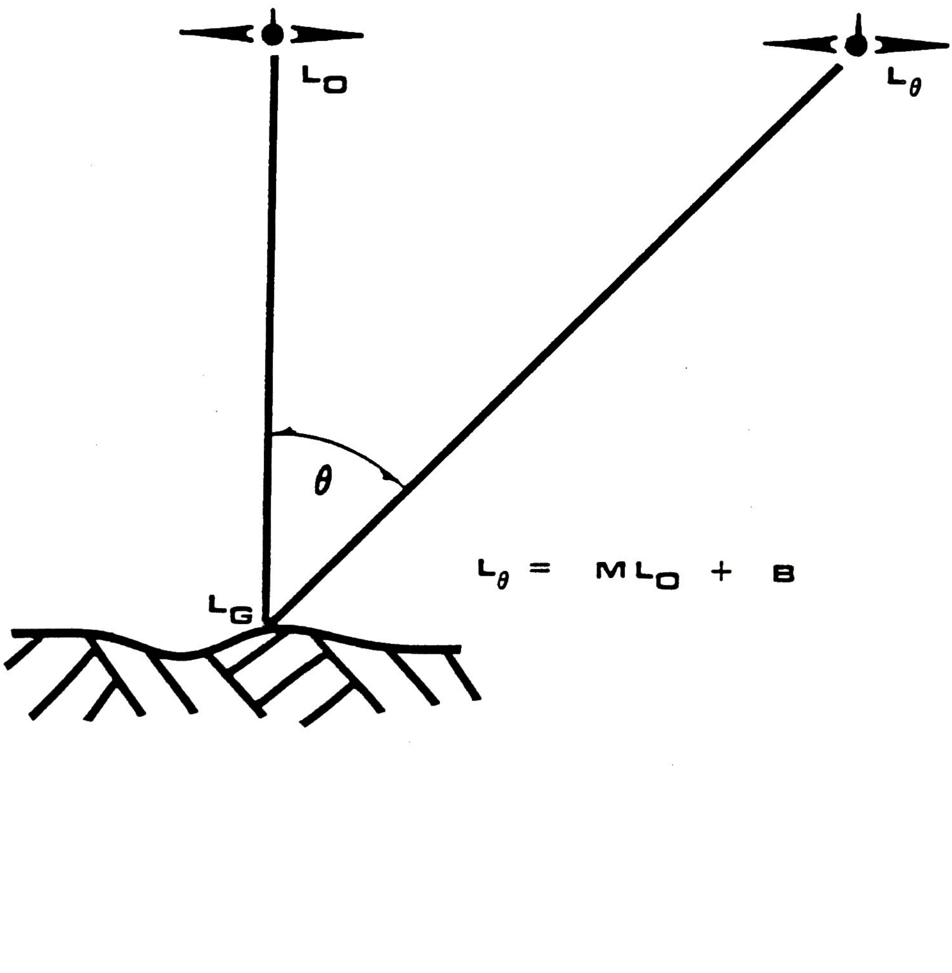

Figure 2. Angular Calibration Flight Format. The Observed Radiance Seen from an Offset View Angle can be Expressed in Terms of the Radiance Seen from Directly Over the Target.

The third technique to be evaluated requires a knowledge of the spectral response of the thermal mapper optics and the radiosonde profile of the atmosphere at the time of imaging. This data is input to a computer atmospheric model, called LOWTRAN[21,45,54] which then predicts atmospheric-path radiance and transmittance. Any path geometry can be analysed, but a 'look-down' configuration was studied to match that of the scanner. The radiosonde data is collected on a twice daily basis at 0000 and 1200 hr GMT at stations around the world. A light weight measurement device, called a radiosonde, is sent aloft to collect information about the atmosphere.[18] The radiosonde, which rises to about 20 km, contains a resistance thermometer, an aneroid barometer, an electrical hygrometer, and a radio transmitter. The radio transmits signals that can be interpreted to give the pressure, temperature, and humidity in the atmosphere.

Each of the atmospheric calibration methods is unique in its own right and enables the determination of the atmospheric parameters necessary for the calculation of absolute ground surface temperatures.

Objective

The objective of this study is three-fold in nature. First, to expand upon the theoretical foundation of the Angular atmospheric calibration technique. Second, to conduct a field evaluation of same. And lastly, to establish a relative order of merit, for the Profile, Angular, and LOWTRAN atmospheric calibration techniques, considering the precision with which predictions of ground surface temperatures can be made.

Historical Background

Thermography[53] is that branch of remote sensing concerned with measuring the radiant temperature of earth surface features from a stand-off distance. The area of interest in a thermographic survey might be as small as a single roof-top or as grand as the ocean currents covering the globe. Although considerable public interest in temperature measurement has been generated from its application to energy conservation studies, the focus of aerial thermographic studies to date has been in a host of other applications.[10,14,17]

The product of an aerial thermographic survey, which employs an IR scanner as the imaging device, is a thermogram. Aerial thermograms can be classified into three broad categories: qualitative, semi-quantitative, and, quantitative.[28] Qualitative thermograms consist of continuous tone analog imagery displayed on black and white film or density sliced imagery displayed on CRT. Such imagery has both inherent systematic noise and geometric distortion, and is not corrected to eliminate the effects of atmospheric attentuation and target emissivity variations. 'Semi-quantitative' is a means of describing imagery which has been corrected for systematic errors (noise and geometry), but not for atmospheric attenuation or emissivity. Quantitative imagery provides absolute surface temperatures, as systematic errors have been removed and atmospheric and emissivity corrections have been applied.[28,41] Obtaining quantitative surface temperature data from thermal scanning systems, however, is a non-trivial task.[14] To accomplish such a task requires some form of calibration of the 'system', usually in the form of referencing to a radiometer or internal blackbody source, air to ground correlations, atmospheric modeling, or repetitive site coverage. Any or all these approaches can be used.[56]

The influence of the atmosphere in attenuating signals has been recognized since 1942 when Elassen studied CO_2 and water absorption band theory.[9] Further work was done by Yates[9] and Ohio State University[8] in this realm but little has been made public up to the late sixties, probably due to military and operational constraints.[14,45]

One of the first to develop an empirical technique for determining atmospheric corrections was Saunders.[30] His approach eliminates the influence of the air layer and of the target reflectivity. He employed a non-scanning radiometer to alternately observe a thermally stable sea surface at zenith angles of 0 degrees and 55 degrees (60 degrees for warm humid atmospheres) from an altitude of 300 metres. He found that the 60 degree reading approximately doubled both the influence of the air layer and reflectivity. Consequently, the difference between the normal and a 60 degree measurement was the total correction required. This approach only applied to water surfaces and has inherent geometric errors in the non-normal readings. The fact, however, that his study was low-altitude in nature would imply reasonable accuracy. In his later paper of 1970,[31] Saunders carried his study one step further to establish the influence of haze as being insignificant when using his technique. Simple analytical forms to extend Saunders' atmospheric corrections have been suggested by Tien.[50]

In 1968, Lorenz[19] discussed at length the use of radiometers to measure the temperature of natural surfaces and the corrections necessary due to its use in such measurements. He cited, as the most significant sources of error, target reflectivity as a function of look-angle and air layer influence. He demonstrated through field experiments that air temperatures at the target surface and radiometer played an important role in radiometer accuracy. Variations of humidity and temperature gradient between the target and radiometer were shown to be of secondary import. From his experiment, Lorenz developed correction graphs for surface temperatures. An accuracy of 0.5°C was claimed for tests conducted over water. The limitations of this approach are two-fold. First, a constant humidity and temperature gradient is used in the calculation of the temperature correction charts, and second, the usually very cold sky is assumed to be the same temperature as the air at the radiometer. These assumptions prompt this author to consider Lorenz's charts with guarded optimism.

Weiss[52] conducted a comparison study of aerial radiometer measurements using bandwidths of 10-12 μm and 8-14 μm. He demonstrated that an atmospheric induced error and a surface reflectivity error can be reduced by working in a narrower region of the atmospheric window centered about 10.5 μm. His experiment involved flying two radiometers differing only in their spectral bandpasses. Comparison of the results indicated the narrower band filter reduced the error in water surface temperature by a factor of 1.8. This claim is to be taken with a grain of salt because Weiss did not have coincident field observations to use as a comparison standard. He simply reviewed his data over the entire period of the tests and surmised 'probable ground truth temperatures'.[52] Further, the radiances emitted in the narrower spectral bandpass of 10-12 μm are 1/2 those emitted in the 8-14 μm bandpass, and so the associated errors are proportionately ratioed. Hence, there is no expected advantage to working in the narrower bandpass. Weiss observed a near linear relation of radiometer readings below 760 metres altitude and hypothesized upon a two-point regression as a quick method at water surface temperature determination. Also, he was unable to completely explain atmospheric optical anomalies found in his data. Unfortunately, Weiss' theory does not make it clear whether he has accounted for sky radiance from the water surface, and hence, his work will not be considered in the study at hand.

Scarpace,[32] in his 1973 studies of thermal plumes, elected to calibrate his scanner outputs using the maximum and minimum temperatures recorded by a boat-mounted portable radiometric thermometer (PRT), or radiometer. The PRT, used with a strip chart, was reported to be accurate to 0.05°C and laboratory calibrations of the scanner indicated a linear output in the range of interest to 0.1°C. The scanner film was digitized with a densitometer to 256 discrete levels and the results compared to the PRT data. Accuracies of better than 0.25°C are reported. In his later work of 1975,[33] Scarpace used multiple 3-metre diameter pools of thermally stable water located at the target site as references. A regression is performed on the data obtained from these water baths of known temperature, giving a calibration curve for the scanner thermogram. This concept will be adopted as a check measure in the study at hand. Scarpace also used routine field observations gathered by the power companies as his calibration data. At some plants, surface water temperatures were measured using thermometers; at other plants, recorded thermocouple intake and discharge temperatures were used. This latter method is routinely employed in thermal plume studies conducted by the Ontario Centre for Remote Sensing.[27] Although it is not discussed in detail, the collection of ground data by plant staff, and the manner in which it is probably collected, makes this latter approach less than ideal. The intake and discharge points are usually displaced from one another by large distances and are difficult to image in the same thermogram. These temperature measurements are sometimes made from inside the intake and discharge ducts, and consequently, do not precisely reflect the water surface temperature in the immediate vicinity of the duct. Further, thermometers, unless they are of ASTM calibre and wholly immersed in the water, do not accurately represent the water temperature. Scarpace does not discuss any of these considerations which casts doubt on the precision of his reported results.

Remote sensing in the 11-13 μm window region, and employing three channels of a Nimbus satellite IR interferometer spectrometer, enabled Prabhakara,[25] in 1974, to estimate sea surface temperature to claimed accuracies of about 1.0°C of field observations. The absorption properties of water vapour in any two channels enabled him to determine the atmospheric correction factor without need for knowledge of profiles of temperature and water vapour. His absorption model was tested on archival satellite data covering 106 locations of the globe for which suitable ground observations were available and which coincided with 'satellite determined'[25] clear skies. Satellite and ground results are claimed to agree well over a sea surface temperature range of 4-29°C. The correction factor calculated from the model led to a slight under-estimation of sea surface temperature for cold waters in the high latitudes and to an overestimation in the tropics. This technique did not see operational use, per se. In later work,[22] it is noted that the selection of wavelength band for optimum radiance difference is a function of the absorption model employed, of which there are many.

In 1975, McMillin[22] conducted sea surface temperature experiments as per Prabhakara, however, in his absorption model he further considered the partial pressure of water vapour. As an improvement over his earlier work involving a linear regression for correction factor determination, McMillin has employed higher order analysis to reduce his claimed error from 0.6°C to 0.4°C. The failing of this work is that McMillin systematically selected a subset of his data set as a reference, thus satisfying his own end. Also, he compares his dual-wavelength results to dual-angle results. These two approaches have theoretically been shown to yield similar results but that is not empirically demonstrated in a rigorous experiment by McMillin in this work.

An experimental simulation of a single-channel, double-angle viewing technique for the determination of sea surface temperature from satellite data was trialled by Chedin,[9] in 1982. His method relies upon the fact that the same area can be coincidently viewed at two different angles (different air masses) by a geostationary and a polar orbiting satellite. Extrapolation of the two air mass observations to zero air mass is shown to give a value of the sea surface temperature which is claimed to be in good agreement with field observations. The complexity of the sensing system is the main disadvantage to this calibration approach, however, it has subsequently been monopolized by other workers.[45,51]

Mintzer,[23] in 1983, demonstrated a means of predicting heat loss from flat-roofed buildings using calibrated digital data from a thermal IR aerial survey. A calibrated thermal reference flat surface of higher temperature than the roof was placed on same. Measurements of wind speed, ambient temperature, reference temperature and sky temperature were also taken to reduce uncertainty in the analysis of the thermograms. A precision of ±0.5°C in the prediction of roof temperature was reported. Mintzer assumes all emissivities, i.e. ice, water, roof material, to be the same as that of the reference surface emissivity. This is considered to be a gross simplification of the problem. Emissivities of ice and snow are listed at $\varepsilon = 0.887$ and $\varepsilon = 0.82$, respectively,[13,16,47] and gravel and tar roofing, as probably used in Mintzer's work, have been shown to vary from 0.84-0.95.[13,40,47] Mintzer's approach is also wrought with extensive ground-based equipment manipulation and data collection which is considered too complex for practical purposes.

To this point, atmospheric calibration has focused on techniques for satellites, those involving extensive field observations, and atmospheric corrections for simple, non-scanning radiometers. Nothing of serious consequence was developed for the small operator which was logistically sound and reasonably accurate, before the work of Schott and, later, Macleod.

Schott,[34] in 1975, devised a method of calibrating for atmospheric effects on thermograms of large water bodies. The method requires no ground-based measurements but relies on establishing an atmospheric absorption profile which is extrapolated to zero altitude to determine apparent ground temperature. This then calibrates any aerial IR scanner over its entire 120 degree scan angle. A radiometer can be used for the calibration, however, a laboratory calibrated scanner can be used on its own. A minimum of four altitudes is recommended for the profiling.[48] Schott's Profile method is much more convenient, less difficult, and sometimes, less expensive than collecting reliable ground-level data. Never-the-less, flying over the same target on multiple passes at different altitudes is an absolute necessity for accurate extrapolation of data to ground temperature values. This technique represents considerable expense in flying time and associated labour. The Profile method has been employed on numerous studies with reported accuracies usually better than 0.5°C.[36,37,39,41,42] Additionally, this method was applied to calibrate satellite data with reported good success.[38]

More recently, Macleod[20] has developed an aerial calibration technique based on a two-angle approach[37] similar to Chedin's satellite method.[9] The technique is intended, for practical purposes, to be used with a vertical and offset angle. Greater precision can theoretically be realized with larger offset angles. This angular approach verified a linear relationship between radiant emittance and atmospheric attenuation for Lambertian targets in the 8-14 μm range. Macleod used archival imagery to develop his method and drew comparisons to ground feature temperatures obtained using Schott's Profile technique. Good correlation of results was reported, but the method has yet to be tested operationally.

Calibration techniques discussed thus far have involved viewing of a target of interest from either a satellite or aircraft platform to establish ground temperature. Some techniques have been more successful than others, but all require on-site viewing for an atmospheric calibration to be effective. A computer atmospheric model called LOWTRAN, developed by McClatchy et al.[21,54] in the early 1970's, can conceptually be employed to calibrate thermograms, even though uncertainties and inadequacies of the LOWTRAN model have been documented in studies[3] involving horizontal path lengths of up to 44 kilometres. Coded standard atmospheric data can be used or empirical atmospheric data can be generated by inputting radiosonde data, i.e. atmospheric pressure, temperature, and dew point depression profiles, to calculate atmospheric-path transmission and radiance between any two points in the terrestrial atmosphere. The model uses U.S. standard atmospheres to establish constituent levels for CO_x, NO_x, etc., but others like water vapour, pollutants, and aerosols are more variable. Radiosonde data only satisfies the water vapour data requirements, so LOWTRAN will assume aerosol and pollutant data unless otherwise provided. The LOWTRAN model deals with band models of absorption spectra as a function of wavelength so it is well suited to radiosonde data. The spectral bandpass of interest can be defined by the user, and through numerical integration methods, a path radiance and transmittance can be calculated which can be manipulated into an atmospheric correction term for thermogram data. Radiosonde data is usually not taken in precise coincidence, both spatially and temporally, with the aerial thermal IR survey thus introducing uncertainty into the results. The radiosonde data profiles the atmosphere to about 30,000 feet altitude.

There has been much effort expended to develop atmospheric calibration methods for satellite and aerial thermal data. Only a select few can be considered as practicible for the practitioner who is after quick and accurate results. The techniques that appear to have the greatest potential as 'business-sound' systems were evaluated in this study. These include Schott's Profile method, Macleod's Angular method, and the LOWTRAN approach.

Theoretical Background

Two types of radiant temperature sensing devices were employed in this study: a thermal radiometer and a thermal mapper.[15,17,26] The former is a non-imaging device which quantitatively measures and records the radiant temperature of objects within its field of view. A simple radiometer is depicted at Figure 3. The scanner, by contrast, builds up a two dimensional record of radiant temperature data for a swath beneath its flight platform. Thermal mapper operation is illustrated at Figure 4.

Implicit to the understanding of these thermal sensing devices is an understanding of the physics of thermal radiation. A description of basic radiation theory is presented at Appendix A.

Interpretation of the radiant energy arriving at our radiance measuring devices requires consideration of the target emissivity and reflectivity character,[28] and atmospheric or path effects over the path length of interest.[41] The intervening medium is a non-homogeneous,

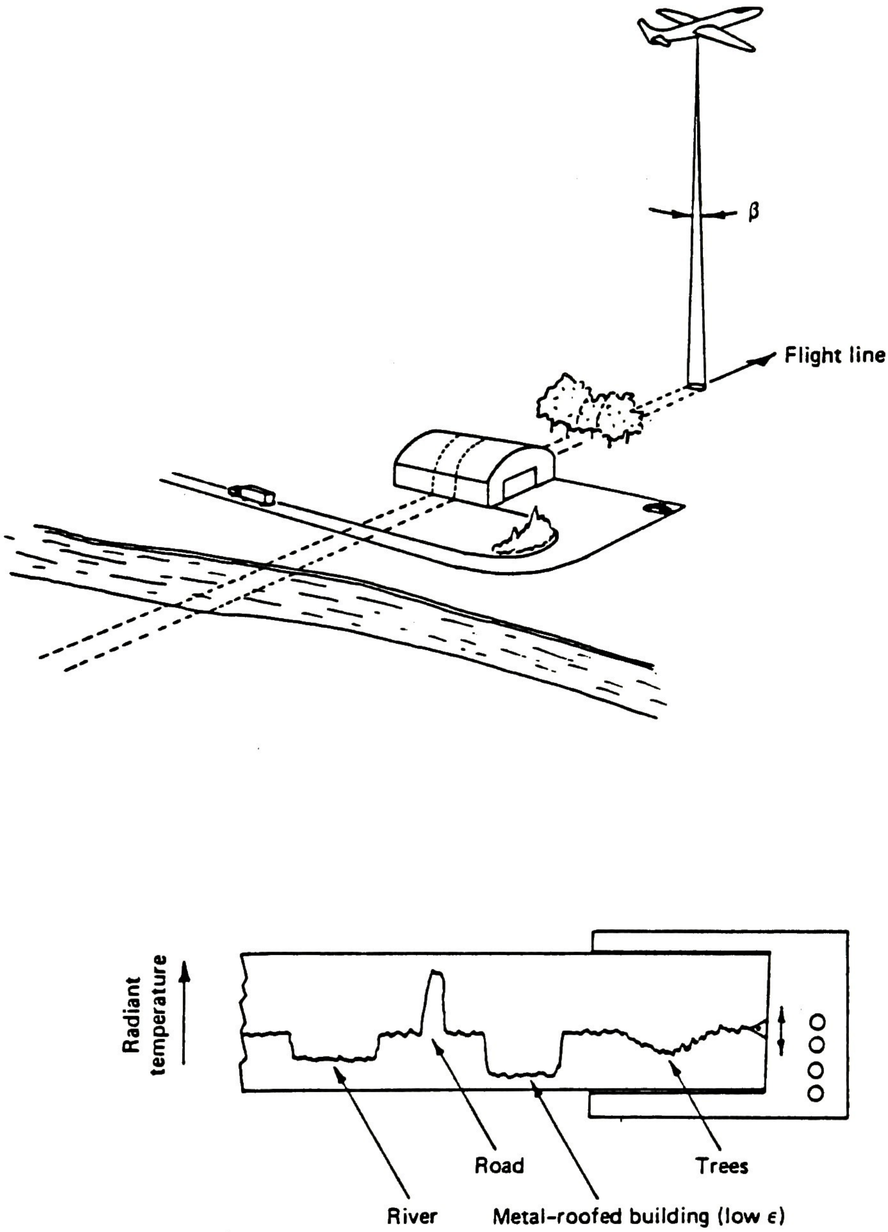

Figure 3. Thermal Radiometer Flight Configuration and Output. (after Lillesand)

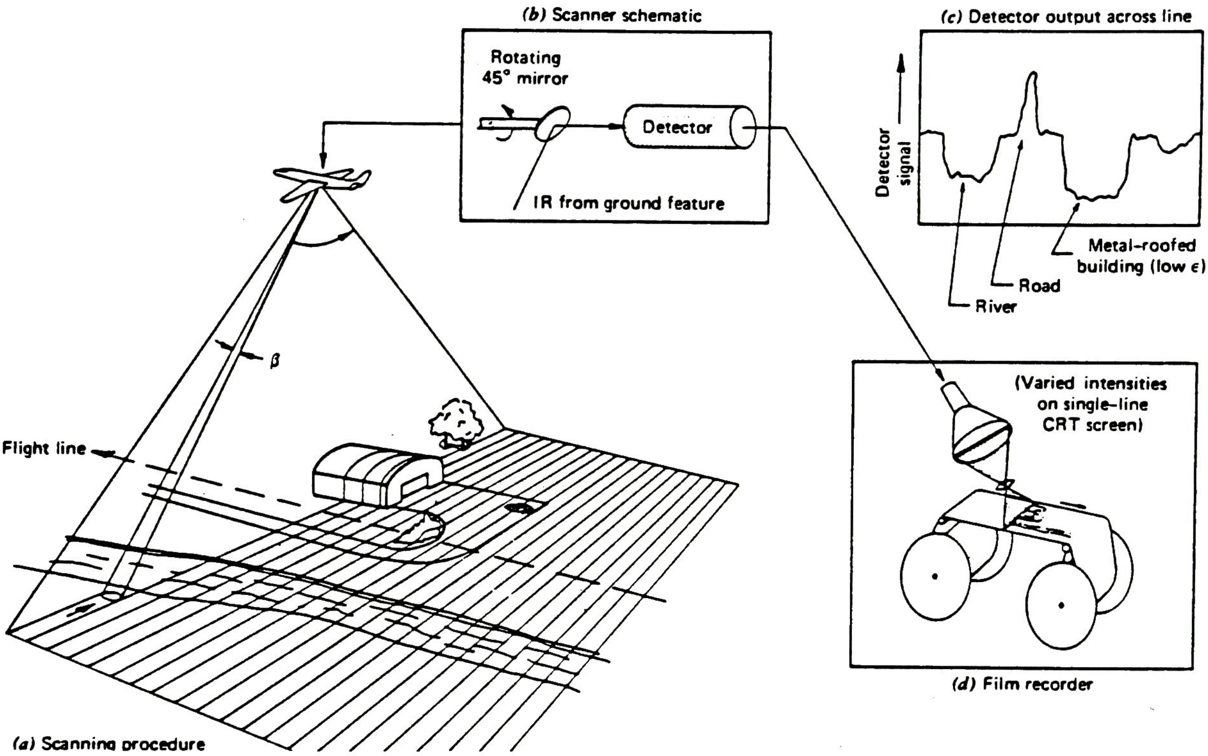

Figure 4. Thermal Scanner (Mapper) System Operation.

(after Lillesand)

dynamic mixture of gases, vapours, and particulate material.[10,15,45,48,54] Primary attenuation in the lower atmosphere is due to absorption by H_2O vapour, CO_2, and OH. These molecules absorb and reradiate as a function of temperature, thereby contributing to the TIR signal which is detected.

These target and air contributions can be summed in a simple expression of radiances, L, of units watts/steradian-centimeter^2:

$$L = \tau \varepsilon L_T + L_u \quad (1)$$

where τ is the atmospheric-path transmission in the spectral bandpass of interest, ε and L_T are the target surface emissivity and radiance, respectively, and L_u is the apparent radiance from the air column between the source and sensor, as well as energy scattered into the sensor as illustrated at Figure 5. The presence or absence of haze or clouds in the sky affects the amount of solar and thermal radiation that can be reflected from the ground or scattered by the air in the path of view.[2,11] The layering character of the atmosphere will vary L_u and τ as a function of the conditions on a given day. Surface emissivity, ε, is included to ensure precise interpretation of the TIR data.[4,28]

In addition to the radiant energy, L_T, from the ground feature, a certain amount of energy originating from the sun and sky collectively will be reflected from the ground surface.[10,48] Solar reflection effects can be avoided by proper orientation of flight lines[2,11] and skylight reflection effects can be expressed as τRL_d and included in the energy equation. Hence,

$$L = \tau \varepsilon L_T + \tau RL_d + L_u \quad (2)$$

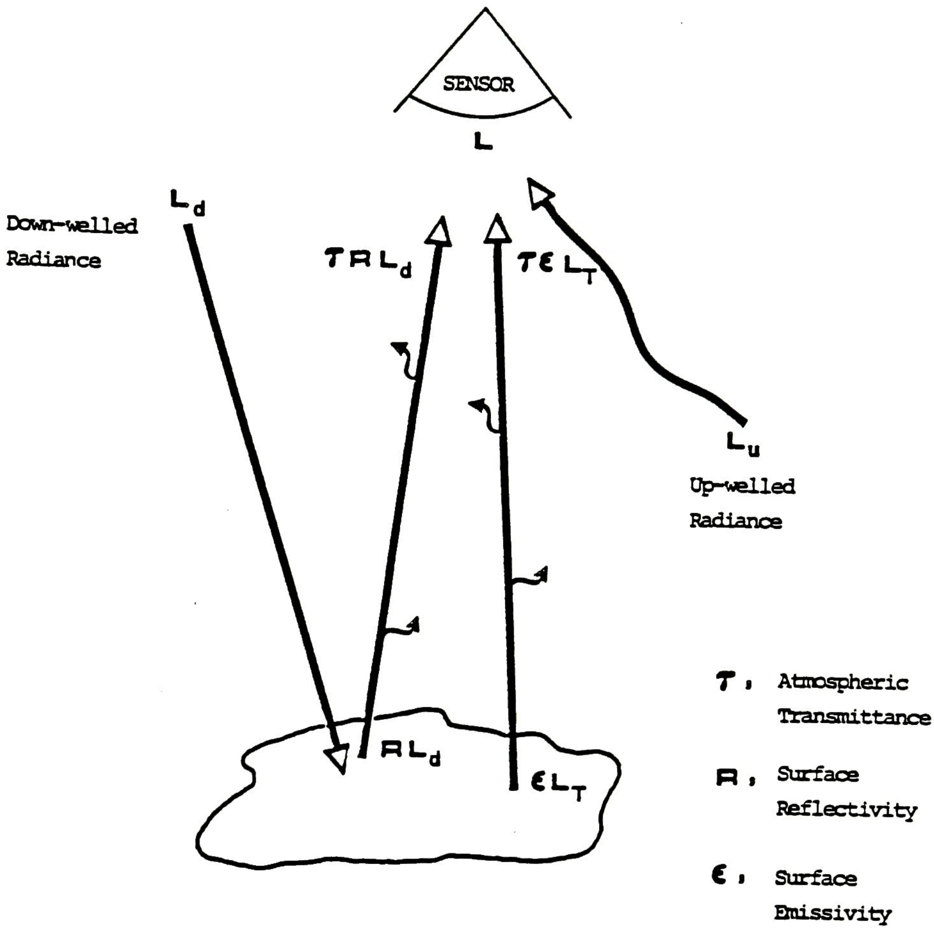

$$L = \tau \epsilon L_T + \tau R L_d + L_u$$

Figure 5. Radiometric Energy Sources Detected in Remote Sensing of the Earth.

where L_d is the downwelled, or sky, radiance from the sky incident on the surface observed, and can be associated with an equivalent sky temperature, T_{sky}. Surface reflectivity is denoted by R.

Skylight irradiation comes from scattered solar radiation, self-emitted radiation from components of the atmosphere, i.e. ozone, water vapour, and energy from the earth reflected by the atmosphere.[10,45,48] All these effects combine to give the sky an apparent radiometric temperature,[2,11] as viewed from the ground, which can be experimentally determined. Radiometers are generally not sensitive or accurate enough to the low sky temperatures, i.e. 230°K, and so other means must be used to estimate the sky radiance. Both an empirical and modelling approach can be employed to solve for L_d. For the empirical derivation, one must make coincident measurements of the surface temperature and radiance of a greybody, such as a sheet of graphite, which is exposed to the sky. Careful orientation of the surface is necessary to prevent radiance contributions incident on the surface from background terrestrial bodies. In this instance, the energy defined at equation (2), can be reduced to the following:

$$L = \tau\varepsilon L_T + \tau R L_d \qquad (3)$$

Terms L, ε,[40] L_T, and R are determined experimentally. L_u is assumed to be negligible and τ is approximately equal to unity in the close quarters of this experiment. Alternatively, the modelling approach in solving for L_d simply involves inputting radiosonde data into a modified LOWTRAN atmospheric model. The model integrates the downwelled radiance over a sky hemisphere to calculate the sky radiance, and equivalent sky temperature.[43]

Ground surface emissivity, ε, is a function of viewing angle,[46] as is reflectivity. In the case of marine surfaces, R and ε are independent of view angle, sea-state, and wind direction for angles less than 45°. A marked functional dependence exists at greater view angles.

It should be recognized that L_u and τ are dependent on the length and composition of the atmospheric-path between the source and observation point. These dependences will be elaborated upon under a discussion of the aerial calibration techniques, to follow.

Profile calibration technique. This approach utilizes infrared thermal mapper data, collected at different altitudes over a given ground target area, to calibrate the scanner output data for atmospheric-path transmittance and radiance. This calibration is employed in the determination of absolute temperatures of ground features imaged in scanner thermograms.

The radiance, or temperature, recorded by the scanner is observed ground radiance, rather than absolute ground radiance, and must be corrected for atmospheric effects.

The observed radiances are interpreted from the thermograms densitometrically and analysed through a series of system calibration curves which are illustrated at Figure 6.

To establish the atmospheric calibration, observed radiance data for a target feature from multiple altitude thermograms, are plotted against altitude, as in Figure 7. An extrapolation to ground level determines the ground apparent radiance for that particular target.

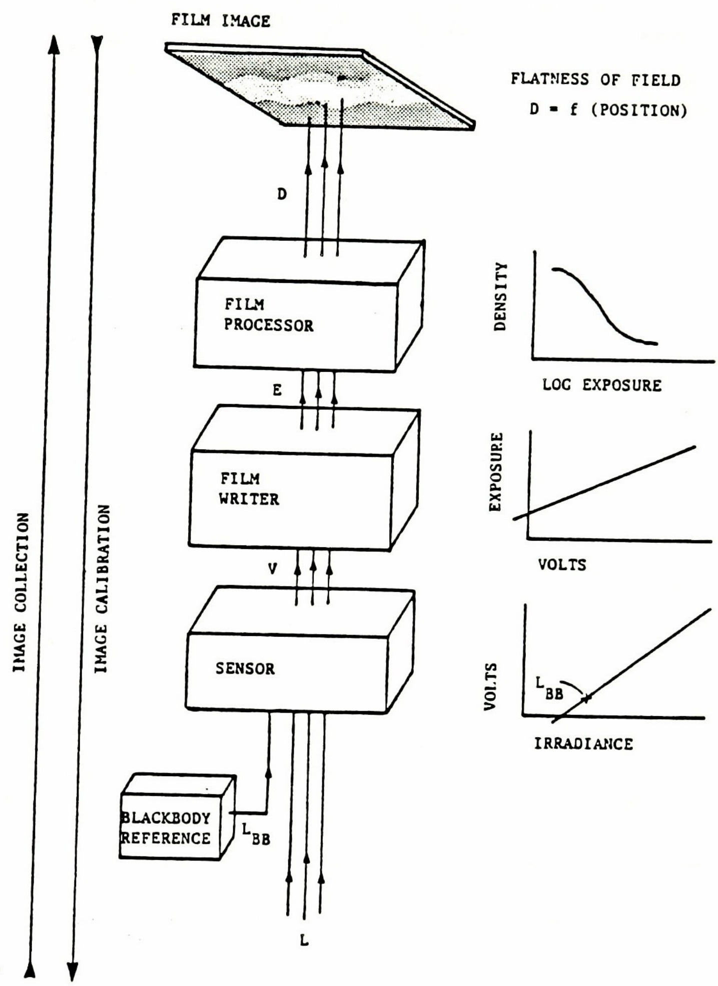

Figure 6. Calibration of Thermograms for Quantitative Data Extraction. The sensor alternately detects the target radiance, L, and the reference blackbody radiance, L_{bb}. These radiances stimulate the sensor to output a proportional voltage, V, which in turn drives a film writer. This device exposes the film which is subsequently developed to an image. The film density can be correlated to the detected radiance.

(after Schott)

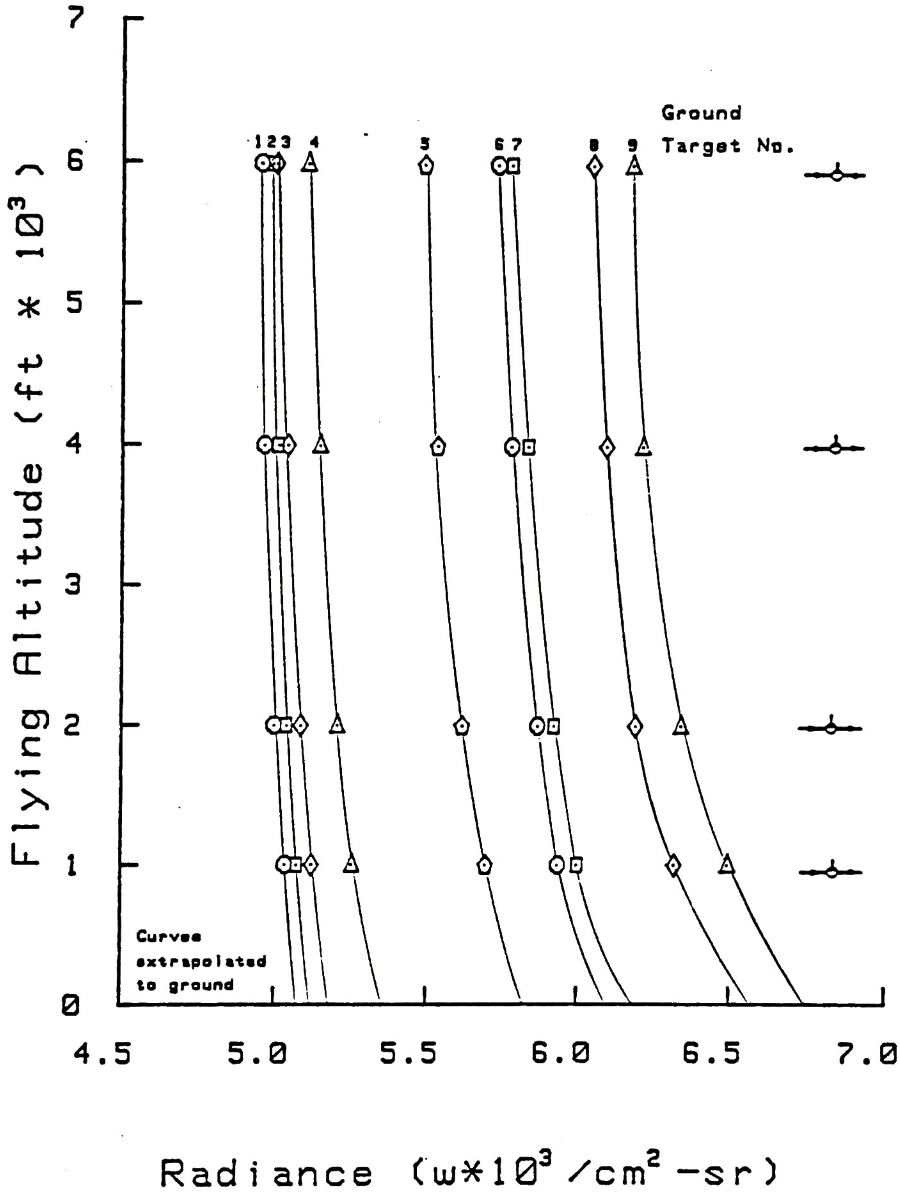

Figure 7. Profile Calibration Atmospheric Radiance Profiles.

This process is repeated for several targets of a wide range of temperatures. The shapes of the curves are established by comparison of the observed radiances for a given target to a series of curves predicted by the LOWTRAN radiosonde-based atmospheric model[43] for a range of defined ground temperatures. A least squares fit is applied for a best fit solution. For each altitude, the observed radiances for all targets are plotted versus the corresponding ground apparent radiances as at Figure 8. The slope of the resultant linear relation is the atmospheric-path transmission at that altitude, and the intercept is the atmospheric-path radiance. This can be shown by considering the energy equation which describes the imaging process,

$$L = \tau \varepsilon L_T + \tau R L_d + L_u \tag{4}$$

and collecting the energy contributions from the ground target,

$$L = \tau(\varepsilon L_T + R L_d) + L_u \tag{5}$$

Let $L_g = (\varepsilon L_T + R L_d)$, and substituting, therefore,

$$L = \tau L_g + L_u \tag{6}$$

Reviewing, the slope is the atmospheric-path transmittance, and the intercept the upwelled radiance. A radiance and transmission profile of the atmosphere can then be generated. Figure 9 summarizes the Profile calibration process.

<u>Angular calibration technique</u>. This method solves for the atmospheric-path radiance and transmission by flying a thermal mapper in a fashion such that the target area is viewed by the thermal scanner from

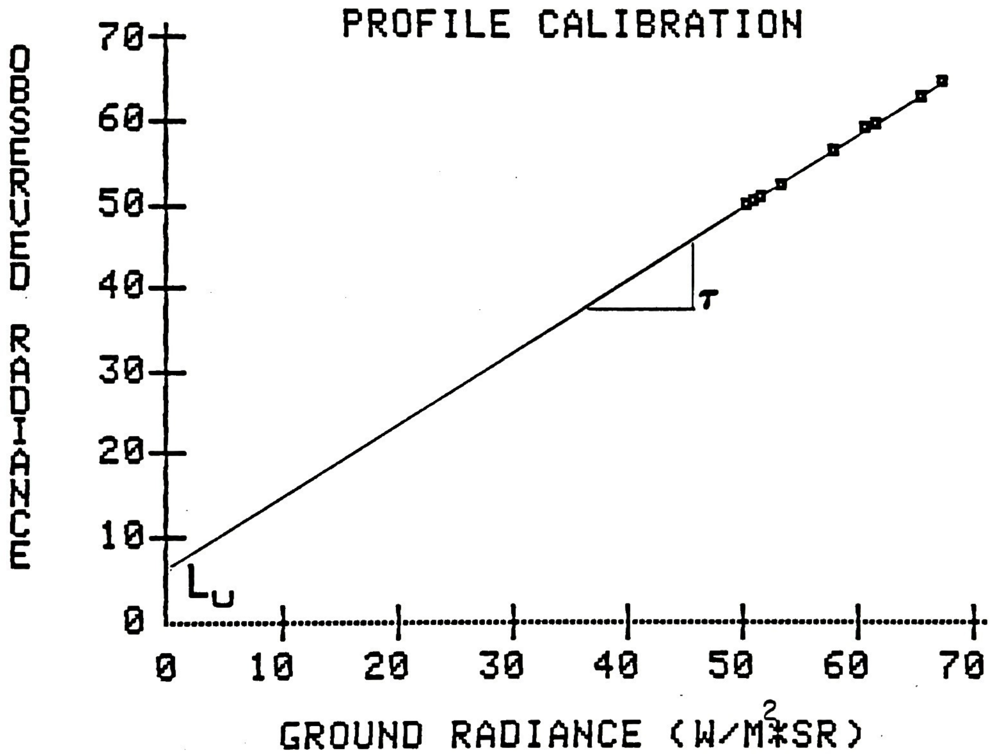

Figure 8. Profile Calibration Determination of Atmospheric-Path Radiance and Transmission.

Step	Process
Density ↓	interpolation on V-D curve
Voltage, V ↓	$T = (V - V_{bb}) \cdot G + T_{bb} + 273.16$
Observed Temperature, T ↓	Planck equation
Observed Radiance, $L(H,\theta)$ ↓	for zenith angle, $\theta = 0°$, extrapolate to ground altitude the plots of observed radiance vs. altitude to determine apparent ground radiance
Apparent Ground Radiance, $L_g(0,0)$ ↓	linear regression of observed radiance vs. apparent ground radiance for several targets of different temperatures (constant altitude) slope = $\tau(H,0)$ intercept = $L_u(H,0)$
$\tau(H,0)$ $L_u(H,0)$	

Figure 9. Profile Calibration Flow Chart. Determination of Atmospheric-path Radiance and Transmission.

two different angles--ideally, from directly overhead and from some offset angle, ϕ. This procedure is repeated for each altitude where the atmosphere is to be characterised.

As with the Profile approach, the radiances of numerous targets of varying temperatures, which can be seen in both the overhead and offset thermograms, are calculated through density calibration relations. The offset, or angled, radiances are plotted versus the corresponding overhead, or vertical, radiances to yield the atmospheric-path radiance and transmission through analysis of the slope and intercept terms, respectively. The theoretical development for this technique has been modified from that first proposed by Macleod[20] and is summarized at Figure 10 and detailed, hence.

Consider that a radiometer is situated at some height, H, above a ground feature, and it is viewing the ground feature at some angle, ϕ, as depicted at Figure 11.

Recalling the functional dependence of surface reflectivity, surface emissivity,[46] and of atmospheric-path radiance and transmittance on altitude and view angle, the energy equation (2) can be rewritten:

$$L(H,\phi) = \tau(H,\phi)\varepsilon(\phi)L_T + \tau(H,\phi)R(\phi)L_d + L_u(H,\phi)$$

$$= \tau(H,\phi)\cdot[\varepsilon(\phi)L_T + R(\phi)L_d] + L_u(H,\phi) \qquad (7)$$

Where $L(H,\phi)$ = observed radiance measured by the radiometer,
$L_T(H,\phi)$ = ground target surface radiance,
L_d = downwelled, or sky, radiance,
$L_u(H,\phi)$ = atmospheric-path upwelled radiance,
$\tau(H,\phi)$ = atmospheric-path transmission, and
$\varepsilon(\phi)$ and $R(\phi)$ are the ground target surface emissivity and reflectance, respectively.

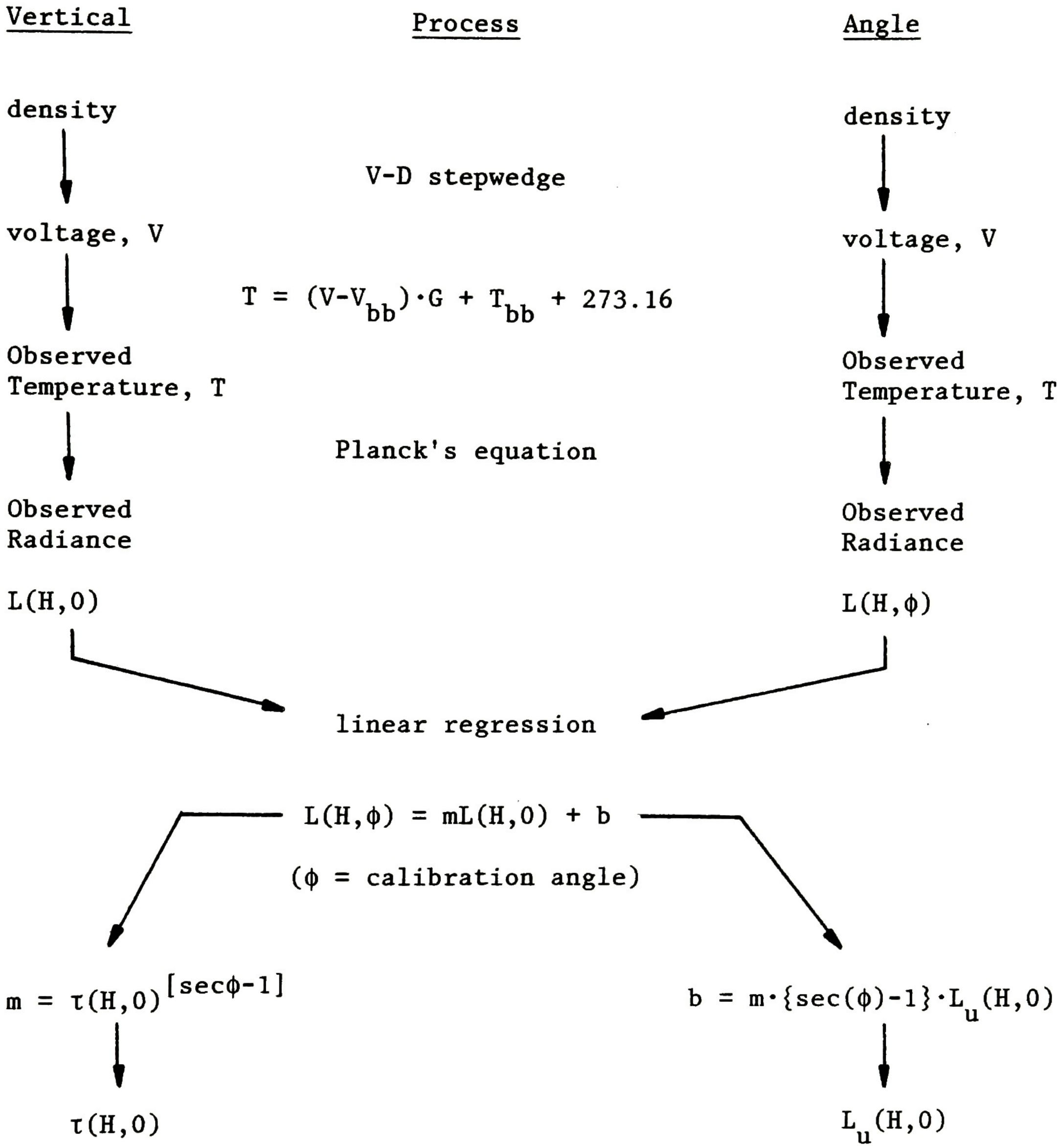

Figure 10. Angular Calibration Flow Chart. Determination of Atmospheric-path Radiance and Transmission.

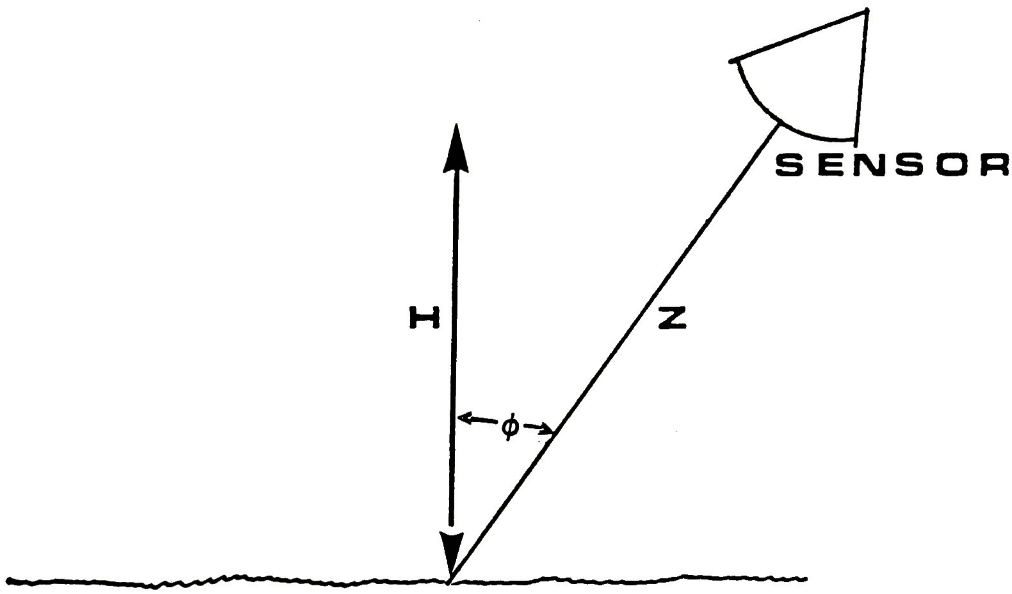

Figure 11. Lambert Cosine Law Geometry.

The symbols 'H' and 'ϕ' refer to the height of the sensor above the target and view angle, respectively, as illustrated in Figure 11. Collecting the ground target contributions together, for an altitude of H = 0:

let $L_g(0,\phi) = \varepsilon(\phi)L_T + R(\phi)L_d$. Therefore,

$$L(H,\phi) = \tau(H,\phi)L_g(0,\phi) + L_u(H,\phi) \tag{8}$$

For vertical viewing, $\phi = 0$,

$$L(H,0) = \tau(H,0)L_g(0,0) + L_u(H,0) \tag{9}$$

The radiance at the ground feature can also be expressed in terms of measured or derived terms,

$$L_g(0,0) = \frac{L(H,0) - L_u(H,0)}{\tau(H,0)} \tag{10}$$

A further computation is necessary to account for the angular dependence of several factors if we are to be able to compare results of differing look-angles. Recall the Bouguer-Lambert Law,[15]

$$P/P_0 = \exp(-\alpha Z) \tag{11}$$

where P/P_0 is the transmittance of flux entering a layer of a medium, α is the absorption coefficient of same, and Z is the path length. Applying this to aerial remote sensing, a change in view angle is equivalent to a change in the atmospheric-path length and we would then expect a greater attenuation of the target signal with larger view angles. Reviewing Figure 11, it is shown that $\cos(\phi) = H/Z$. Considering this, the atmospheric-path transmission can then be stated as,

$$\tau(H,\phi) = \tau(H,0)^{\sec(\phi)} \qquad (12)$$

This expression is a reasonable statistical approximation for view angle correction, for $\phi < 80°$.[43] Examining the bandwidth of interest in increments of $\Delta\lambda$, the equivalent absorber amounts, w^*, of each increment vary from zero to unity as per the atmospheric absorption window.[21,48,54] When the $\sec(\phi)$ factor is applied to the bandwidth increments characterised with $w^* = 0$, little contribution is made to the absorber amounts in the summation over the entire bandwidth of interest. This statistically balances the strong effect of the $\sec(\phi)$ factor on the wavelength increments which have near unity w^* values. For view angles greater than 80°, air index of refraction and earth sphericity corrections are needed.[43]

But, unlike Macleod who expressed $L_u(H,\phi)$ as $L_u(H,0)/\cos(\phi)$, this term, $L_u(H,\phi)$, can be more appropriately represented by the expression $L_u(H,0)\cdot\tau^{[\sec(\phi)-1]}(H,0)/\cos(\phi)$, as derived at Appendix B.

Assuming Lambertian character of the target surface,[48] i.e. $L_g(0,0) = L_g(0,\phi)$, then,

$$L(H,\phi) = \tau(H,\phi)\cdot L_g(0,\phi) + L_u(H,\phi) \qquad (13)$$

$$= \tau(H,0)^{\sec(\phi)}\cdot L_g(0,\phi) + \frac{L_u(H,\phi)\cdot\tau^{[\sec(\phi)-1]}(H,0)}{\cos(\phi)}$$

$$= \frac{\tau^{\sec(\phi)}(H,0)\cdot[L_u(H,0)-L_u(H,0)]}{\tau(H,0)} + \frac{L_u(H,0)\cdot\tau^{[\sec\phi-1]}(H,0)}{\cos(\phi)}$$

Therefore $L(H,\phi) = L(H,0)\cdot\tau^{[\sec(\phi)-1]}(H,0)$

$$+ L_u(H,0)\cdot\tau^{[\sec(\phi)-1]}(H,0)\cdot[\sec(\phi)-1] \qquad (14)$$

Rewriting, $L(H,\phi) = m\cdot L(H,0) + b$

Then,

$$m = \text{slope} = \tau^{[\sec(\phi)-1]}(H,0) \qquad (15)$$

and,

$$b = \text{intercept} = m\cdot[\sec(\phi)-1]\cdot L_u(H,0) \qquad (16)$$

To review, the measured or derived values are $L(H,\phi)$ and $L(H,0)$. Linear regression of this data, as illustrated in Figure 12, results in the determination of the desired atmospheric parameters.

LOWTRAN calibration technique. The last atmospheric calibration method to be examined uses the LOWTRAN computer-based atmospheric model. It is more empirically derived, but is reported[54] to be less accurate than other models, such as the Aggregate model. Determination of the atmospheric-path radiance and transmittance, using LOWTRAN, is easily done. All that is required of the user is to input the appropriate radiosonde data and to define the type of atmosphere and viewing geometry.

The algorithms for LOWTRAN are based on a series of graphs developed by the U.S. Air Force Geophysics Laboratory. One graph is used to determine the equivalent horizontal or slant path absorber amount and four others to calculate spectral transmittance due to absorption by atmospheric gases. Scattering is calculated by the use of yet another graph. Slant paths are accommodated in the model.

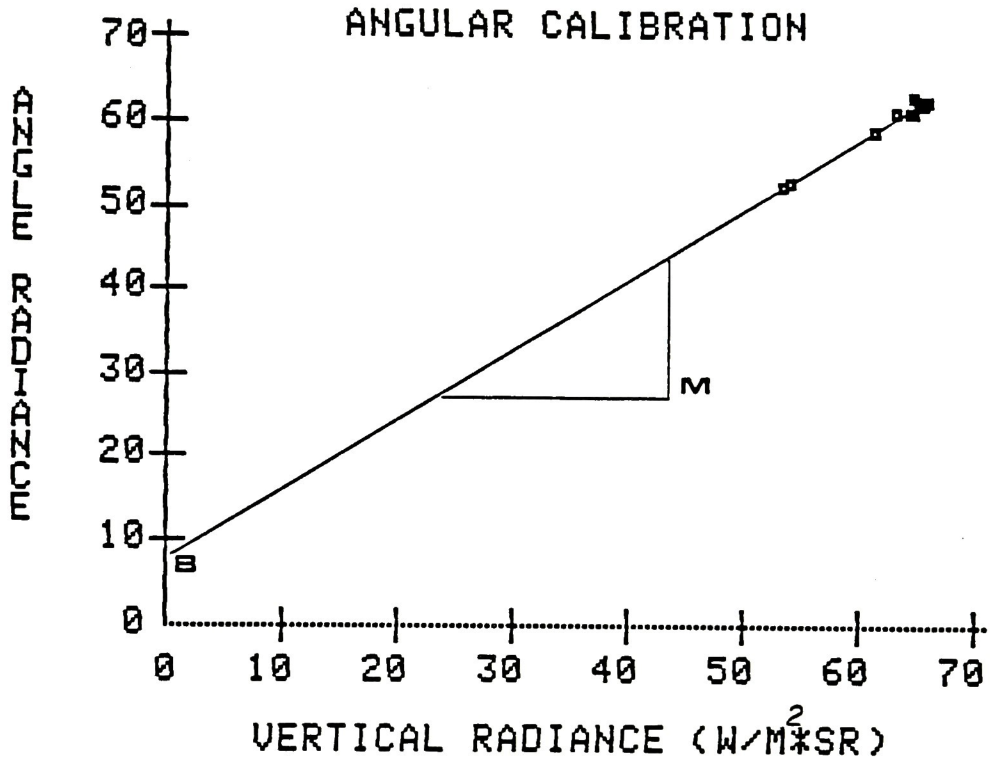

Figure 12. Angular Calibration Determination of Atmospheric Parameters.

Input data comprises altitude profiles of atmospheric pressure, temperature, and dew point depression values.

The spectral response function within the spectral bandpass of interest can be suitably defined in the LOWTRAN computer code to correspond to the thermal sensing device which generated the thermograms. The values of τ and L_u are appropriately factored.[55] This procedure is described in the 'Results' section.

Ground temperature prediction. With the atmosphere calibrated for transmission and upwelled radiance, the temperature of ground targets imaged in aerial thermograms can then be determined. The process, summarized at Figure 13, requires that density measurements of the targets be made from the thermograms; these results converted to voltage through the density-voltage curve; and these results substituted into equation (17), below. This equation defines the equivalent temperature, T, of the thermal mapper output voltage, V, hence:

$$T = (V - V_{bb}) \cdot G + T_{bb} + 273.16 \tag{17}$$

where G is the scanner gain; and V_{bb} and T_{bb} are the scanner blackbody voltage and temperature, respectively. T_{bb} is measured in degrees celsius. Derivation of this relation is made at Appendix C.

Numerical integration of Planck's equation over the spectral bandpass of the thermal mapper, i.e. 8-14 μm, yields the equivalent radiance, $L(H,\theta)$, for a given altitude, H, and observer view angle, θ. This is then corrected for atmospheric effects through the following equation.

Step	Process
Density	
↓	interpolate on V-D curve
Voltage	
↓	$T = (V-V_{bb})\cdot G + T_{bb} + 273.16$
Observed Temperature, T	
↓	integrate Planck's equation over interval 8-14 μm
Observed Radiance $L(H,\theta)$	
↓	
Apparent Ground Radiance $L_g(0,\theta) = \dfrac{L(H,\theta) - L_u(H,\theta)}{\tau(H,\phi)}$	; given $L_u(H,\theta)$, $\tau(H,\theta)$ and observation angle θ.
↓	
Ground Radiance $L_T(0,\theta) = \dfrac{L_g(0,\theta) - L_d\cdot R(\theta)}{\varepsilon(\theta)}$	; given L_d, $R(\theta)$, $\varepsilon(\theta)$.
↓	point-wise interpolation of tabulated radiance values
Ground Temperature	

Figure 13. Prediction of Ground Temperature Flow Chart.

$$L_g(0,\theta) = \frac{L(H,\theta) - L_u(H,\theta)}{\tau(H,\theta)} \tag{18}$$

where $\tau(H,\theta) = \tau^{\sec(\theta)}(H,0)$, as per equation (12)

and

$$L(H,\theta) = \frac{L(H,0)\cdot\tau^{[\sec(\phi)-1]}(H,0)}{\cos(\theta)} \tag{19}$$

Accounting for the ground surface characteristics of emissivity and reflectivity, then ground target radiance is defined:

$$L_T(0,\theta) = \frac{L_g(0,\theta) - L_d\cdot R(\theta)}{\varepsilon(\theta)} \tag{20}$$

where L_d = sky radiance,

$R(\theta)$ = target reflectivity, and

$\varepsilon(\theta)$ = target emissivity.

A point-wise linear interpolation of tabulated radiance values for L_T will yield a predicted surface temperature for the ground target.

EXPERIMENTAL

The experimental element of this study comprised three parts: a field experiment, thermogram analysis, and data analysis.

Field Experiment

This work involved calibration of all instruments, collection of aerial thermographic data, and processing of film.

The thermal mapper was calibrated as described in Appendix C, which established the reference blackbody temperature and system gain, i.e. °C/volt. The gain calibration was necessary for a proper analysis of output signals which were to be recorded on magnetic tape before film writing, and for those signals which were to be recorded direct to film. The former required a 15 step voltage-density (V-D) wedge, and the latter a 6 step V-D wedge. The V-D wedge is written in increments of one volt, beginning at zero volts.

The thermistors and the PRT-5 radiometer were collectively calibrated against an ASTM thermometer over the temperature range 1-55°C. For this exercise, the thermistors were immersed in a stable water bath and the radiometer was directed at the surface of same. The radiometer was held approximately 12" from the surface of the water. The calibration process was repeated before and after the field measurements.

The thermal mapper was flown along the shoreline of Lake Ontario at the outfall of the Genesee River and Little Pond at Rochester, New York, between the hours of 1030 hr and 1200 hr on 11 and 25 June, 1983. The sky was cloudless. The thermal mapper output signal was recorded by a glow-tube type film recorder and on magnetic tape, the latter being a backup measure. The format of parallel flight lines is depicted at Figure 14 which included 6 altitudes for the Profile technique and 4 complementary offset flight lines over land to accommodate the Angular technique. Each leg was about two miles in length requiring some two hours flight time for each of the two replicate missions. All legs were flown east to west in order to arrange the blackbody stripe on the side of the film which imaged the lake waters. The aircraft was rented from Calspan Corporation of Buffalo, New York.

Coincident with the flights, surface temperatures of Lake Ontario, the Genesee River, and Little Pond were being made with thermistors[27] and a PRT-5 radiometer.[6] Transportation consisted of an 18 foot open-bow motor launch. Four thermistors were affixed to the underside of a styrofoam flotation device. All temperature measurements were made at the bow of the boat to minimize the heating effect on the water surface by the boat's motor radiator discharge. Since the boat always had effective forward motion, the radiometer emulated the thermal mapper in its integration of the signal over a large area.[33] Position fixing of the boat during temperature measurement was facilitated with a marine compass. Bearings were taken on at least two prominent, stationary landmarks. This data was subsequently triangulated on a 1":200' scale orthophoto map.

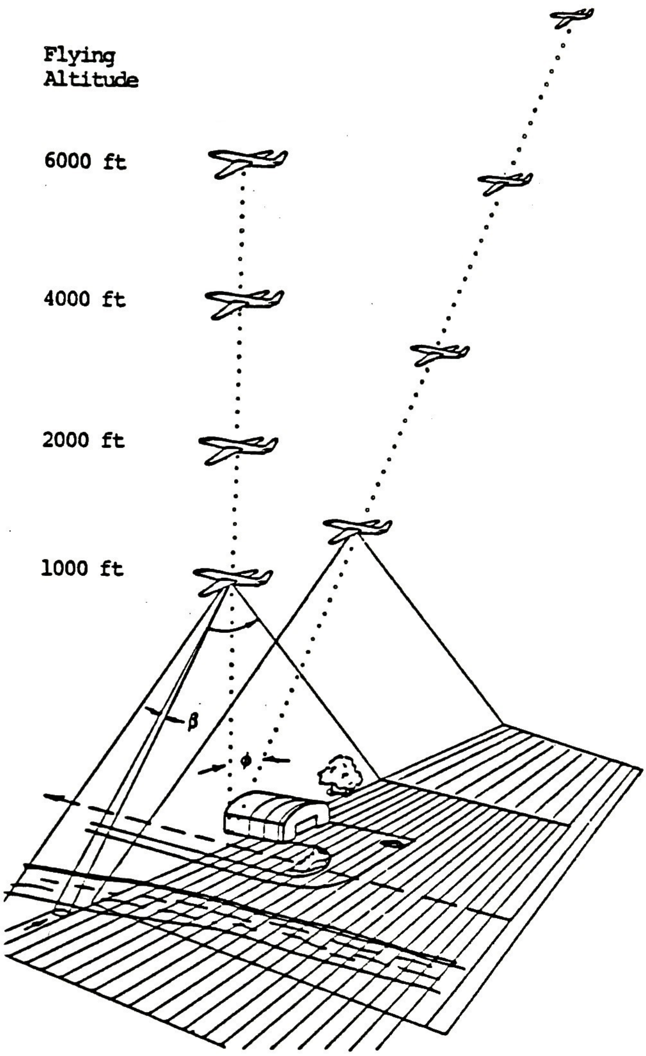

Figure 14. Flight Format Used in Experiment.

The tape recorded thermal mapper signal was played back in the laboratory and rerecorded on film through a Visicorder oscillograph. The film generated in this manner, as well as that written by the glow-tube film recorder, were developed in a Versamat film processor. Each strip of film was appropriately tagged with a sensitometric step wedge.

Radiosonde atmospheric data for the Buffalo and Albany, New York weather stations were procured from the National Oceanic and Atmospheric Administration for the mission days. This data formed the data base for the LOWTRAN atmosphere model.

Equipment reliability for this experiment is listed at Table 1.

Table 1. Equipment Serviceability Record

Equipment Description	11 Jun Mission	25 Jun Mission
Thermal Mapper	O.K.	O.K.
In-flight Film Writer	O.K.	Failed
Tape Recorder	Failed	Limited Failure
Versamat Film Processor	Failed	O.K.
Visicorder Film Writer	Not Used Since Tape Recorder Failed	O.K.

The 11 June mission suffered failure of the magnetic tape recorder. Also, the film which was written in-flight was non-homogeneously developed due to a failure of the Versamat processor.

The 25 June mission was tainted with a failure of the in-flight film writer and a partial failure of the tape recorder. The video signal was recorded on tape without its complementary synchronization signal. As the name implies, this latter signal is necessary to synchronize the sweep of a film writing facility, such as a Visicorder oscillograph. A pseudo-synchronization signal was eventually substituted from a pulse-generator whose frequency was manually manipulated to maintain the monitored video signal in a relatively stable configuration. The oscillograph-generated thermograms suffered increased degradation of geometric fidelity with increased altitude.

Thermogram Analysis

All densitometric analyses involved three trials, each one being replicated six times.

Analysis of thermograms was initiated with establishing the appropriate densitometer aperature size. Too large an aperature, i.e. 450 μm, could not accommodate the smaller features in the images, and too small an aperature, i.e. 50 μm, was characterised with too much density noise. A 150 μm aperature proved to be the best compromise.

Sensitometric compatibility of the thermograms to the reference V-D step wedge was established for each image frame by comparison of the sensitometric step wedges written on each frame. Density values obtained from thermograms were sensitometrically corrected to the V-D curve.

Several preliminary tests were conducted on the imagery before proceeding with the atmospheric calibration techniques. First, the blackbody stripe density variability and mean value were established for each frame. Next, the temperature discrimination, i.e. °C/density unit, and the relationship of view angle to film distance from the nadir line were examined.

A 1000-foot altitude thermogram of the experiment site taken on 11 June, 1983 was digitally analysed[5] with density slicing techniques and false colours applied to produce the image of Figure 15. The temperature spread in the waterways represents approximately 15°C.

Profile calibration. This calibration technique involved studying select features which were common to each of the Profile thermograms generated at different altitudes. The features selected were situated along the nadir line of each image and covered a broad range of temperatures. Thermograms of altitudes 1000, 2000, 4000, and 6000 feet were found suitable for this analysis.

Angular calibration. This technique required analysis of complementary pairs of thermograms, imaged at the same altitude, whose flight paths were parallel. Common features were selected from each image such that the view angle between the two perspectives of viewing remained constant. Features were selected along the nadir line of one image to simplify the study. The analysis was completed for the same altitudes studied in the Profile calibration.

Primary ground-truth targets. Densities of water features whose temperature were measured with thermistors and PRT-5 radiometer were taken from the imagery used in the Profile analysis. This data set served as a ground-truth data base.

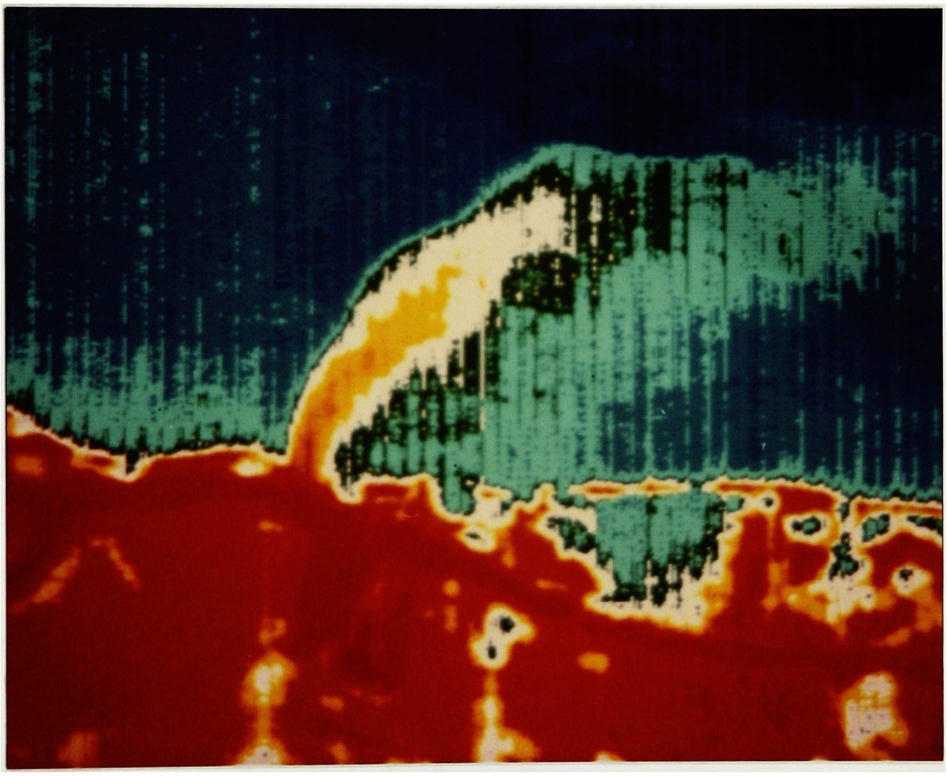

Figure 15. Digitally Enhanced Thermogram of Field Experiment Site. The thermal plume (yellow, white and green) is seen at its outfall into Lake Ontario (blue). The outline of a road can be seen running parallel to the shoreline (red).

Data Analysis

Reduction of the thermogram density data was facilitated with computer software[29] written for the Apple II Plus personal computer. This software is listed as an appendix.

Profile and Angular calibration. The flow diagrams of Figures 9 and 10 list the algorithms incorporated into the Apple software used to solve for the atmospheric-path radiance and transmittance as defined by the Profile and Angular techniques, respectively.

LOWTRAN calibration. The LOWTRAN calibration simply required inputting radiosonde data into the LOWTRAN computer code resident in the R.I.T. VAX computer. A 23 km rural aerosol model, a spring/summer season, and a look-down viewing geometry were selected. This program calculated the atmospheric-path radiance and transmittance for the defined altitudes. These results were factored with the spectral response function of the thermal mapper optics. The algorithms for this are described in the 'Results' section. The LOWTRAN program could not predict atmospheric-path radiance and transmittance for vertical path lengths ending at the earth's surface which originated at an altitude lower than the lowest radiosonde data point.

Ground-truth temperature prediction. The software for the determination of the ground-truth surface temperatures was also written in Applesoft Basic. The flow chart for this procedure has been summarized at Figure 13. For this calculation, water surface emissivity was taken as $\varepsilon = 0.986$,[13,16,46] and the sky radiance value, L_d, was calculated using the modified LOWTRAN code, according to Schott.[43]

Ground-truth targets were studied on 1000, 2000, 4000, and 6000-foot altitude thermograms. Unfortunately, because of geometric infidelities and inadequate feature discrimination on the higher altitude thermograms, only the 1000-foot altitude thermograms could be analysed with the necessary degree of precision. The R.M.S. errors in the prediction of ground-truth surface temperatures for all altitudes are listed at Table 2, and illustrated at Figure 16. The altitude depen-

Table 2. R.M.S. Errors in Primary Ground-Truth Temperature Predictions.

Altitude (ft)	Angular	Profile (note 1)	Profile (note 2)	LOWTRAN	LOWTRAN (note 3)
1000	1.026	0.711	0.704	0.643	0.680
2000	2.382	1.934	2.380	1.409	1.890
4000	4.314	3.003	3.621	2.443	2.510
6000	4.649	3.740	4.281	3.499	3.630

Note 1. Analysis of data by an independent agent.

Note 2. Analysis of data using least squares regression.

Note 3. LOWTRAN results spectrally corrected for thermal mapper optics.

dency in ground-truth data that is evident in these results is considered unsatisfactory above 1000-foot altitude since the error propagation study indicates errors of only 1.06°C at 1000-foot altitude, and 1.27°C at 6000-foot altitude. Errors in Primary ground-truth temperature predictions, $E_{predict}$, were calculated using the following equation and solving for $E_{predict}$:

$$E^2_{observed} = E^2_{ground\text{-}truth} + E^2_{predict} \tag{21}$$

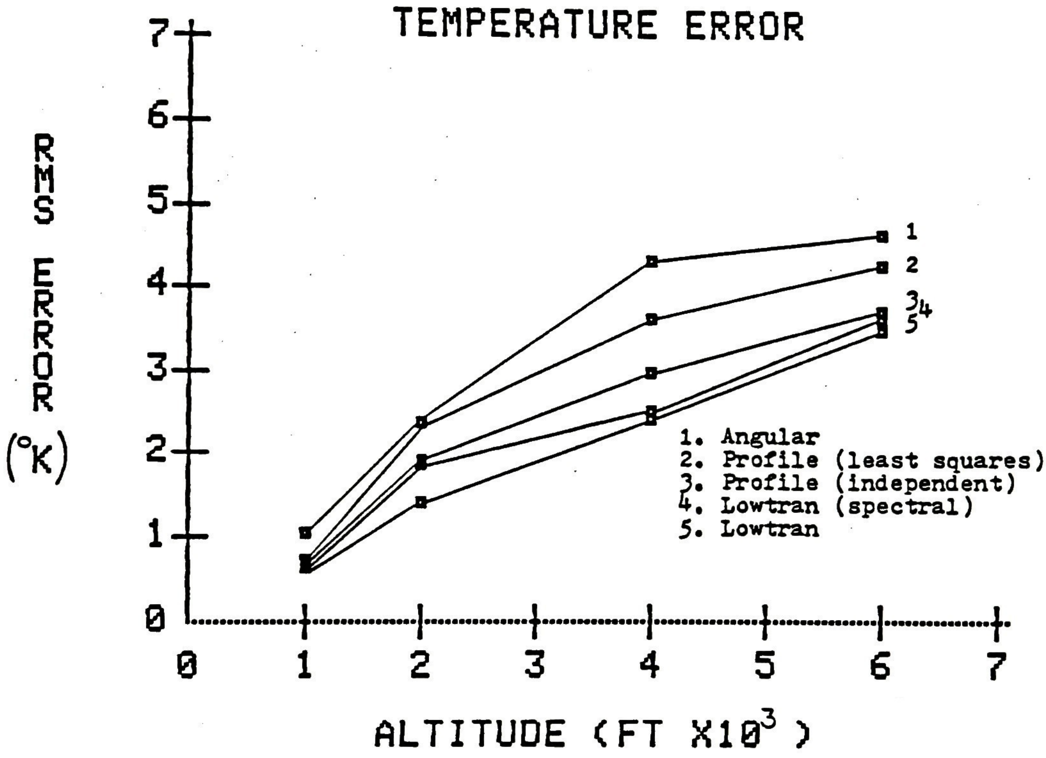

Figure 16. R.M.S. Error in Predicted Ground-Truth Temperature.

To extend the study to the higher altitudes, secondary, or new ground-truth targets of large area, uniform temperature, and which were imaged at all altitudes, were sought out. Coincidentally, the targets used for the Profile calibration technique satisfy these requirements and were accordingly utilized to establish a new ground-truth data base at altitudes 2000, 4000, and 6000 feet.

The prediction of the ground temperatures for the new ground-truth observed radiances was accomplished through a technique adopted from Scarpace.[33] In this approach, the thermogram-predicted radiances of the primary ground-truth features were regressed against the corresponding thermistor derived ground (water) radiances. The resultant linear relation leads to an atmospheric τ and L_u (c.f. Appendix H and Figure 21), which were then used in conjunction with the graphical interpolations of new ground-truth data found in the 1000-foot thermograms to predict the surface temperatures of these new ground-truth features. These predicted ground temperatures were then used as new ground-truth data for comparison to the 2000 to 6000-foot altitude thermogram observed temperatures.

Errors in the new ground-truth temperature predictions were calculated using equation (21), but substituting the $E_{\text{ground-truth}}$ term with the $E_{\text{new ground-truth}}$ value, as follows:

$$E^2_{\text{observed}} = E^2_{\text{new ground-truth}} - E^2_{\text{predict}} \qquad (22)$$

RESULTS

Field Measurements

Results of the thermal mapper calibration for gain and blackbody temperature settings are illustrated at Appendix C. For the mission settings, the blackbody temperature was established at 22.15°C, and the gain for the system, which included the tape recorder in the film writing process, was found to be 2.434°C/volt.

The thermistor calibration curve is illustrated at Figure 17. The thermistors exhibited greater stability than did the PRT-5 radiometer in the replications of this exercise. Drift in the radiometer response became evident in the after-mission check calibrations and, for this reason, the radiometer data were discarded. It is suspected that water splashed onto the radiometer detector during the field experiment on Lake Ontario was the cause of the anamolies in the radiometer readout.

The water surface temperatures, i.e. primary ground-truth, as determined by the thermistors, are listed at Appendix D. The range of temperature for these reference targets is about 15°C. The variability in the thermistor data translated into a precision of ±0.16°C in these water surface temperature values.

A thermal front survey[7] conducted by Rochester Gas & Electric at the Nuclear Ginna Plant validated that a cyclic temperature power spectrum characterizes the water body at the power plant cooling water outfall. Two degree celsius temperature swings in three minute cycles

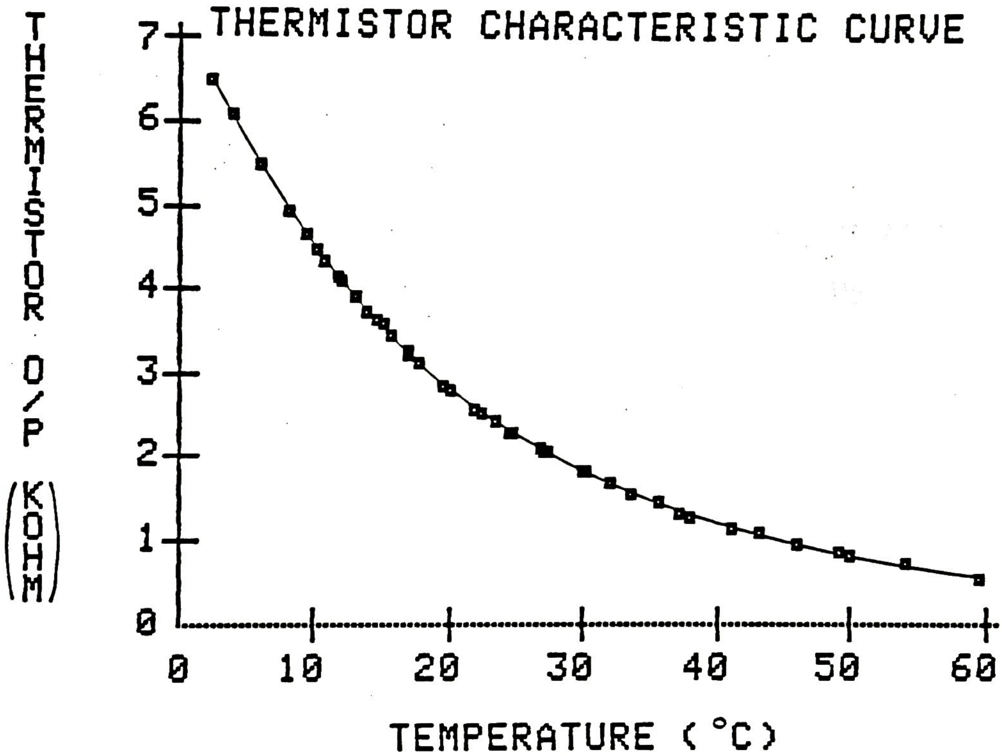

Figure 17. Characteristic Response Curve of Thermistors.

at 4.5 foot and 6.5 foot depths at 100 feet from the outfall were chronicled. This indicates that temperature power spectra are a potential source of variability in aerial TIR studies involving ground-truth correlation. Only two ground-truth measurements were taken near the Russell Station outfall at Little Pond, one at the 20 foot and another at 200 foot distance. Review of this data, (c.f. Figure 21 data points 2 & 6, and Appendix D), indicate little influence from temperature power spectra. This result is expected since the outfall of 25 June, 1983 could be characterized as a rough-water plume[12] where wave momentum and the turbulence associated with breaking waves dominates all the processes. Here, temperature differences serve merely as tracers of plume water, which is transported over relatively large distances along the shore by littoral currents. The outfall of 11 June, 1983 illustrated in Figure 15 is characteristic of a normal plume.[12]

Thermogram Analysis and Atmospheric Calibration

The radiance values referenced in this section were derived from thermogram density measurements and represent the mean values of three trials, each replicated six times.

Profile calibration. Thermogram observed radiances and extrapolated apparent ground radiances are tabulated at Appendix E, and the atmospheric profile curves generated from this data set are illustrated therein. As already discussed, the extrapolated ground radiances for all ground targets are regressed against their corresponding data set for a single altitude. The slope of the linear relation is the atmospheric-path transmittance for that altitude, and the intercept is the corresponding path radiance. (c.f. Figure 8)

Angular calibration. The radiance data for the Angular calibration technique are listed at Appendix F. A regression of the offset and vertical radiance values for a single altitude, as shown in Figure 12, leads to a computation of the atmospheric-path radiance and transmittance through the slope and intercept.

LOWTRAN calibration. The radiosonde data used in the LOWTRAN atmospheric model are listed at Appendix G. The atmosphere temperature profile generated from this data is illustrated at Figure 18 and indicates an insignificant atmospheric temperature inversion. The calculated sky radiance, $L_d(\theta)$, is plotted as a function of view angle, θ, at Figure 19. Integration of this result over a hemi-sphere yields the calculated downwelled sky radiance, L_d,[2,43]

$$\begin{aligned} L_d &= \int_\Omega L_d(\theta)d\Omega/\pi \qquad (23) \\ &= 1.48399\text{E-}3 \ \text{W/cm}^2 \end{aligned}$$

where Ω is the solid angle of the hemi-sphere.

The spectral response function of the thermal mapper and its IR filter is shown at Figure 20. This function was used to modify the LOWTRAN-model computation of atmospheric parameters. In this fashion, the LOWTRAN model better emulates the thermal mapper IR response. The LOWTRAN output data is modified as per the following equation,[44]

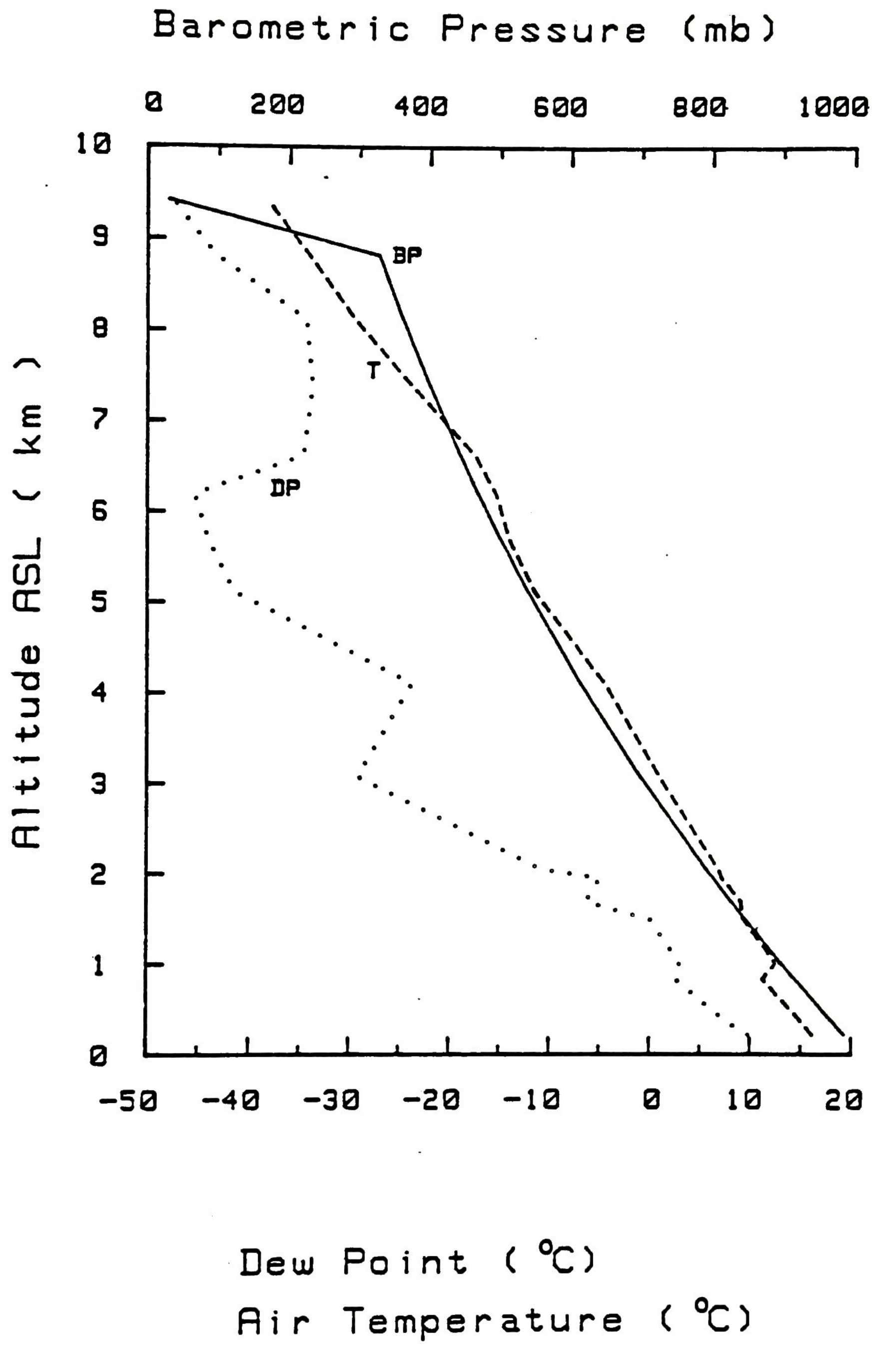

Figure 18. Atmosphere Temperature Profile on Day of Field Experiment, 25 June, 1983.

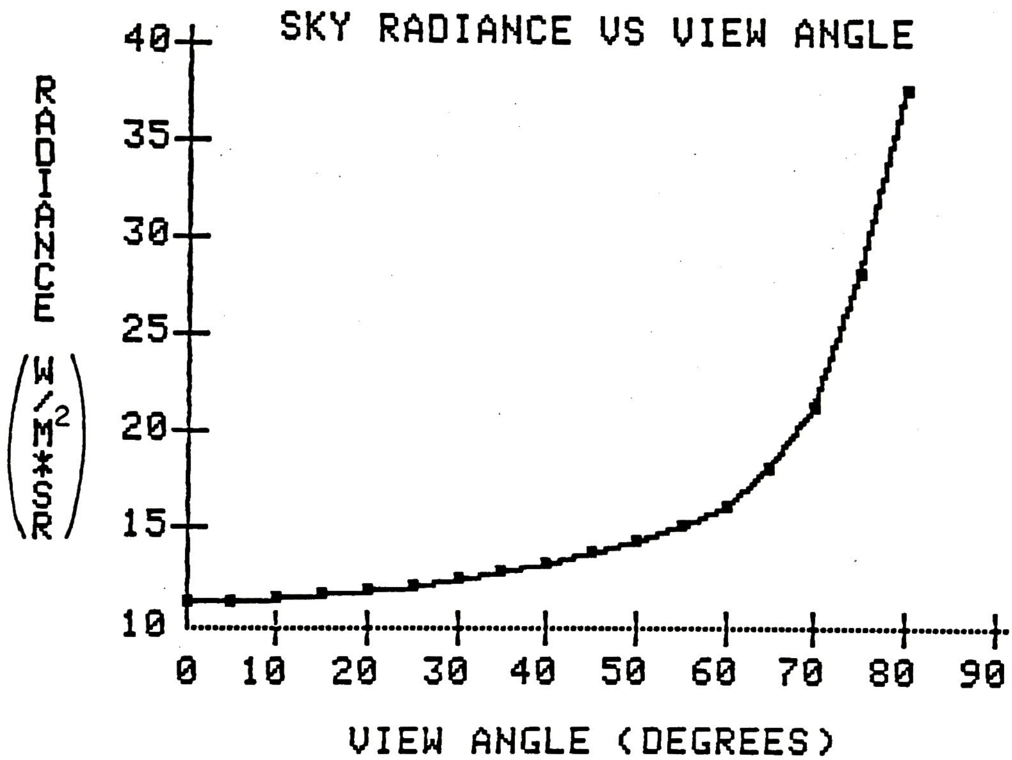

Figure 19. Sky Radiance as a Function of View Angle on Day of Field Experiment, 25 June, 1984.

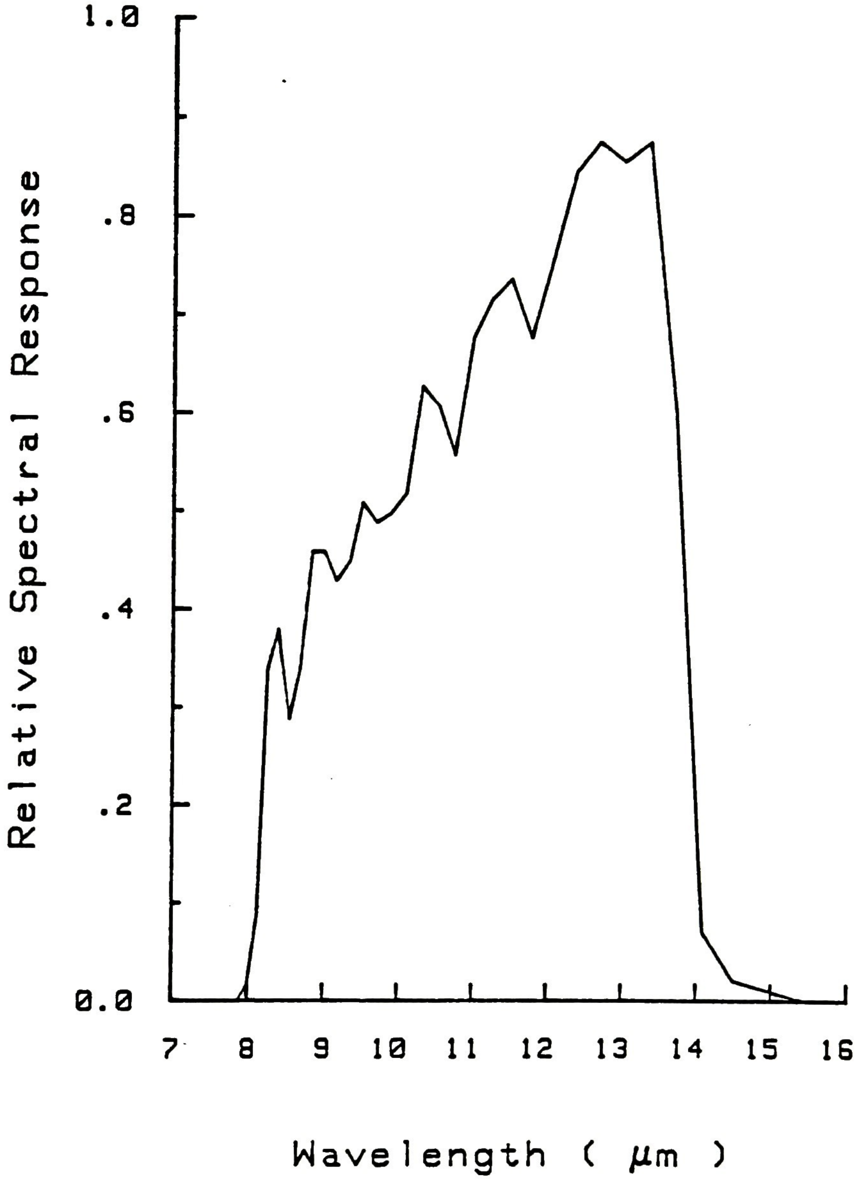

Figure 20. Thermal Scanner with IR Filter Spectral Response Function.

$$L_{spectral_{T,d\lambda}} = \int_{\lambda_1}^{\lambda_2} \frac{\int_{\lambda_1}^{\lambda_2} L_{lowtran_{T,\Delta\lambda}} \cdot R_{\Delta\lambda} \cdot d\lambda}{\int_{\lambda_1}^{\lambda_2} R_{\Delta\lambda} \cdot d\lambda} \cdot d\lambda \tag{24}$$

where the integration is applied within the spectral bandpass of interest; $L_{lowtran_{T,\Delta\lambda}}$ is the LOWTRAN radiance within a step of the spectral bandpass; and $R_{\Delta\lambda}$ is the relative spectral response of the scanner optics in the same spectral step. To calculate an atmospheric-path τ and L_u, the above analysis is repeated for LOWTRAN outputs of two defined ground temperatures.[44] These results are then regressed against corresponding blackbody calculations where $L_{bb_{T,\Delta\lambda}}$ is substituted for $L_{lowtran_{T,\Delta\lambda}}$ in equation (24). The slope of the resulting linear relation is τ, and the intercept is the L_u. The LOWTRAN model was run in both a spectrally modified and unmodified mode.

<u>Primary ground-truth targets</u>. As a check on the atmospheric calibration methods, the predicted primary ground-truth radiances derived from the thermograms were regressed against the corresponding thermistor ground-truth radiances, as at Figure 21, (c.f. Appendix D for data). This is a simple calibration method adapted from Scarpace[33] and illustrates the degree of data correlation. The results of Appendix H indicate that a correction factor is needed if a perfect one-to-one correlation is to be realized. Atmosphere parameters τ and L_u were calculated from this relation for each altitude data set. The value of τ varied inversely with altitude, and L_u varied as some direct function of altitude. This trend indicated high confidence in the trend of the

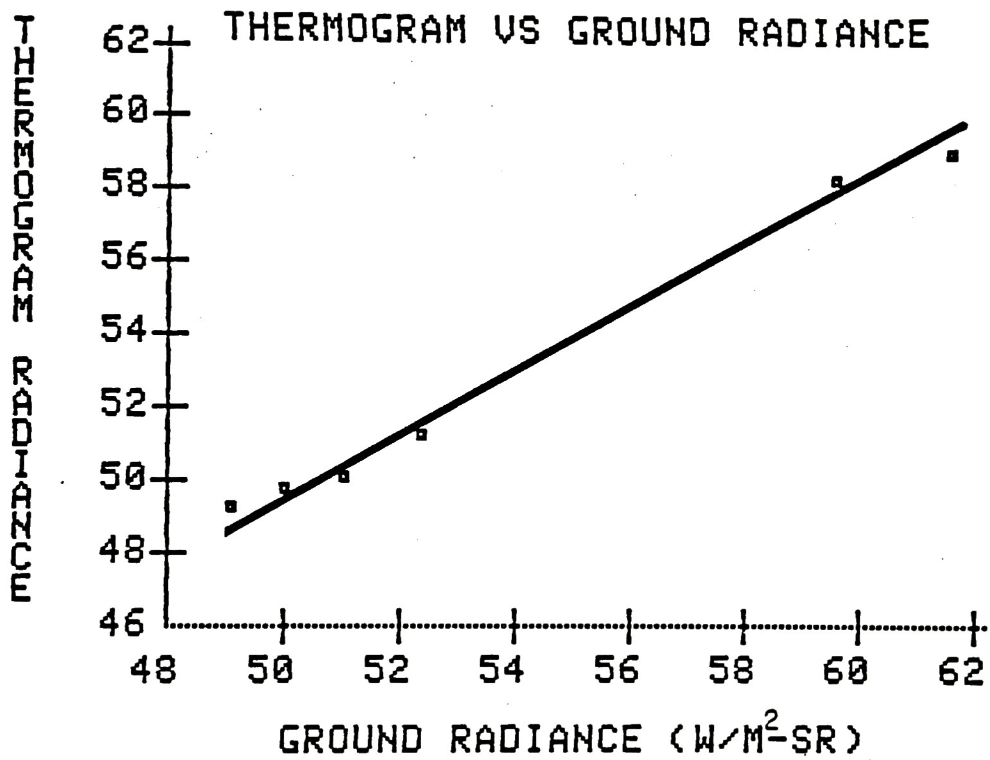

Figure 21. 1000-Foot Altitude Thermogram Versus Thermistor Derived Radiances for Primary Ground-Truth Features.

atmospheric calibration results, but the poor temperature discrimination, i.e. flat curves, and the R.M.S. errors noted in Figure 16 lend credibility only to the 1000-foot altitude data set. Subsequently, the 1000-foot results were used in establishing new ground-truth temperatures for this study, as earlier described.

Atmospheric calibration parameters. The atmospheric-path radiances and transmittances calculated by each atmospheric calibration method are summarized at Table 3 and graphically represented for comparison purposes at Figures 22 and 23, respectively.

Ground Temperature Prediction

At Table 4 and Figure 24, are detailed the R.M.S. temperature errors resulting from the comparison of the new ground-truth temperature data to the corresponding observed ground temperatures generated from the thermograms. These experimental R.M.S. errors, with the exception of the Angular error results for altitudes greater than 1000 feet, are of the same relative magnitude as those predicted in the error propagation study of Appendix I. A significant altitude dependence is noted only with the Angular calibration results.

The error in the primary and new ground-truth temperature measurements were established at 0.16°C and 0.58°C, respectively, (c.f. Field Measurements, and Appendix H). Use of equation (21) for the 1000 foot data and equation (22) for all other altitudes, resulted in the ground temperature prediction errors listed at Table 5. These ground temperature errors with ground-truth determination errors removed differ from the observed temperature errors of Table 4 by less than 0.1°C. This

Table 3. Atmospheric-Path Radiance and Transmittance as Determined by Atmospheric Calibration Techniques.

Transmittance

Altitude (ft)	Angular	Profile (note 1)	Profile (note 2)	Lowtran	Lowtran (note 3)
1000	0.8143	0.9062	0.8757	0.8974	0.9045
2000	0.7835	0.8651	0.8125	0.8534	0.8592
4000	0.7396	0.8157	0.7618	0.7973	0.8006
6000	0.7459	0.7944	0.7461	0.7699	0.7721

Radiance, $L_u \times 10^{-4}$

1000	9.961	14.424	5.974	5.168	4.793
2000	12.928	6.249	8.884	7.225	6.905
4000	16.101	8.331	11.075	9.622	9.473
6000	16.158	9.135	11.580	10.615	10.563

Note 1. Analysis of data by an independent agent.

Note 2. Analysis of data using least squares regression.

Note 3. Lowtran results spectrally corrected for thermal mapper optics.

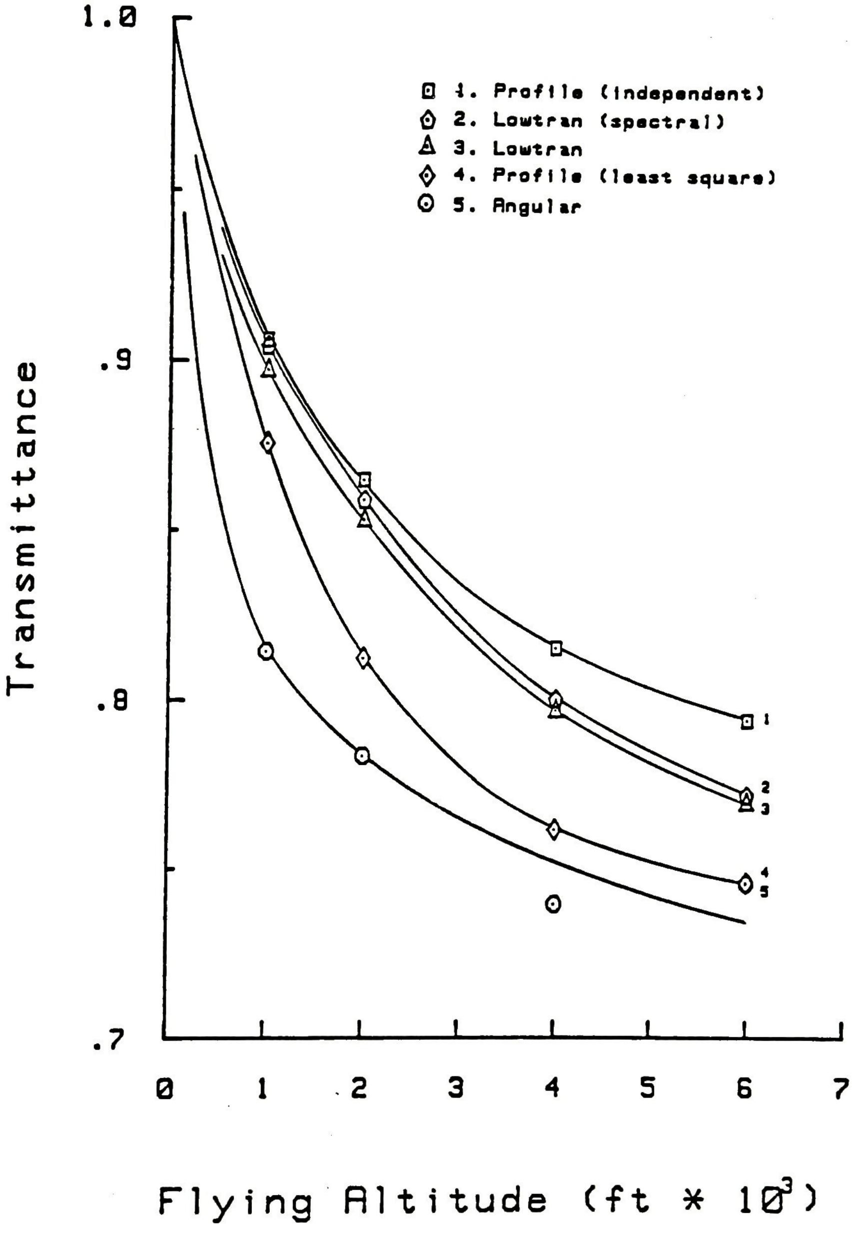

Figure 22. Atmospheric-Path Transmission Profiles. Error in Angular and Profile Calibration Techniques is 1.6% and 1.0%, respectively.

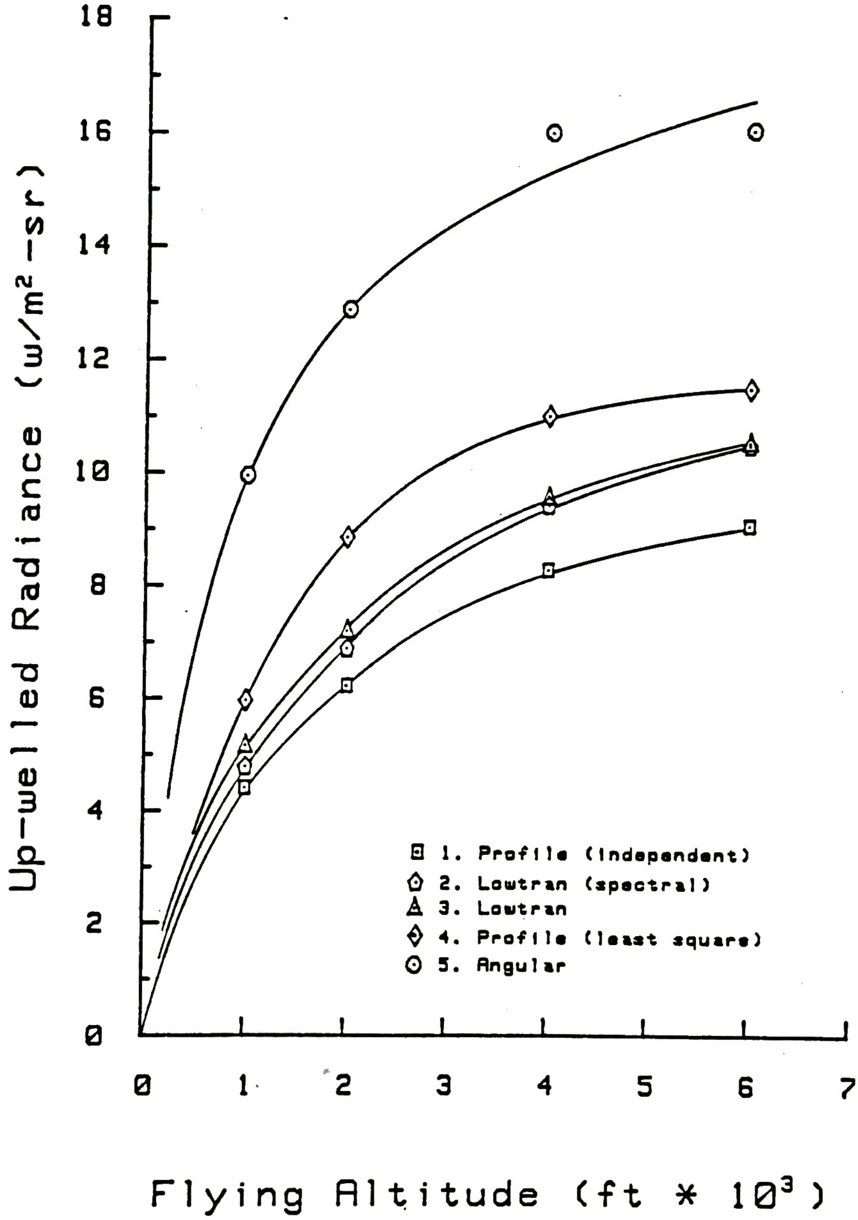

Figure 23. Atmospheric-Path Upwelled Radiance Profiles. Error in Angular and Profile Calibration Techniques is 3.2% and 3.0%, respectively.

Table 4. R.M.S. Errors in Ground Temperature Predictions for New Ground-Truth Data.

Altitude (ft)	Angular	Profile (note 1)	Profile (note 2)	Lowtran	Lowtran (note 3)
1000 (note 4)	1.026	0.711	0.704	0.643	0.680
2000	3.547	0.776	1.144	0.904	0.892
4000	5.202	1.330	1.963	1.181	1.136
6000	6.871	1.541	2.055	1.601	1.548

Note 1. Analysis of data by an independent agent.

Note 2. Analysis of data using least squares regression.

Note 3. Lowtran results spectrally corrected for thermal mapper optics.

Note 4. 1000 foot data from primary ground reference analysis (c.f. Table 2).

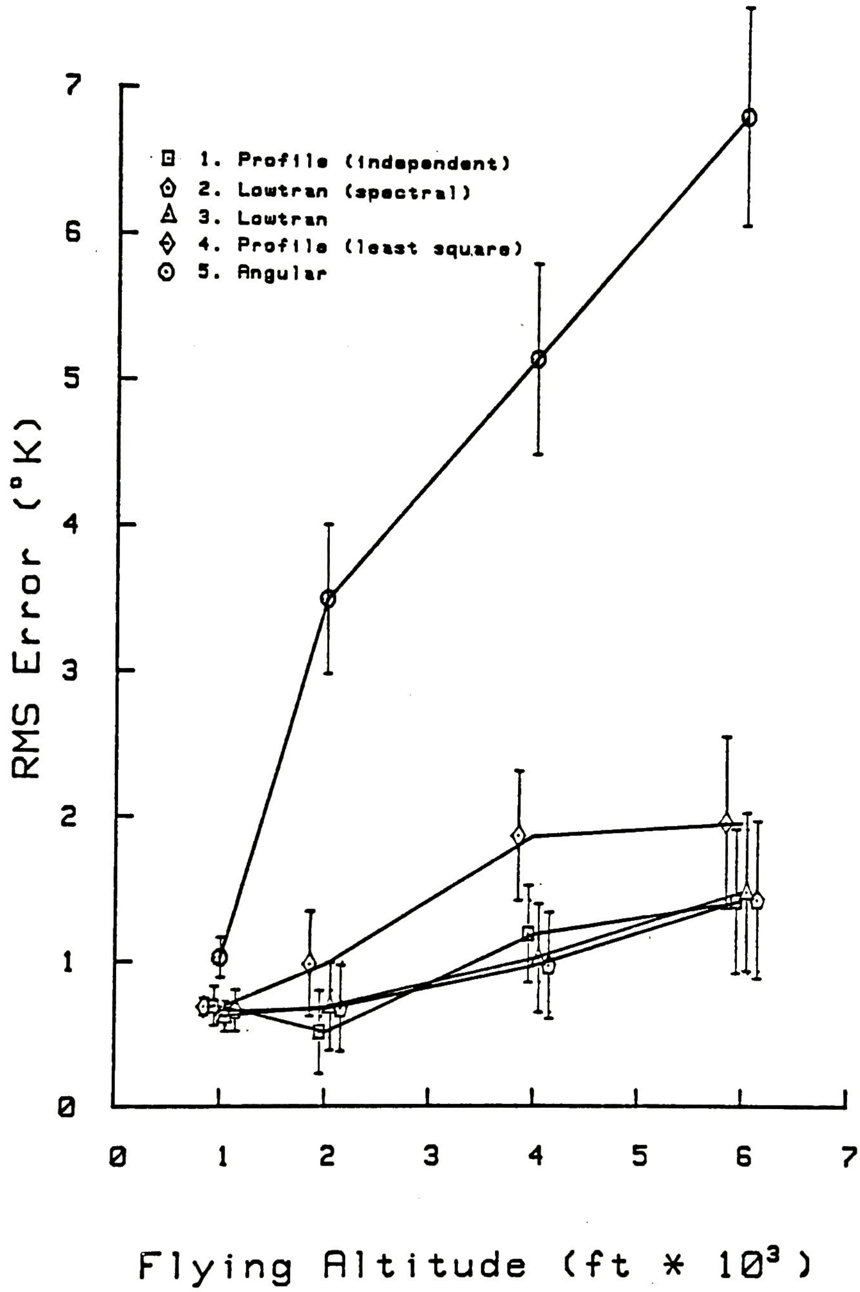

Figure 24. R.M.S. Error in Predicted Ground Temperature for New Ground-Truth Features. One-sigma error bars are indicated.

Table 5. R.M.S. Errors in Ground Temperature Prediction for New Ground-Truth Features, with Ground-Truth Error Removed.

Altitude (ft)	Angular	Profile (note 1)	Profile (note 2)	Lowtran	Lowtran (note 3)
1000 (note 4)	1.031	0.693	0.686	0.623	0.661
2000	3.499	0.512	0.984	0.691	0.675
4000	5.169	1.195	1.874	1.027	0.975
6000	6.846	1.426	1.971	1.491	1.434

Note 1. Analysis of data by an independent agent.

Note 2. Analysis of data using least squares regression.

Note 3. Lowtran results spectrally corrected for thermal mapper optics.

Note 4. 1000 foot data from primary ground reference analysis (c.f. Table 2).

high degree of correlation is evidence that the variability in the imaging system calibration process represents an insignificant error source in this study.

DISCUSSION

Calibration of Instruments

The calibration of equipment was conducted very meticulously and was considered successful. The correlation coefficients of the ensuing relationships were very high and the coefficients of regression fit were very small.

Thermistors. The exercise of calibrating thermistors was repeated three times, each measurement being replicated four times for each of the four thermistors. Each calibration yielded a thermistor response curve which was identical to that of the others, to 99% confidence. The calculated precision of this calibration was ±0.16°C. The sensitivity of the thermistors was observed to be ±0.01 kohms, which is equivalent to ±0.01°C. This observation correlates well with the calculated precision.

Thermal Mapper. Dual water baths of different temperatures were employed in this calibration process. The water bath temperatures were measured using the thermistors calibrated above. A total of 50 measurement sets were taken to establish the system gain and blackbody temperature calibration for the ranges indicated in Appendix C. The vernier potentiometers of the scanner made for high confidence in the repeatability of control settings. This calibration process involved measurements of scanner output-voltage, water bath temperatures, and film densities. The precision of the gain calibration was found to be

0.269°C/volt, and the precision on the blackbody calibration was set at 0.112°C. When this variability is applied to the temperature defining relation at equation (17), a temperature determination error of about 0.5°C is expected.

Field Measurements

Weather. The weather on the day of the field operation was clear, with winds from the NNW. Wind speeds of 17 mph were recorded at the start of the data collection and decreased to 5 mph upon completion of the field work. The ground air temperature was 68°F. This data was collected at the Coast Guard Station situated at the data collection site.

Radiosonde atmosphere data. This data was collected at the Buffalo weather station at 6 a.m. local time. This was some 4.5 hours prior to the field operation at Rochester some 70 miles away. The radiosonde atmosphere temperature profile (c.f. Figure 18) indicates that a negligible thermal inversion existed prior to the field operation, and in all likelihood, the atmosphere was characterised by a linear temperature profile during the data collection process. The fact that the radiosonde data was collected a large distance from the experiment site introduces uncertainty into the analysis involving LOWTRAN atmosphere modelling. The two sites are, however, similar in being located adjacent to large bodies of water which could influence the atmosphere character in similar ways.

Water surface temperature. The gusting winds created swells on the lake up to six feet in height making surface temperature measurement difficult. It was a lake swell which soaked the PRT-5 radiometer rendering it unserviceable. The thermistors were attached to the underside of a styrofoam slab which placed the thermistors slightly under the water surface. The wave action churned the water sufficiently that a thermal gradient across the surface layer, due to evaporative cooling,[54] was less likely to exist. Hence, the measured temperatures at the depth of the thermistors was most probably a good representation of the surface temperature. The average standard deviation of these thermistor readings was very small at 0.13°C.

Thermal mapper. The serviceability record of the recording devices used in conjunction with the thermal mapper was very poor. The onboard filmwriter and tape recorder functioned only one of two times, and the tape recorder only recorded one of the two required signals when it did operate. The scanner itself functioned flawlessly. The two sorties in this study were both late on the target due to aircraft and scanner system unserviceabilities, but these problems were quickly rectified by the experienced scanner operator. Since the scanner was already installed in the aircraft prior to the experiment and removal is a major task, it was not removed for calibration until after the missions were completed. It was assumed that the scanner calibration did not shift in the time between the first mission and when the system was calibrated in the laboratory.

Thermogram Analysis for Atmosphere Calibration

Thermogram generation. The transfer to film of the tape recorded scanner output-signal was facilitated with a Visicorder oscillograph.

Several attempts were necessary to generate an acceptable thermal image for each of the 10 frames, or passes of the aircraft. Each frame was characterised by a unique, but very similar, sensitometric curve. These multitude of sensi-curves were corrected to the sensi-curve of the reference V-D stepwedge.

V-D stepwedge. Generation of the reference voltage-density step wedge was accomplished by recording the scanner output step-voltage onto tape, and writing that signal onto film under identical conditions as that for the thermogram writing process.

An anomaly was identified in the shoulder region of the V-D curve; hence, only data which fell within the linear portion of the curve were used in the study.

Thermogram densitometry. The Roscoe II analog densitometer, equipped with a 150 μm fibre-optic probe, was used to analyse the thermograms. This densitometer was calibrated within the noise level of density measurements, i.e. 0.01 D, to a confidence level greater than 99%. The variability in the density of the blackbody stripe situated on the edge of the thermograms was found to be ± 0.009 D, well within the system noise level. The temperature discrimination of the thermogram ranged from 0.41°C/0.01 D near the shoulder of the D-Log E curve,[49] and 0.12°C/0.01 D in the toe region. These indicate the best temperature discrimination that can be realized if errors due to calibration drift and probe position are minimal. The densitometer did require occasional readjustment, and the marginally workable higher altitude images coupled with the inherent reduced scale made probe positioning a serious concern. Target identification was enhanced by correlating film position to a 1":200' scale orthophoto map. But even on the 4000 and 6000-foot altitude thermograms, it was difficult to be absolutely certain about target identification.

The nadir,[17] or flight line projected to ground, was established from the center line of the thermograms and transferred to the map. All but the 6000-foot altitude flight lines were parallel.

Atmosphere calibration results. The altitude dependence of the atmospheric-path transmission and radiance illustrated in Figures 22 and 23, respectively, indicate a consistent data trend. There is an inverse order of the L_u and τ altitude dependencies, as would be predicted, i.e. greater path transmission implies less path radiance, and vice versa. The calibration lines do not cross one another and exhibit smooth trends except for the Angular results. This anomoly will be dealt with under a discussion of that technique.

Profile calibration. Few identical ground features were imaged along the nadir lines at all altitudes. The nine satisfactory targets represented a predicted ground temperature spread of 15°C which is adequate for an atmospheric calibration. Systematic error was evident in generating the target temperature profiles in that every target of each altitude is characterised with a positive or negative displacement from the least squares regressed curve. The R.M.S. temperature displacement ranges from 0.7°C at 1000-foot altitude to 0.4°C at 6000-foot altitude. This variability could have its origins in a multitude of factors, but the most significant includes the variability of the exposure and chemical processing of each thermogram, and the ability to predict thermogram feature temperatures being constrained by experimental limitations of temperature discrimination, i.e. 0.4°C/0.01 density units. Also, mapping of the temperature distribution of the thermal plume took the better part of an hour to complete, during which time the plume may have changed.[12]

Using new ground-truth targets, the regression, as at Figure 8, of thermogram observed radiances versus apparent ground radiances for each altitude, in the determination of τ and L_u, were well correlated. Correlation coefficients greater than 0.999 and standard deviations of regression fit less than 0.20°C were realized. The derived values of τ and L_u followed the expected dependence on altitude.

This calibration was performed by an independent agent using these study results for observed target radiance. Similar Profile calibration regressions, as at Figure 32, but with a more conservative ground cusp, were predicted. The calibration results were also similar in trend but yielding greater transmissions and reciprocally lower path radiance values.

The R.M.S. errors in ground temperature prediction, for both Profile calibration trials, were essentially identical at 0.7°C at 1000-foot altitude. The errors of the independent agent were marginally smaller at the higher altitudes by a consistent 0.5°C. This departure of precision most likely reflects in the greater experience of the independent agent in the application of the Profile calibration technique.

<u>Angular calibration</u>. This analysis proved to be the most difficult. It required the greatest amount of density data and so took much more time. Several drawbacks cited below are an expected major

source of error in this technique. The scanner was flown in an east-west arrangement over the experiment site with the blackbody stripe being imaged on the north side of the thermogram. It was intended to use the same nadir line data set as used by the Profile calibration so as to minimize system errors, but the ground distance between same-altitude flight line pairs was too great to permit viewing of the north flight line from the complementary south thermogram. This occurred because the scanner blackbody occupied 10° of view to the north and obstructed this view. Consequently, the south flight lines of each altitude were used in the calibration process. Each altitude employed a different set of ground density data, and each line of targets is displaced from the Profile nadir line, located at the shoreline, by a distance equivalent to its altitude. In this approach, one of the four nadir lines required a site familiarization before data could confidently be extracted. A further tribulation of this analysis was a lack of suitable inland targets on the higher altitude thermograms. This was exacerbated by the narrow strip of urban development being concentrated only along the Lake Ontario shoreline with farmland and highways being the main features along nadir lines of high altitude thermograms.

Regression of vertical density data versus offset density data yielded a linear relation with high correlation for all altitudes. A similar regression of the corresponding radiances yielded a linear relation only for densities less than 1.85 D. A pronounced falloff, as illustrated at Figure 25, was typical. The vertical densities, and radiances, registered higher than the V-D reference curve indicated were

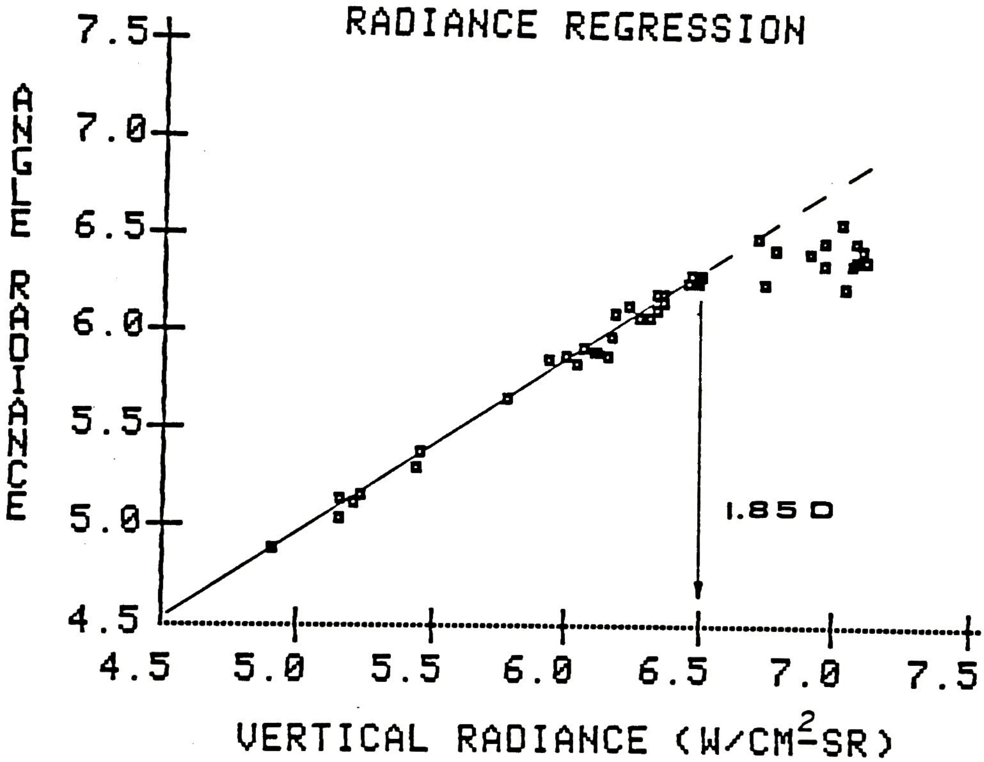

Figure 25. Offset Radiance Versus Vertical Radiance for Angular Calibration Technique Illustrating Non-linearity of Regression Above Equivalent Film Density of 1.85 D.

possible. As the validity of the upper portion of the V-D curve remains in doubt, all density values above 1.85 D were discarded.

The range of target densities spanned the full range of the valid V-D curve and enabled good regression results (c.f. Figure 12). Correlation coefficients for all altitudes were greater than 0.98, and standard deviations of fit less than 0.7°C resulted, except for the 4000-foot data, where a value of 1.2°C resulted. This last anomoly could explain the out-of-form path transmission and radiance results at 4000 feet (c.f. Figure 22 & 23).

Predictions of ground temperature for the 1000-foot data resulted in R.M.S. errors consistent with those of the other calibration results, within the variability of the error.

<u>LOWTRAN</u>. The spectrally corrected LOWTRAN values for τ were greater than those of the spectrally uncorrected results, as expected. This can be seen by considering the spectral windows used in each LOWTRAN atmosphere model; the uncorrected window is a rectangle function of unity height, and the spectrally corrected window is as per Figure 20. When the atmosphere absorption profile (c.f. Figure 27) is superimposed on the LOWTRAN spectral windows, it is obvious that a higher percentage of the spectrally corrected LOWTRAN window overlaps the atmosphere window than does the uncorrected rectangle window. This gives the perception of increased transmission and is reflected in the magnitude of the τ values.

The calculation of the path radiance is consistent with the inverse relation between τ and L_u.

The R.M.S. errors resulting from both LOWTRAN approaches to atmospheric calibration rival the results of the independent Profile calibration at all altitudes. The difference in errors is within 0.15°C. These favourable results must be considered within the limitations of the technique. The radiosonde data, and the spectral response function are all that are needed as inputs to calibrate the atmosphere. If the radiosonde data accurately reflects the atmosphere at the experiment site, then good results can be expected as noted in this study. The assumption of applicable radiosonde data is not always valid and must be guarded against. Radiosonde data taken at Buffalo, New York, 70 miles from the experiment site at Rochester, New York, was used yielding good results. Both Buffalo and Rochester weather are strongly influenced by the Great Lakes. By contrast, the radiosonde data from Albany, New York, which is 290 miles from Rochester and much less influenced by the Great Lakes, was found to be appreciably different in comparison to the Buffalo radiosonde data. The best guarantees when using the LOWTRAN calibration method is to have radiosonde data taken coincidently at, or very near, the experiment site.

Ground-Truth Target Temperature Analysis

Primary ground-truth targets. The process of making density measurements of those ground features where thermistor measurements were made was complicated by the fact that thermistor readings were taken very close to the shoreline. This made proper placement of the densitometer probe very difficult, particularly at the higher altitudes, and required trade-offs of several factors. First, poor image contrast and quality necessitated placing the densitometer probe farther out into the water body so as not to include landform densities. The densities farther out into the water body were found to vary from the shore density. Also, the scale of the thermogram directly effects how much ground feature the density probe sees. For example, the probe covers 36 times more ground area on the 6000-foot thermogram than on the 1000-foot thermogram. And, assuming a non-homogeneous temperature distribution on the lake surface as in thermal plume, it is obvious that apparent ground radiance derived from thermograms is a function of the densitometer probe spot size.

Primary ground-truth temperature prediction. The compromises in taking ground-truth target densities point to systematic errors in the prediction of these ground temperatures. This hypothesis was clearly borne out in the ensuing temperature predictions. A trend of increasing temperature error, as a function of altitude, is illustrated in Figure 16. At 1000-foot altitude, these results indicate good prediction within about 1°C for all calibration techniques which is within the predicted experimental error. The trend of increased error with altitude was also evident in the regression results of thermogram predicted radiances versus primary ground-truth radiances for single altitudes, (c.f. Figure 21). This led to establishing a new set of ground-truth data that was based on the 1000-foot altitude data of the primary ground-truth data.

New ground-truth temperature prediction. The premise of this study is that ground temperatures can be predicted with precision, given a calibrated thermogram.[44] Accepting this precept, the previous results of ground-truth temperature predictions should enable reasonable predictions of other ground target temperatures, for purposes of generating new ground-truth data. This new ground-truth data consisted of large ground features of uniform temperature which were recorded on all thermograms. The ground temperatures of these features were predicted by application of Scarpace's calibration method,[33] (c.f. Appendix H), as applied to the 1000-foot altitude primary ground-truth data set. The L_u and τ values generated from the Scarpace analysis of 1000-foot primary ground-truth data were used in this process as earlier described. This procedure yielded expected R.M.S. errors in the new ground-truth data of approximately 0.5°C.

The ground temperature prediction process, for each atmosphere calibration technique, using the 2000-foot to 6000-foot altitude observed radiances of the new ground-truth data set, yielded optimistic results when compared to the previous analysis. Only the results of the Angular calibration maintained the prominent rising trend in R.M.S. error as a function of altitude as previously seen, i.e. 6°C/5000 feet. Contrasted to this, the other calibration techniques produced a very slight altitude dependence in the R.M.S. error of 1°C/5000 feet.

Summary

Results. This study shows that the Profile, and LOWTRAN calibration techniques yield comparatively good results at all altitudes. The Profile results are consistent with operator experience, and the LOWTRAN spectrally corrected approach yields slightly better results than the uncorrected LOWTRAN approach. The 1000-foot altitude results for the

Angular calibration are the same as that predicted for the other calibration techniques, within variability of the errors. This is consistent with the comparisons reported by Macleod even though night-time TIR imagery was used in his study.[20] The higher altitude Angular results reflect much greater error and indicate an altitude dependency. The poor image quality at these altitudes is an obvious culprit in this regard, but another factor to consider is the different thermal inertias of ground-truth features[10,11] coupled with diurnal effect.[11,17] Also, the assumption of Lambertian surface character[48] is not necessarily valid for all the ground-truth features at all view angles. These factors were not quantified in this study.

Ease of use. The LOWTRAN calibration of the atmosphere is the simplest of all evaluated in this study. Radiosonde data obtained from the weather service is input to the LOWTRAN5A atmosphere computer model. The required atmospheric-path parameters are outputs. In the case of spectrally corrected LOWTRAN, the output is modified by the spectral response function of the thermal mapper optics.

The Profile calibration technique is the next simplest approach and requires a modest amount of work to extract thermogram data. A minimum amount of experience with the technique and some scientific insight are prerequisites to realize satisfactory results.

The Angular calibration method required an extensive amount of work to extract thermogram data and it is the least favoured for this reason. By contrast, however, it does not require the scientific insight needed to execute a Profile calibration and could effectively be carried out by those less knowledgeable in the discipline.

Feasibility. Equipment, information, and personnel resources will be prevailing considerations in the selection of an atmosphere calibration technique. Hence, there is no winner, per se, since all methods are limited in their scope and application.

The Profile method requires multiple passes over the same site area. This is expensive, time consuming, and impractical for denied access areas. Where this is of little concern, the lower the final altitude the more precise the results. This is feasible over water where altitude restrictions are less stringent than over land.

The Angular technique requires paired, parallel passes over the site of interest. Compared to the Profile method, this represents a significant reduction in flight time over the site. Again, this has limited application for denied access areas.

The atmosphere calibration via the LOWTRAN approach is effectively divorced from the flying element of aerial thermography operations. A single pass of the thermal mapper over the target site is needed simply for collection of target data. This single pass concept then is the least expensive in respect of flight time, and has potential for denied access areas if radiosonde data of the target site, or its equivalent, can be obtained.

Application. All the atmosphere calibration methods can be employed for virtually any scenario. The Profile method has been demonstrated to be most satisfactory for the study of water surfaces because the thermal mapper is flown very close to the water surface, and this has been used to advantage to successfully calibrate satellite imagery. For terrestrial bodies, such as urban and industrial areas, the Angular technique could be viable, if only for safety reasons with respect to the Profile method. The LOWTRAN method would be ideal for all scenarios if satisfactory radiosonde data were available. The calibration of satellite imagery is a case in point, wherein the satellite may overfly a radiosonde station which can be underflown coincidently with a low altitude thermal mapper.[38] This concept can be extended to analysis of satellite imagery of denied access regions.[42]

CONCLUSIONS

A coefficient for atmospheric-path radiance, which accounts for the increased path length due to acute viewing angles, has been derived and shown to be effectively equivalent to that derived by Schott.[41] The derivation of these coefficients is based on a layered, non-homogeneous atmosphere. This is a marked improvement over the Lambert-Cosine law coefficient[20] which assumes a homogeneous atmosphere.

The experimental results of this study indicate that the field evaluation of the Angular atmospheric calibration technique was a success at 1000-foot altitude. Ground temperatures were predicted consistent with those of other atmospheric calibration techniques, within variability of the error. The experimental results of the Angular calibration method, for altitudes 2000 to 6000 feet, indicate a pronounced altitude dependence in the errors of ground temperature prediction.

The experimental results also indicate that an order of merit, based on performance in ground temperature predictions with regard to experimental error, should be assigned as follows:

1. spectrally corrected and uncorrected LOWTRAN,
2. Profile, and
3. Angular.

Each atmospheric calibration method evaluated in this study has inherent limitations which must be considered when selecting one technique over another.

RECOMMENDATIONS

The objectives of this study were not fully achievable due to the geometric infidelities in the thermograms at altitudes greater than 1000 feet. This factor could very well have been the bane of the Angular atmospheric calibration technique, hence, this study should be repeated using non-distorted thermograms. Additionally, efforts should be made to quantify the Lambertian and thermal inertia character of the ground-truth features.

The very promising results obtained in this study using the LOWTRAN atmospheric calibration method indicates that further study into the limitations of this approach is warranted.

BIBLIOGRAPHY

1. Y. Beers, Introduction to the Theory of Errors, Addison-Wesley Publishing Co., Cambridge, Mass., 1953.

2. E.E. Bell, et al., "Spectral Radiance of Sky and Terrain at Wavelengths Between 1 and 20 Microns. II. Sky Measurements", Journal of the Optical Society of America, 50, 1313-1320 (1960).

3. A. Ben-Shalom, et al., "Spectral Characteristics of Infrared Transmittance of the Atmosphere in the Region 2.8-14 Microns--Preliminary Measurements", Infrared Physics, 20, 165-174 (1980).

4. K.J.K. Buettner and C.D. Kern, "Determination of Infrared Emissivities of Terrestrial Surfaces", Journal of Geophysics Research, 70, 1329-1337 (1965).

5. K.K. Castleman, Digital Image Processing, Prentice-Hall, New Jersey, 1979, pp. 68-83.

6. J. Cataldo, Report to NYSER&DA, "Infrared Water Temperature Measurements Performed by Wormser Scientific Corp. for NY State Energy Research and Development Authority", 1976.

7. J. Cataldo, personal communication, "Thermal Front Survey", Sept. 14, 1978.

8. R.M. Chapman, et al., Ohio State University Research Foundation Report No. cnW44-099eng.400, "Atmospheric Transmission of Infrared--Summary Report", 1949.

9. A Chedin, et al., "A Single-Channel, Double-Viewing Angle Method for Sea Surface Temperature Determination from Coincident METEOSAT and TIROS-N Radiometric Measurements", Journal of Applied Metereology, 21, 613-618 (1982).

10. R. Colwell, ed., Manual of Remote Sensing, 2nd Ed., American Society of Photogrammetry, Virg., 1983.

11. L. Eisner, et al., "Spectral Radiance of Sky and Terrain at Wavelengths Between 1 and 20 Microns. III. Terrain Measurements", Journal of the Optical Society of America, 52, 201-209 (1962).

12. T. Green, et al., "Types of Thermal Plumes in Coastal Waters", Water Research, 11, 123-125 (1977).

13. G. Gubarov, et al., Thermal Radiation Properties Survey, Honeywell Research Center, Minn., 1960, Ch. 3.

14. R.B. Haynes and J. Whipple, Technical Memo No. RADC/IR/TM-71-2, "Problems in Applying Infrared Reconnaissance Technology to Water Temperature Surveillance", 1971.

15. R.D. Hudson, Infrared System Engineering, John Wiley & Sons, New York, 1969.

16. V. Leeman, Report No. NASA-CR-115757, "The NASA Earth Resources Spectral Information System--A Data Compilation", 1971.

17. T.M. Lillesand and R.W. Kiefer, Remote Sensing and Image Interpretation, John Wiley & Sons, New York, 1979, Ch. 7.

18. R.W. Longley, Elements of Meteorology, John Wiley & Sons, New York, 1970, pp. 27-32.

19. D. Lorenz, "Temperature Measurements of Natural Surfaces Using Infrared Radiometers", Applied Optics, 7, 1705-1710 (1968).

20. I.D. Macleod, An Airbone Thermal Remote Sensing Calibration Technique, M.S. Thesis, Rochester Institute of Technology, Rochester, NY, 1983.

21. R.A. McClatchey, et al., Report No. AFGL-72-0497, "Optical Properties of the Atmosphere", 3rd Ed., 1972.

22. L.M. McMillen, "Estimation of Sea Surface Temperatures From Two Infrared Window Measurements With Different Absorption", Journal of Geophysical Research, 80, 5113-5117 (1975).

23. O.W. Mintzer, et al., "Measuring Heat Loss from Flat Roof Buildings with Calibrated Thermography", Photogrammetric Engineering and Remote Sensing, 49, 777-788 (1983).

24. K. Piech and J.R. Schott, "Atmospheric Corrections for Satellite Water Quality Studies", Proceedings of SPIE, 51, San diego, 1974.

25. C. Prabhakara, et al., "Estimation of Sea Surface Temperature from Remote Sensing in the 11-13 Micron Window Region", Journal of Geophysical Research, 79, 5039-5044 (1974).

26. Kaplan, "Thermosense I, Thermal Infrared Sensing Technology in Energy Conservation Programs", Proceedings of the American Society of Photogrammetry, Chattanooga, Tenn., 1978.

27. D.I. Ross, Report of Ministry of the Environment of Ontario, "Evaluation of Airborne Thermal Infrared Mapping of Cooling Water Discharges from Generating Stations", 1976.

28. D.I. Ross and S.E. Franklin, "Current Limitations on Quantitative Airborne Thermography", Proceedings of 8th Canadian Symposium on Remote Sensing, Montreal, Canada, 1983.

29. F.R. Ruckdeschel, BASIC Scientific Subroutines, Vol. I & II, Byte/McGraw-Hill, New York, 1981.

30. P.M. Saunders, "Aerial Measurements of Sea Surface Temperature in the Infrared", Journal of Geophysical Research, 72, 4109-4117 (1967).

31. P.M. Saunders, "Corrections for Airborne Radiation Thermometry", Journal of Geophysical Research, 75, 7596-7601 (1970).

32. F.L. Scarpace and T. Green III, "Dynamic Surface Temperature Structure of Thermal Plumes", Water Resources Research, 9, 138-153 (1973).

33. F.L. Scarpace, et al., "Scanning Thermal Plumes", Photogrammetric Engineering and Remote Sensing, 41, 1223-1231 (1975).

34. J.R. Schott and R.H. Tourin, "A Completely Airborne Calibration of Aerial Infrared Water Temperature Measurements", Proceedings ERIM 10th International Symposium on Remote Sensing of Environments, Ann Arbor, Mich., 1975.

35. J.R. Schott, Calspan Report No. NA-6019-M-1, NTIS#TB-269-471, "Thermal Remote Sensing Calibration Techniques", 1978.

36. J.R. Schott, Calspan Report, "Aerial Infrared Thermal Surveys of Rochester Gas and Electric Power Stations", 1978.

37. J.R. Schott, "Temperature Measurement of Cooling Water Discharged from Power Plants", Photogrammetric Engineering and Remote Sensing, 45, 753-761 (1979).

38. J.R. Schott, et al., Calspan Report No. 6175-M-1, NAS5-24263, "Data Use Investigations for Applications Explorer Mission A (Heat Capacity Mapping Missions)", 1981.

39. J.R. Schott and E. Wilkinson, NYSER&DA Report, "Aerial Measurement of Heat Loss--Phase II", 1982.

40. J.R. Schott and C.B. Kirby, NYSER&DA, USDOE and C.B. Kirby, NYSER&DA, USDOE and Calspan Report, "An Emissivity Measurement Method Suitable for Large Irregular Surfaces", 1983.

41. J.R. Schott, et al., "A Comparison of Techniques for Radiometric Calibration of Aerial Infrared Thermal Images", Proceedings of the Conference on Techniques for Extraction of Information from Remotely Sensed Images, Rochester, NY, 1983.

42. J.R. Schott and J. Biegel, "Comparison of Modelled and Empirical Atmospheric Propagation Data", Proceedings of SPIE 27th Annual International Technical Symposium, San Diego, 1983.

43. J.R. Schott, Naval Research Laboratories Report, "Target and Background Infrared Calculations for Tactical Space-Based Sensor Applications", 1983.

44. J.R. Schott, personal communication, Dec. 1983.

45. M. Shuler, et al., Report No. AFGL-TR-78-0216, "Remote Sensing of Atmospheric Visibility--A Critical Review", 1978.

46. M. Sidran, "Broadband Reflectance and Emissivity of Specular and Rough Water Surfaces", Applied Optics, 20, 3176-3183 (1982).

47. R. Siegel, Thermal Radiation Heat Transfer, 2nd Ed., McGraw-Hill, New York, 1981.

48. P.N. Slater, Remote Sensing--Optics and Optical Systems, Addison-Wesley, Mass., 1980, Ch. 8, 10.

49. W. Thomas, ed., SPSE Handbook of Photographic Science and Engineering, John-Wiley & Sons, New York, 1973, p. 768.

50. C.L. Tien, "Atmospheric Corrections for Airborne Measurements of Water Surface Temperatures", Applied Optics, 13, 1745-1746 (1974).

51. L. Wald, et al., "Reflectance Contrast Observed by Landsat Between a Calm and a Rough Sea", Photogrammetric Engineering and Remote Sensing, 49, 241-242 (1983).

52. M. Weiss, "Airborne Measurements of Earth Surface Temperature (Ocean and Land) in the 10-12 Micron and 8-14 Micron Regions", Applied Optics, 10, 1280-1287 (1971).

53. R.S. Williams, "Thermography", Photogrammetric Engineering and Remote Sensing, 28, 881-883 (1972).

54. W.L. Wolfe and G.J. Zissis, The Infrared Handbook, Environmental Research Institute of Michigan, Michigan, 1978.

55. W.D. Wood, Thermal Radiative Properties, No. 3, Plenum Press, New York, 1964, pp. 4-29.

56. V. Zsilinszky, Report of Ministry of Natural Resources of Ontario, "Ontario Centre for Remote Sensing--Program Review 1980-82", 1982.

APPENDIX A

Thermal Radiation Theory

This appendix is an extraction from several works.[15,20,47,48,54,55] Specifically, it is a description of the development of equations used in the section 'Theoretical Background' in this study.

Theoretical Development of Radiometry Equations

The physics of radiometry can be described in accordance with the precepts of electromagnetic theory. In the case of explaining the energy distribution in the spectrum of a thermal radiator, the concept of a blackbody as a comparison standard is needed. A blackbody is a hypothetical, ideal radiator in that all energy which is incident on it is also reradiated.

Any body having a temperature greater than absolute zero emits radiation of spectral intensity that is a function of the body's material. The spectral radiant emittance of the body can be characterised by a blackbody curve. A family of blackbody curves is illustrated in Figure 26, indicating the shift of energy peak as a function of temperature. The curve at 300°K is of particular concern in studies involving the earth.

The blackbody curves are a representation of Planck's blackbody law which is a function of temperature and wavelength,

$$L_\lambda = \frac{2hc^2\lambda^{-5}}{e^{(ch/\lambda kT)} - 1} \tag{25}$$

where L_λ = spectral radiance, Wcm^{-2} - $s.r.^{-1}$,

λ = wavelength, μm

h = Planck's constant, 6.6256E-34 $Wsec^2$,

T = absolute temperature, °K,

c = velocity of light, 2.997925E10 $cm\text{-}sec^{-1}$,

k = Boltzmann's constant, 1.38054E-23 $Wsec\text{-}°K.^{-1}$

Integration of this equation yields the total radiation at all wavelengths and accounts for all incident flux radiated into a hemisphere above a blackbody of unit area. The resulting equation is known as the Stefan-Boltzmann law,

$$\pi \int_0^\alpha L_\lambda = L = \sigma T^4 \tag{26}$$

where L = radiant emittance, $W\text{-}cm^{-2}$,

σ = Stefan-Boltzmann constant, 5.6697E-12 $Wcm^{-2}\text{-}°K^{-4}$,

and indicates that the total power radiated from a blackbody varies as the fourth power of the absolute temperature.

If Planck's equation is differentiated and the result set to zero, one can determine the wavelength at which the spectral emittance is a maximum and also the amount of spectral radiance, L_λ, at this wavelength. Wein's displacement law gives the wavelength for maximum L_λ as,

$$\lambda_{max} = \frac{2897.8}{T} \ \mu m \tag{27}$$

and L_λ at λ_{max} as:

$$L_{\lambda_{max}} = 1.288E\text{-}15\ T^5 \text{ watt cm}^{-2}\mu m^{-1} \tag{28}$$

Notice that the higher the temperature, the shorter the wavelength at which the peak occurs and that L_λ at the peak varies as the fifth power of the absolute temperature.

To solve for the temperature dependence of L in a specified spectral bandpass, numerical integration via Simpson's rule or blackbody table interpolation can be employed. Greater precision is realized by the numerical approach, but adequate results can be obtained with a finely stepped lookup table. Both approaches are employed in the study reported herein.

Consideration of the real world must be accounted for in the application of radiometry theory. Planck's equation describes a perfect blackbody, one which reradiates all incident energy, but the real world comprises less efficient radiators, i.e. greybodies. An efficiency factor, which is a measure of a body's radiating efficiency when compared to a blackbody, is needed. Emissivity, ε, is such a parameter. Hence, a greybody has an emissivity less than unity and can be described,

$$L = \varepsilon L_T \tag{29}$$

where L = radiant emittance of the body,

ε = emissivity, and

L_T = radiant emittance of a blackbody at the same temperature as the body.

Radiant energy incident upon a surface is characterised by three processes: a fraction, α, of the incident energy may be absorbed, a fraction, ρ, may be reflected, and a fraction, τ, may be transmitted. Since conservation of energy must prevail, the following relation describes this interaction,

$$\alpha + \rho + \tau = 1 \tag{30}$$

By definition, a blackbody absorbs all incident radiant energy such that $\alpha = 1$, and $\rho = \tau = 0$. Kirchoff observed that, for a prescribed temperature, the ratio of radiant emittance of a greybody to the greybody's absorptance was a constant for all materials, and further, that this ratio is equivalent to the radiant emittance of a blackbody at that temperature. This relation is known as Kirchoff's law, expressed hence,

$$\frac{\varepsilon L}{\alpha} = \sigma T^4 \tag{31}$$

Using the Stefan-Boltzmann law,

$$\frac{\varepsilon \sigma T^4}{\alpha} = \sigma T^4 \tag{32}$$

Reducing then,

$$\varepsilon = \alpha \tag{33}$$

This states that the emissivity of any material at a prescribed temperature is numerically equivalent to its absorptance. Extending this concept, since an opaque material does not transmit energy, i.e. $\tau = 0$, therefore,

$$\varepsilon + \rho = 1 \tag{34}$$

This is the character of most terrestrial materials encountered in remote sensing of the earth in the 8-14 μm spectral band.

When viewing the earth, the sensor not only detects terrestrial energy, but also sees energy originating from the atmosphere. The intervening atmosphere is an inhomogeneous and dynamic mixture of gases, vapours, and particulate matter. The constituents of primary concern are water vapour, carbon dioxide, nitrous oxides, and ozone.

The spectral transmission window of the atmosphere within the 8-14 μm band is as shown in Figure 27. This window passes the radiance energy peak associated with terrestrial bodies of 300°K temperature.

Radiant emittance from a ground target is attenuated by material effects, i.e. ε, and by atmosphere effects, i.e. τ. Since the atmospheric-path through which a sensor detects a ground target signal will also emit radiance, then the detected signal will be,

$$L = \tau\varepsilon L_T + L_u \tag{35}$$

where L = observed radiance at the detector,

τ = atmospheric-path transmission,

L_u = atmospheric-path radiance,

ε = target emissivity, and

L_T = blackbody equivalent radiance from target.

Additionally, there is an energy contribution from the sky dome which reflects from the ground target surface. This term is modified by the atmosphere transmission and target reflectivity. Therefore, the total radiant energy seen by the sensor is,

$$L = \tau\varepsilon L_T + \tau R L_d + L_u \tag{36}$$

where L_d = downwelled sky radiance, and

R = target reflectivity.

This completes the derivation of the fundamental equations governing this study and described in the section 'Theoretical Background'.

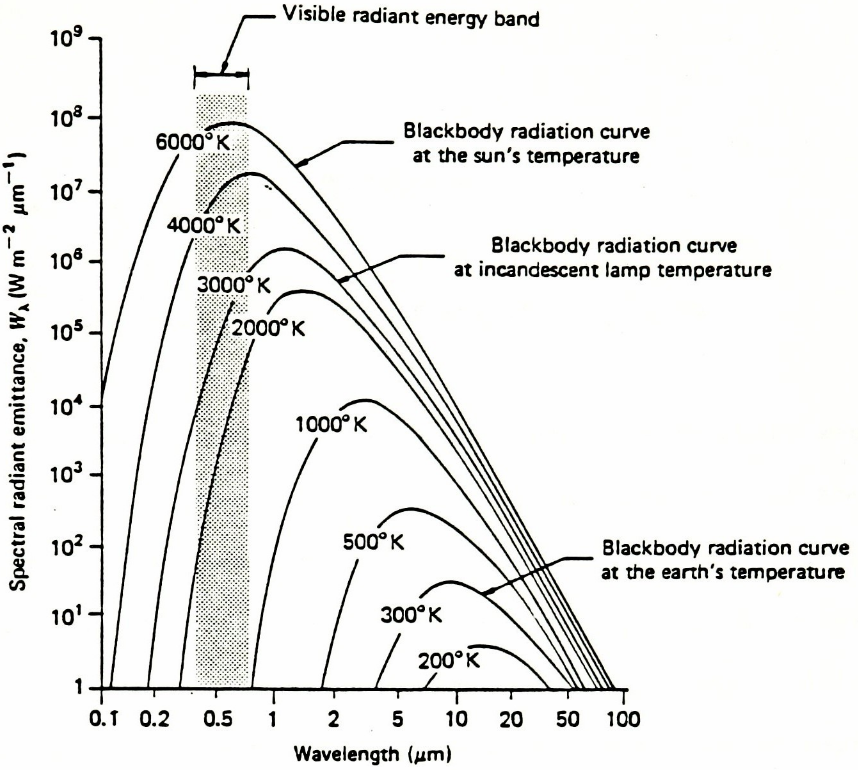

Figure 26. Spectral Distribution of Energy Radiated from Blackbodies of Various Temperatures.

(after Lillesand)

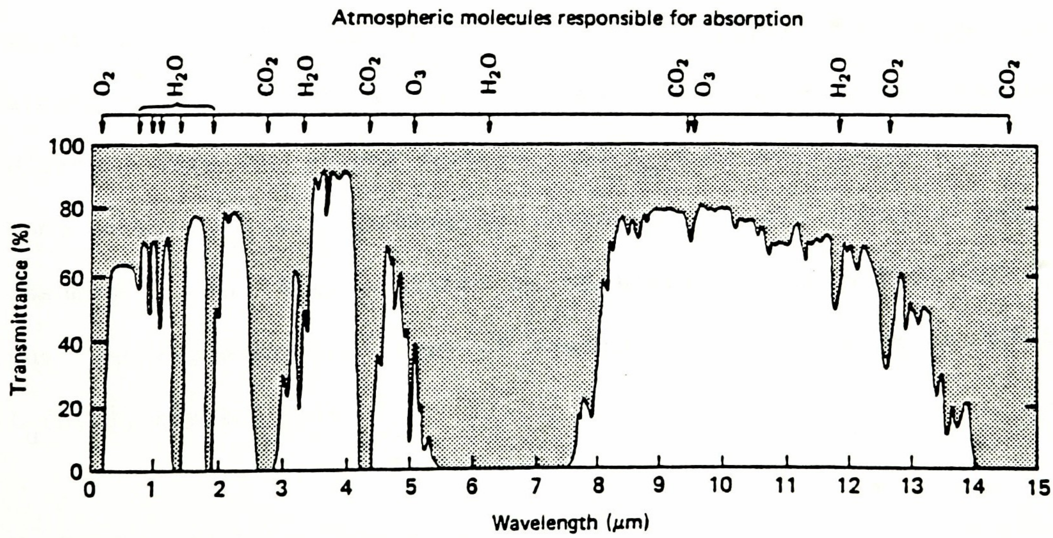

Figure 27. Atmospheric Transmission in the 0 to 15 μm Wavelength Band. Note the atmospheric windows in the 3 to 5 μm and 8 to 14 μm thermal wavelength regions.

(after Lillesand)

APPENDIX B

Upwelled Radiance Coefficient Derivation

Measurement of ground feature thermal radiance requires knowledge of the radiometric character of both the ground feature and the atmosphere separating the sensor and the earth. The radiance reaching the sensor is the sum of these two quantities factored by the atmospheric spectral transmittance. Expressed mathematically, the spectral radiance at the sensor, for a given look angle and altitude, can be expressed:

$$L(H,\theta) = \frac{\tau(h,\theta)\cdot[L_T(H,0) - L_u(H,0)]}{\tau(H,0)} + L_u(H,0)$$

where $L_T(H,0)$ is the ground radiance, $L_u(H,0)$ and $\tau(H,0)$ are the atmospheric-path radiance and transmission, respectively, as observed directly over the ground feature, and $L_u(H,\theta)$ and $\tau(H,\theta)$ are values at some other angle. Lambertian character of the earth's surface is assumed.[48] For this equation to be useful, terms $\tau(H,\theta)$ and $L_u(H,\theta)$ must be expressed in terms of measurable values, such as $\tau(H,0)$ and $L_u(H,0)$, respectively.

Macleod τ and L_u Coefficients

The increased atmospheric-path length due to slanted viewing angles will necessarily decrease transmission by the factor:

$$\tau(h,\theta) = \tau^{\sec(\theta)}(H,0)$$

Reciprocally, the magnitude of the upwelled radiance will be increased. This expected increase has been quantified by some (Macleod, 1983)[20] by application of Lambert's Cosine Law, such that:

$$L_u(H,\theta) = \frac{L_u(H,0)}{\cos(\theta)},$$

and in so doing, are assuming a single layer homogeneous atmosphere. The atmosphere has been shown to be more appropriately modelled as a layered atmosphere, although the Cosine Law is a good first approximation. A more precise result is sought based on the premise of a layered atmosphere.

Schott L_u Coefficient

Use of the atmosphere extinction coefficient, τ_i', will satisfy this problem (Schott, 1983).[41] First, consider a layered atmosphere as depicted in Figure 28, with a thin i^{th} layer at ground level. The transmission for the i^{th} layer is:

$$\tau_i = e^{-\tau_{ext}}$$

$$= e^{-\tau_i'}$$

The ratio of atmospheric-path radiance as seen from directly overhead and at some other angle for 'n' layers of atmosphere is then:

$$\sum_{i=1}^{n} \frac{L_{u_i}(\theta)}{L_{u_i}(0)} = \frac{L_{T_i}[1-\tau_i^{\sec\theta}]\cdot\tau_j^{\sec\theta}}{L_{T_i}[1-\tau_i]\cdot\tau_j}$$

$$= [\frac{1-\tau_i^{\sec\theta}}{1-\tau_i}]\cdot\tau_j^{\sec\theta-1}$$

$$= [\frac{1-e^{-\tau_i'\sec\theta}}{1-e^{-\tau_i}}]\cdot\tau_j^{\sec\theta-1};\quad e^x \cong 1 + x$$

$$= \frac{\tau_i'\sec\theta}{\tau_i'} \cdot \tau_j^{\sec\theta-1}$$

therefore $$\frac{L_u(\theta)}{L_u(0)} = \tau_j^{\sec\theta-1}\cdot\sec\theta$$

or $$L_u(\theta) = L_u(0) \cdot \frac{\tau_j^{\sec\theta-1}}{\cos\theta}$$

Hence, we have the result derived by Schott[41] for upwelled atmospheric-path radiance which is similar to that for the Cosine Law result, but is factored by the transmittance.

Byrnes L_u Coefficient

The author's approach in deriving a coefficient for $L_u(0)$ also assumes a layered atmosphere and as with Schott's approach:

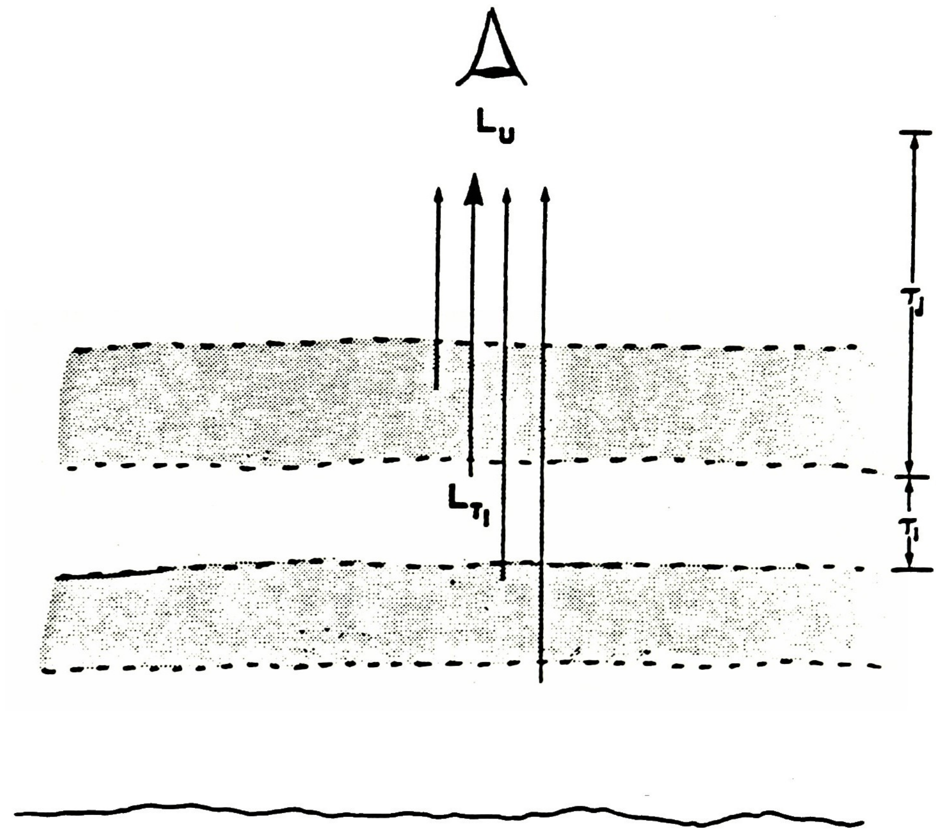

$$L_U = \sum_i L_{\tau_i} \cdot (1-\tau_i) \cdot \tau_j$$

Figure 28. Summation of the Atmosphere Layer Contributions to Upwelled Radiance.

(after Schott)

$$\sum_{i=1}^{n} \frac{L_{u_i}(\theta)}{L_{u_i}(0)} = \left[\frac{1-\tau_i^{\sec\theta}}{1-\tau_i}\right] \cdot \tau_j^{\sec\theta-1}; \qquad a^x \cong 1 + x\log_e a$$

$$\cong \left[\frac{1-(1+\sec\theta\cdot\log_e\tau_i)}{1-\tau_i}\right] \cdot \tau_j^{\sec\theta-1}$$

$$= \left[\frac{\sec\theta\cdot\log_e\tau_i}{\tau_i-1}\right] \cdot \tau_j^{\sec\theta-1}; \qquad \log_e a \cong (a-1) - \tfrac{1}{2}(a-1)^2$$

$$\cong \frac{\sec\theta}{\tau_i-1}\left[(\tau_i-1)-\tfrac{1}{2}(\tau_i-1)^2\right] \cdot \tau_j^{\sec\theta-1}$$

$$= \sec\theta\cdot\left[1 - \frac{\tau_i}{2} + \tfrac{1}{2}\right] \cdot \tau_j^{\sec\theta-1}$$

$$= \frac{3}{2}\sec\theta\cdot\tau_j^{\sec\theta-1} - \frac{\sec\theta}{2}\cdot\tau_i\cdot\tau_j^{\sec\theta-1}$$

When $i = 1$, as in Figure 28, then $\tau_{i=1} = 1$ and $\tau_j \cong \tau(H,0)$. Therefore:

$$\frac{L_u(\theta)}{L_u(0)} \cong \frac{3}{2}\sec\theta\cdot\tau(H,0)^{\sec\theta-1} - \frac{\sec\theta}{2}\cdot\tau(H,0)^{\sec\theta-1}$$

$$= \frac{\tau(H,0)^{\sec\theta-1}}{\cos\theta}$$

Recognize this as that derived by Schott previously.

Also, when $i = n-1$ as in Figure 28, with the j^{th} layer comprising only a thin layer near the sensor, then $\tau_{i=n-1} = \tau(H,0)$ and $\tau_j \cong 1$.

Therefore:

$$\frac{L_u(\theta)}{L_u(0)} = \frac{3}{2}\sec(\theta) - \frac{\sec(\theta)\cdot\tau(H,0)}{2}$$

$$= \frac{\sec(\theta)\cdot[3-\tau(H,0)]}{2}$$

Assuming a homogeneously layered atmosphere over short altitudes to be a reasonable approximation, we will then expect an average of these two limits on the derivation to represent a plausible relation of $L_u(\theta)$ and $L_u(0)$ such that:

$$\frac{L_u(\theta)}{L_{u(0)}} \cong \frac{\dfrac{\tau(H,0)^{\sec\theta-1}}{\cos\theta} + \dfrac{1}{\cos\theta}\cdot\left(\dfrac{3-\tau(H,0)}{2}\right)}{2}$$

$$= \frac{3 + 2\tau(H,0)^{\sec\theta-1} - \tau(H,0)}{4\cos\theta}$$

or

$$L_u(\theta) = L_u(0)\left[\frac{3 + 2\tau(H,0)^{\sec\theta-1} - \tau(H,0)}{4\cos\theta}\right]$$

Summary

Three expressions have been derived for upwelled atmospheric-path radiance for any look angle; two of which assume a layered homogeneous atmosphere. These expressions are plotted at figure 29 for view angles 0 to 90 degrees. The limit of thermal mapper FOV is usually ± 60 degrees. It is evident there is little difference between the two coefficients derived herein for this FOV, but these two are significantly different from the Cosine Law coefficient at angles less than 45 degrees. Schott's coefficient equals the Cosine Law value at 60 degrees.

Since observation angles of less than 40° were employed in this study, Schott's coefficient was used for computational efficiency.

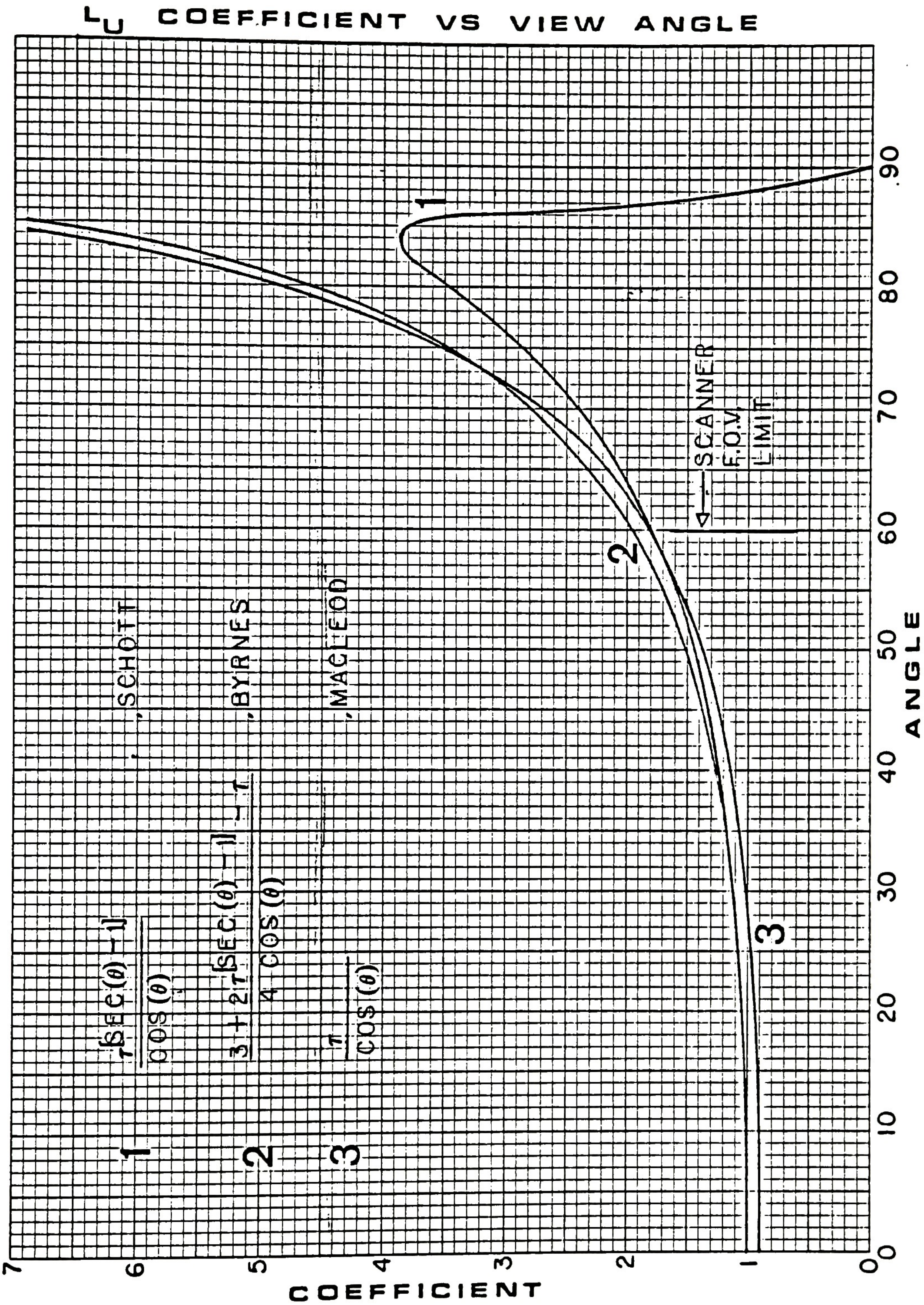

Figure 29. Upwelled Radiance Coefficient Versus View Angle.

APPENDIX C

Calibration of Bendix LN-3 Thermal Mapper

To be able to use the output data of a thermal mapper, the system must first be calibrated for gain, i.e. °C/volt, and blackbody temperature.

The initial step requires establishing the relation between output voltage of the scanner system and the resultant density written onto film. A 0 to 15 volt density step wedge was required to calibrate the Bendix LN-3 mapper since the output signal was being recorded on magnetic tape before being written to film. This relation was produced for the velocity/height (V/H) setting used for data gathering.

With the scanner viewing two thermally stable water baths of different temperature and with a constant blackbody setting, the system gain setting is changed in an ordered fashion. The procedure is repeated for a number of blackbody settings and can be repeated for various water bath temperature differences to improve upon the precision of calibration.

Knowledge of the difference between the water bath temperatures and that of the corresponding densities, and hence voltages, imaged on the film, one is able to establish the system's gain characteristic curve. That determined for this study is at figure 30. Similarly, knowing the temperatures of the water baths will enable finding the system blackbody temperature through densitometric analysis of the water bath images and the adjacent blackbody stripe on the film. The blackbody temperature calibration curve is at figure 31. Neither characteristic curve was found to be linear over the range of control settings.

The mission settings were as follows: Gain = 55, (2.434 °C/volt), and Blackbody = 9-361, (22.15°C).

This calibration data is employed in the following algorithm for determining an unknown temperature, i.e.,

$$V = (T/G) + V_0$$

where V = output voltage, G = gain, T = unknown temperature, and V_0 = initial voltage or the intercept of the response curve.

Using the calibration data, the value of V, or V_{bb}, is obtained densitometrically from the blackbody stripe on the film which is converted through the density-voltage step wedge. Knowing the blackbody temperature, T_{bb}, and the gain, G, then V_0 can be solved, i.e.

$$V_0 = V_{bb} - (T_{bb}/G)$$

Substitution into the equation for an unknown temperature yields:

$$T = (V - V_{bb}) \cdot G + T_{bb}$$

Hence, measurement of the target density, converted to voltage as previously discussed, and then substituted into the above equation will yield the corresponding temperature.

APPENDIX C

Thermal Mapper Blackbody Temperature Calibration

Control Setting	Temperature (average °C)
9-000	14.23
9-100	16.04
9-200	16.99
9-300	19.95
9-400	23.48
9-500	26.48
9-600	30.95

For mission setting of 9-361, T = 22.15°C

System Gain Calibration

Control Setting	Gain (°K/volt)	Control Setting	Gain (°K/volt)
10	21.461	80	2.992
20	11.141	90	2.864
30	8.333	100	2.595
40	6.259	110	2.333
50	4.893	120	1.848
60	4.187	130	1.867
70	3.658	140	1.583

For mission setting of 100, Gain = 2.434°K/volt.

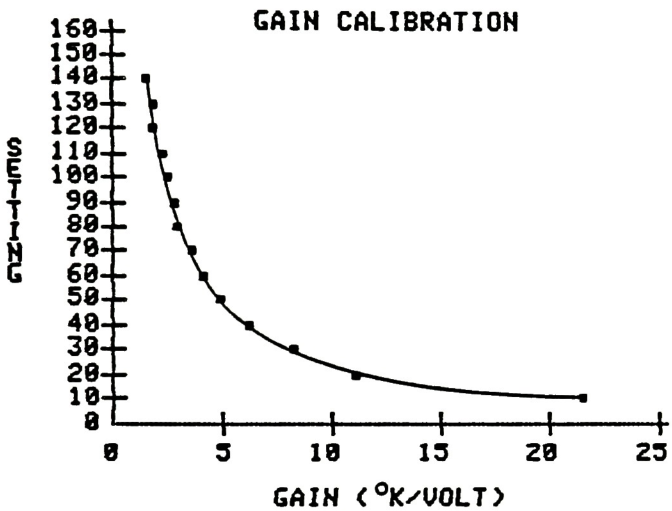

Figure 30. Thermal Mapper Gain Calibration Curve.

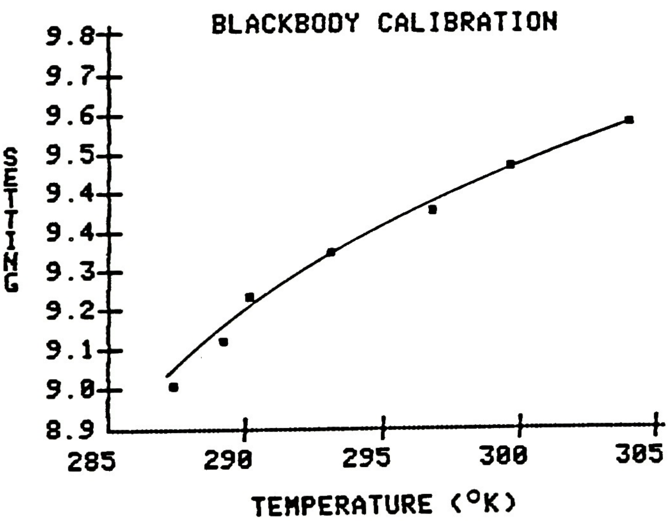

Figure 31. Thermal Mapper Blackbody Calibration Curve.

APPENDIX D

Primary Ground-Truth Radiances-- Thermistor and Thermogram Derived

Thermistor Data

	Target	Temperature (°K) (measured)	Radiance (W/cm^2-s.r.) (calculated)
1.	Lake Ontario west of pond	292.779	4.9076E-3
2.	Lake Ontario east of river	293.965	5.0010E-3
3.	Lake Ontario west of river	295.262	5.1043E-3
4.	Genesee River west pier	296.952	5.2409E-3
5.	Little Pond east bank	305.407	5.9568E-3
6.	Pond Outfall into lake	307.722	6.1624E-3

APPENDIX D (continued)

Thermogram Data

Altitude (ft)	Target	Temperature (°K)	Radiance (W/cm^2-s.r.)	View Angle (degrees)
1000	1	292.971	4.9227E-3	6.8
	2	293.606	4.9727E-3	9.9
	3	294.093	5.0112E-3	33
	4	295.553	5.1278E-3	33
	5	303.960	5.8305E-3	8.5
	6	304.825	5.9058E-3	0
2000	1	293.775	4.986E-3	18.6
	2	293.678	4.9783E-3	16
	3	295.343	5.1109E-3	27.7
	4	296.610	5.2132E3	27.7
	5	304.593	5.8855E-3	11.3
	6	305.337	5.9508E-3	15.4
4000	1	293.990	5.003E-3	24.8
	2	294.087	5.0107E-3	22.4
	3	294.877	5.0735E-3	28.3
	4	296.044	5.1673E-3	28.3
	5	304.327	5.8624E-3	23.9
	6	305.163	5.9355E-3	23.3
6000	1	294.385	5.0344E-3	15.6
	2	294.336	5.0305E-3	17.6
	3	295.115	5.0926E-3	21.8
	4	296.300	5.188E-3	21.8
	5	304.422	5.8707E-3	13.4
	6	305.386	5.955E-3	14.9

APPENDIX E

Profile Calibration Data Summary

Altitude / Target	0	1000	2000	4800	6000
	Radiance (watt E-3/cm^2-s.r.)				
Radiance Values Generated from Thermogram Data					
1		5.024	4.987	4.997	4.940
2		5.075	5.016	5.041	4.990
3		5.171	5.049	5.064	4.998
4		5.282	5.193	5.140	5.098
5		5.499	5.575	5.547	5.565
6		5.902	5.886	5.829	5.706
7		5.957	5.885	5.887	5.775
8		6.182	6.181	6.105	6.078
9		6.251	6.200	6.251	6.206
Radiance Values Generated by Least Squares Analysis					
1	5.060	5.034	4.997	4.962	4.950
2	5.108	5.073	5.038	5.008	4.988
3	5.170	5.122	5.085	5.040	5.000
4	5.335	5.255	5.205	5.145	5.103
5	5.813	5.695	5.617	5.532	5.485
6	6.080	5.935	5.865	5.775	5.725
7	6.170	6.000	5.920	5.830	5.770
8	6.550	6.320	6.190	6.090	6.040
9	6.730	6.495	6.340	6.210	6.170
Radiance Values Generated by Independent Agent					
1	5.090	5.040	5.020	4.970	4.950
2	5.120	5.070	5.050	5.000	4.970
3	5.180	5.130	5.100	5.050	5.010
4	5.320	5.250	5.200	5.150	5.110
5	5.760	5.660	5.610	5.540	5.500
6	6.000	5.920	5.870	5.800	5.760
7	6.080	5.980	5.920	5.850	5.810
8	6.500	6.310	6.210	6.090	6.030
9	6.650	6.450	6.350	6.220	6.150

APPENDIX E (continued)

	Target Description	New Ground-Truth Temperatures (°K)
1.	Lake Ontario, east of river	294.883
2.	Lake Ontario, west of pond	295.637
3.	Lake Ontario, west of river	297.043
4.	Genesee River at west pier	298.645
5.	Roof of pumphouse	301.708
6.	West pier at river	307.186
7.	Little Pond by road	307.913
8.	Road by pond	310.845
9.	Y-intersection in road	311.731

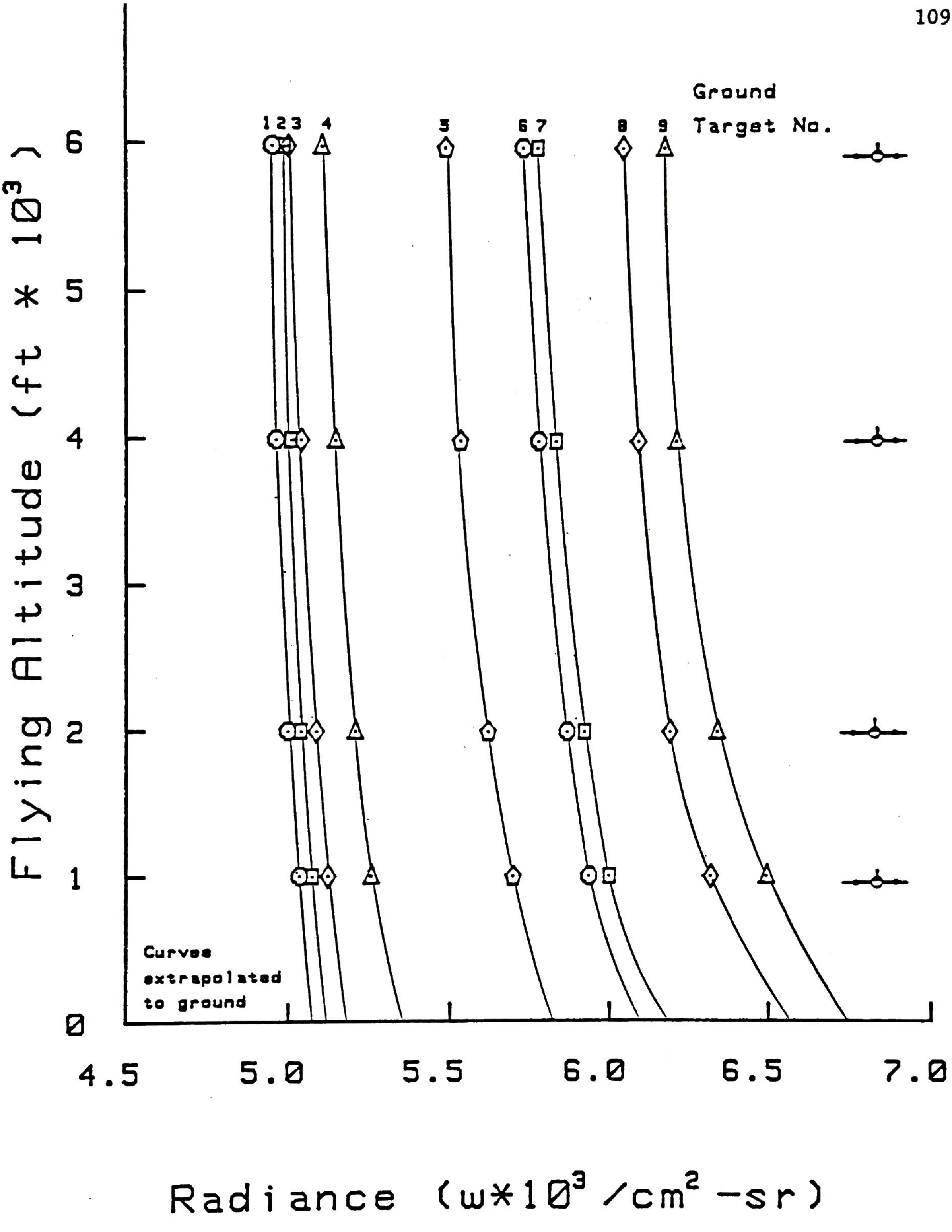

Figure 32. Profile Calibration--Observed Radiances versus Altitude for New Ground-Truth Features.

APPENDIX F

Angular Calibration Data Summary

Target	Radiance (watt E-3/cm^{-2}-s.r.) Vertical	Angle
Altitude: 1000 feet		
Calibration Angle: 49.5°		
1. asphalt lot	6.1841	6.1067
2. river	5.1565	5.0486
3. concrete pier	6.1226	5.9076
4. warehouse roof	6.2761	6.0792
5. warehouse roof	6.0609	5.9239
6. asphalt lot	6.1750	5.9917
7. asphalt road	6.3381	6.1922
8. asphalt road	6.1155	5.9112
9. asphalt road	6.0393	5.8520
10. house roof	6.7807	6.4256
11. asphalt road	6.5031	6.2887
12. asphalt road	6.2449	6.1313
13. house roof	6.7177	6.4974
14. sand pit, golf	6.3100	6.0832
15. sand pit, golf	6.3384	6.1242
16. asphalt lot	6.4998	6.2781
17. asphalt lot	6.4980	6.2646
18. shed roof	6.7439	6.2593
19. gravel lot	5.9354	5.8591
20. asphalt road	6.0041	5.8904
21. pond	5.2427	5.1671
22. gravel road	6.3719	6.1944
23. power plant roof	6.3438	6.1906
24. asphalt lot	6.4758	6.2959
25. concrete pad	5.4441	5.3146
26. asphalt road	6.3686	6.1460
27. asphalt strip	6.4545	6.2574
28. driveway	6.1613	5.8972
29. house roof	7.0294	6.5697
30. golf green	4.9145	4.8870
31. marina	5.2138	5.1369
32. concrete pad	5.1569	5.1568
33. wood pier	5.7823	5.6732
34. golf green	5.4530	5.3822

APPENDIX F (continued)

Target	Radiance (watt E-3/cm^{-2}-s.r.) Vertical	Angle
Altitude: 2000 feet		
Calibration Angle: 53.9°		
1. marina	5.4168	5.3274
2. concrete pad	6.1315	5.9294
3. river	5.3531	5.2684
4. shed roof	6.5143	6.2853
5. asphalt road	6.4646	6.1524
6. asphalt lot	6.5808	6.2748
7. driveway	6.5571	6.2548
8. asphalt road	6.4295	6.1619
9. gravel lot	6.3147	6.1256
10. store roof	6.4546	6.3133
Altitude: 4000 feet		
Calibration Angle: 43.1°		
1. marina	5.1845	5.2297
2. asphalt lot	6.2821	6.2310
3. river	5.2523	5.2015
4. warehouse roof	6.5104	6.4089
5. asphalt lot	5.8892	5.8543
6. asphalt road	6.3272	6.2670
7. sand quarry	6.1033	6.0847
8. golf green	5.4551	5.3370
9. asphalt road	6.2763	6.1387
10. house roof	6.7391	6.3601
11. pond	5.2559	5.1324
Altitude: 6000 feet		
Calibration Angle: 39.1°		
1. warehouse roof	5.6761	5.6489
2. warehouse roof	5.5177	5.4897
3. asphalt lot	6.3460	6.2749
4. marina	5.3368	5.3170
5. factory roof	6.2707	6.1909
6. river	5.3356	5.2745
7. asphalt lot	6.1376	6.0520
8. asphalt road	6.4001	6.2851
9. sand quarry	6.2384	6.1876

APPENDIX G

Atmosphere Radiosonde Data Summary

Location: Station Buffalo, New York
Date: 25 June, 1983
Time of Release: 1100 GMT
ASC. No.: 349

Altitude ASL (km)	Barometric Pressure	Temperature (°C)	Dew Point (note 1)
0.218	990	16.1	9.8
0.383	971	14.9	7.5
0.836	920	11.2	2.6
1.011	901	12.5	3.0
1.497	850	9.3	0.1
1.695	830	9.1	-6.3
1.958	804	7.2	-4.9
2.06	794	6.8	-10.8
3.084	700	0.9	-29.1
4.113	615	-4.5	-23.7
5.124	540	-11.5	-41.5
5.711	500	-14.1	-44.1
6.196	469	-15.4	-45.4
6.625	443	-17.5	-34.6
7.380	400	-23.7	-33.7
8.121	361	-29.5	-34.4
8.821	327	-34.1	-43.3
9.419	300	-38.3	-47.6

Note 1. Dew Point = Temp - Dew Point Depression

APPENDIX H

Regression Analysis of Thermogram versus Thermistor[33] Derived Radiances for Primary Ground-Truth Features

Altitude (ft)	1000
Intercept, A	7.413E-4
Slope, B	0.8439
Correlation Coefficient	0.995
Standard Error of Regression Fit (w/cm^2-s.r.)	4.901E-5
Standard Error of Regression Fit (°K)	0.583 (Error in New Ground-Truth Data)
τ	0.856
L_u (w/cm^2-s.r.)	7.235E-4

Sample Calculation

$$L = \tau\varepsilon L_T + \tau R L_d + L_u$$

$$= BL_T + A$$

$$B = \tau\varepsilon$$

$$\tau = B/\varepsilon$$

$$A = \tau R L_d + L_u$$

$L_u = A - BRL_d/\varepsilon$; where $\varepsilon = 0.986$, $L_d = 1.48399E-3$

APPENDIX I

Error Propagation Study[2] of Ground Temperature Predictions

Analysis

This error study defines the propagated errors associated with the ground temperature prediction process outlined in Figure 13.

Starting with the ground radiance equation,

$$L_T = \frac{L_g - L_d R}{\varepsilon}$$

The defining error equation is,

$$\delta(L_T) = [(\frac{\partial L_T}{\partial L_g} \cdot \delta(L_g))^2 + (\frac{\partial L_T}{\partial L_d} \cdot \delta(L_d))^2 + (\frac{\partial L_T}{\partial R} \cdot \delta(R))^2 + (\frac{\partial L_T}{\partial \varepsilon} \cdot \delta(\varepsilon))^2]^{\frac{1}{2}}$$

$$= [(\frac{\delta(L_g)}{\varepsilon})^2 + (\frac{-R}{\varepsilon} \cdot \delta(L_d))^2 + (\frac{-L_d}{\varepsilon} \cdot \delta(R))^2 + ((\frac{L_g - RL_d}{\varepsilon^2}) \cdot \delta(\varepsilon))^2]^{\frac{1}{2}}$$

The defined values are:

$$\delta(L_d) \equiv \pm 10°K \equiv 0.362E\text{-}3 \text{ w/cm}^2\text{-s.r.}$$

$$\delta(R) = \delta(\varepsilon) = \pm 0.005$$

To find $\delta(L_g)$, the equation of L_g is reviewed,

$$L_g = \frac{L - L_u}{\tau}$$

The defining error equation, here, is,

$$\delta(L_g) = [(\frac{\partial L_g}{\partial L} \cdot \delta(L))^2 + (\frac{\partial L_g}{\partial L_u} \cdot \delta(L_u))^2 + (\frac{\partial L_g}{\partial \tau} \cdot \delta(\tau))^2]^{\frac{1}{2}}$$

$$= [(\frac{\delta(L)}{\tau})^2 + (\frac{-\delta(L_u)}{\tau})^2 + ((\frac{L - L_u}{\tau^2}) \cdot \delta(\tau))^2]^{\frac{1}{2}}$$

The defined values are:

$\delta(L_u)$ = 3% for Profile, (ref: Schott); 3.2% for Angular (ref: Macleod)

$\delta(\tau)$ = 1% for Profile (ref: Schott); 1.6% for Angular (ref: Macleod)

To find $\delta(L)$, the equation of L through the equivalent temperature, T, is examined,

$$T = (V - V_{bb})\cdot G + T_{bb} + 273.16$$

The defining error equation is,

$$\delta(T) = [(\frac{\partial T}{\partial V} \cdot \delta(V))^2 + (\frac{\partial T}{\partial V_{bb}} \cdot \delta(V_{bb}))^2 + (\frac{\partial T}{\partial T_{bb}} \cdot \delta(T_{bb})^2 + (\frac{\partial T}{\partial G} \cdot \delta(G))^2]^{\frac{1}{2}}$$

$$= [(G\cdot\delta(V))^2 + (-V_{bb}\cdot\delta(V_{bb}))^2 + (\delta(T_{bb}))^2 + ((V-V_{bb})\cdot\delta(G))^2]^{\frac{1}{2}}$$

The defined values are,

$$\delta(T_{bb}) = 0.112°K$$

$$\delta(G) = 0.269°K/Volt$$

Errors on voltage, i.e. V_{bb}, V, are based on the noise level of the densitometer, i.e., 0.01 D. Hence,

$\delta(V_{bb}) = \pm\ 0.195$ Volts

$\delta(V)$ in the toe region of the D-V calibration curve = ± 0.195 Volts.

$\delta(V)$ in the linear region of the D-V calibration curve = ± 0.05 Volts.

Results

This analysis predicted the following errors for the process of determining ground temperatures in this study:

Predicted Ground Temperature Error, $\delta(T_T)$, (°K)

Calibration Technique	1000' Altitude	6000' Altitude
Profile	1.06	1.27
Angular	1.42	1.58

These error predictions, except for the 6000' altitude Angular error, are consistent with the experimental results of Tables 4 and 5. The anomoly with the Angular error result at altitudes greater than 1000' altitude indicates that all error sources were not fully accounted for.

APPENDIX J

Software Listings

```
5     REM  ****************************************************
10    REM  ****** PROFILE ATMOSPHERIC CALIBRATION: PART I ******
20    REM  ****************************************************
22    REM  THIS PROGRAM CALCULATES TEMP & RADIANCE
24    REM  FOR THE 'PROFILE' CALIBRATION TECHNIQUE
26    REM  FILM DENSITY IS THE PRIMARY INPUT
28    REM  AND THE OUTPUT IS TEMPERATURE AND RADIANCE.
29    REM  REFERENCE: FIGURE 9
30    REM  ****************************************************
50    DIM D(100),DT(100),DBB(100),V(100),VB(100),Z(100)
52    DIM TAPP(100),X(100),Y(100),WN(100),A(100),W(100,L(100),C(100)
55    REM  DATA: TBB, GAIN
60    DATA 22.15,2.434
70    READ TBB,G
80   D$ = CHR$ (4)
200   HOME
205   INVERSE
210   INPUT "INPUT WEDGE FROM <D>ISC or <K>EYBOARD?";W$
220   IF W$ = "K" THEN  GOSUB 9000
230   IF W$ = "D" THEN  GOTO 238
235   IF W$ <  > "D" THEN  GOTO 210
238   FLASH : PRINT : PRINT "YOU MUST WORK WITH ONLY"
239   PRINT "ONE V-D CURVE AT A TIME!": INVERSE
240   PRINT "TBB, GAIN SET CORRECTLY?": PRINT "TBB = ";TBB;", GA IN =
      ";G;""
245   GOSUB 7900
250   PRINT "PROFILE CALIBRATION": PRINT
255   PRINT : INPUT "HOW MANY DENSITIES TO PROCESS?";Q
260   FOR I = 1 to Q
270   PRINT I: PRINT "INPUT ALT, D, DBB, WEDGE #"
290   PRINT : INPUT A(I),DT(I),DBB(I),WN(I)
300   NEXT I
302   HOME : PRINT "ALT           DEN           DEBB"
303   NORMAL : FOR I = 1 to Q
304   PRINT A(I),DT(I),DBB(I)
305   NEXT I
306   PRINT : INVERSE : INPUT "I/P DATA OK?";N$
308   IF N$ = "N" GOTO 255
309   NORMAL : PRINT  TAB( 10)"DATA ANALYSIS IN PROGRESS"
310   FOR I = 1 to Q
340  A = DBB(I)
350   GOSUB 5000
360   LET VBB(I) = B
370  A = DT(I)
380   GOSUB 5000
390   V(I) = B
392  TAPP(I) = G * (V(I) - VBB(I)) + TBB) + 273.16
394  C(I) = COS (Z(I) *3.14159 / 90)
395  A(I) = INT ((A(I) / C(I)) * 10 + .5) / 10
410   GOSUB 750
412  TAPP(I) = INT (TAPP(I) * 1000 + .5) / 1000
```

```
413     V(I) = INT (V(I) * 1000 + .5) / 1000
414     VBB(I) = INT (VBB(I) * 1000 + .5) / 1000
415     L(I) = INT (L(I) * 10000000000 + .5) / 10000000000
417      NEXT I
418      HOME : PRINT CHR$ (7)
420      PRINT : PRINT : GOSUB 700
500      INPUT "HARD COPY OF DATA?";C$
510      IF C$ = "Y" THEN  GOTO 550
520      IF C* = "N" THEN  GOTO 1000
530      GOTO 500
550      INPUT "TITLE?";H$
552      IF H$ = "Y" GOTO 558
554      IF H$ = "N" GOTO 562
558      PR# 1: PRINT
560      GOSUB 600
561      GOTO 565
562      PR# 1: PRINT : GOSUB 630
565      PR# 0
570      INput 'COPY OF WEDGE DATA?";F$
575      IF F$ = "Y" GOTO 645
580      PR# 0
590      GOTO 1000
600      PRINT : PRINT : PRINT "PROFILE DATA SUMMARY"
605      PRINT "--------------------"
608      PRINT
610      PRINT "W#","RADIANCE","TAPP","DBB","VBB","ALT","D","V"
615      PRINT "--","--------","----","---","---","---","--","--"
620      PRINT
630      FOR I = 1 TO Q
640      PRINT WN(I),L(I),TAPP(I),DBB(I),VBB(I),A(I),DT(I),V(I)
641      NEXT I
642      RETURN
645      PR# 1: PRINT : PRINT : PRINT "STEP WEDGE DATA"
646      PRINT "V"; TAB( 5)"DENSITY"
647      PRINT "----------"
651      PRINT
652      FOR I = 1 to 17
653      PRINT Y(I); TAB( 5);X(I)
654      NEXT I
660      GOTO 580
700      PRINT "ALT  DEN DBB  TAPP   WN  RADIANCE"
705      PRINT "---------------------------------------"
711      FOR I = 1 TO Q
712      PRINT A(I); TAB( 6)DT(I); TAB( 10)DBB(I); TAB( 15)TAPP(I);
         TAB( 23)WN(I); TAB( 26)L(I)
713      NEXT I
715      PRINT : PRINT
716      NOTRACE
720      RETURN
750      REM  RADIANCE CALCULATION BY INTEGRATING PLANCK'S B.B. LAW.
         REF:SLATER,PG.37
```

```
760   REM  WAVELENGTH INTERVAL
765   B = 14:E = 8
766   W1 = (B - E) / 40
768   W = E
770   GOSUB 850
772   Y1 = F
774   W = B
776   GOSUB 850
778   Y2 = F
780   C = 0
782   D = 0
784   REM  LOOP FOR EACH INTERVAL
786   FOR Z = 1 TO (B - E) / W1 - .5
788   W = E + Z * W1
790   GOSUB 850
792   Y = F
794   REM  INTERVAL EVEN OR ODD?
796   T2 = Z / 2:R = INT (T2)
798   IF T2 = R THEN 808
800   REM  SUM ALL ODD INTERVALS
802   C = C + Y
804   GOTO 810
806   REM  SUM ALL EVEN INTERVALS
808   D = D + Y
810   NEXT Z
812   REM  COMPUTE INTEGRAL
814   L(I) = W1 / 3 * (Y1 + (C * 4) + D * 2 + Y2)
820   RETURN
850   REM  DEFINE RADIANCE FUNCTION
852   K = 37415.1 / 3.14159
854   M = 14387.9
856   U = M / (W * TAPP (I))
858   F = (K / (W ^ 5)) * (1 / ( EXP (U) - 1))
860   RETURN
1000  INPUT "DO YOU WISH TO REPEAT STUDY?";Q$
1010  IF Q$ = "Y" THEN GOTO 200
1020  IF Q$ = "N" THEN GOTO 1100
1025  GOTO 1000
1030  INPUT "START POINT: <W>EDGE I/P OR <A>LT I/P?";R$
1040  IF R$ = "W" THEN  GOTO 200
1050  IF R$ = "A" THEN  GOTO 250
1060  GOTO 1030
1100  PRINT "YOU ARE ABOUT TO EXIT 'PROFILE CALIB':
1110  INPUT "DO YOU WISH TO EXIT? (Y/N)";S$
1120  IF S$ = "N" THEN  GO TO 1000
1130  FLASH : HOME : NORMAL : PRINT  CHR$ (&): END
5000  GOTO 10000
5005  REM  CURVALINEAR INTERPOLATION
5010  P = 9: REM  # OF WEDGE STEPS
5020  REM  ENTER 'X' COORD OF PT TO BE INTERPOLATED
5050  B = 0
```

```
5055   REM  LAGRANGE INTERPOLATION
5060   FOR J = 0 to P
5070  T = 1
5080   FOR K = 0 to P
5090   IF K = J THEN 6010
6000  T = T * (A - X(K)) / (X(J) - X(K))
6010   NEXT K
6020  B = B + T * Y(J)
6030   NEXT J
6040   RETURN
7000   REM  STEP WEDGE DATA FILE SAVE
7004   PRINT : PRINT "FILE NAME MUST BE"
7005   PRINT "OF FORM: WN'I':
7006   PRINT "WHERE 'I' = DATA SET NO."
7007   PRINT "IE. WN1, WN2, ETC."
7008   PRINT
7010   INPUT "INPUT FILE NAME: ";N$
7020   PRINT D$;"OPEN";N$: PRINT D$;"DELETE";N$: PRINT D$;"OPEN";N$:
       PRINT D$;"WRITE";N$
7040   FOR I = 1 TO 17
7050   PRINT D(I)
7060   NEXT I
7080   PRINT D$;"CLOSE";N$
7085   PRINT  CHR$ (7): PRINT "WEDGE DATA SAVED"
7090   RETURN
7900   REM  AUTO V-D DATA RETRIEVAL
7920   PRINT "TYPE IN WEDGE 'FILENAME':
8000   REM  STEP WEDGE DATA FILE RETRIEVAL
8010   PRINT : INPUT " FILE NAME: ";N$
8020   PRINT D$;"OPEN";N$: PRINT D$;"READ";N$
8030   FOR I = 1 to 17
8040   INPUT D(I)
8042  X(I) = D(I)
8044  Y(I) = I - 4
8046   PRINT Y(I),X(I)
8050   NEXT I
8060   PRINT D$;"CLOSE";N$
8070   PRINT "";N$;" DATA RETRIEVED"
8080   PRINT : RETURN
9000   REM  KEYBOARD I/P OF WEDGE DATA
9010   PRINT "I/P WEDGE DENSITY DATA": PRINT : PRINT
9020   FOR I = 1 to 17
9030   PRINT "D(";I - 1;") = "
9035   INPUT D(I)
9040   NEXT I
9050   PRINT : PRINT
9060   PRINT "WEDGE DATA TO BE SAVED TO DISC": GOSUB 7000
9080   PRINT " INPUT "I/P ANOTHER WEDGE DATA SET?";B$
9090   IF B$ = "Y" THEN  GOTO 9010
9100   PRINT : GOTO 238
10000  REM  LINEAR INTERPOLATION
```

```
10005  P = 17
10010   FOR J = 1 TO P
10015   IF X(J) > A GOTO 10025
10017   IF X(J) = A GOTO 10035
10020   NEXT J
10025  B = Y(J - 1) + (Y(J) - Y(J - 1)) / (X(J) - X(J - 1)) *
        (A - X(J - 1))
10030   RETURN
10035  B = Y(J)
10040   GOTO 10030

]
```

```
1       REM  *******************************************************
2       REM  ******* PROFILE ATMOSPHERIC CALIBRATION: PART II *******
3       REM  *******************************************************
4       REM  THIS PROGRAM REGRESSES THE GROUND VS ALTITUDE
5       REM  VALUES OF RADIANCE OR TEMPERATURE FOR SEVERAL TARGETS
6       REM  VALUES OF RADIANCE OR TEMPERATURE FOR SEVERAL TARGETS
6       REM  INPUT DATA IS FROM 'PART I' OF THIS PROGRAM SERIES.
8       REM  *******************************************************
10      DIM X(20),Y(20),TG(20),TAPP(20)
20      NORMAL : HOME : PRINT "PROFILE CALIBRATION: DETERMINATION"
25      PRINT "                          OF LU & TAU"
26      PRINT "-------------------------------"
28      PRINT : PRINT : PRINT "WHAT ALTITUDE WILL YOU"
30      INPUT "BE WORKING AT?";E
40      PRINT : INPUT "HOW MANY TARGETS?";N
42      PRINT : INPUT "INPUT TEMP OR RADIANCE DATA (T/R)";U$
44      IF U$ = "T" GOTO 50
46      IF U$ = "R" GOTO 400
48      GOTO 42
50      PRINT : PRINT "INPUT APPARENT AND"
60      PRINT "GROUND TEMP DATA:"
70      FOR I = 0 TO N - 1
80      PRINT I + 1: PRINT "TAPP, TGRD"
85      PRINT : INPUT TAPP(I),TG(I)
90      NEXT I
100     HOME : PRINT : PRINT "TAPP             TGRD": PRINT
110     FOR I = 0 TO N - 1
120     PRINT TAPP(I); TAB( 16)TG(I)
130     NEXT I
140     PRINT : PRINT : INPUT "DATA OK?";S$
150     IF S$ = "N" GOTO 40
160     FLASH : PRINT : PRINT : PRINT "CONVERSION OF TEMP TO RADIANCE"
170     PRINT "IN PROGRESS": NORMAL
180     FOR I = 0 TO N - 1
190    T = TAPP(I)
200     GOSUB 1000
210    Y(I) = L(I)
220    T = TG(I)
230     GOSUB 1000
240    X(I) = L(I)
250     NEXT I
255     PRINT : INPUT "NEW OR ORIGINAL REGRESSION ROUTINE? (N/O)";G$
257     IF G$ = "N" GOTO 265
259     IF G$ = "O" GOTO 276
261     GOTO 255
265     HOME : FLASH : PRINT "LINEAR REGRESSION OF L(ALT) VS L(GRD)"
267     PRINT "IN PROGRESS"
269     GOSUB 3500
271     GOTO 310
276     HOME : FLASH : PRINT "LINEAR REGRESSION OF L(ALT) VS L(GRD)"
278     PRINT "IN PROGRESS"
```

```
280     GOSUB 3500
310     GOSUB 1980
315     GOSUB 1900
316     GOTO 350
320     INVERSE : PRINT : PRINT : INPUT "HARD COPY OF DATA?";U$
330     IF U$ = 'N' GOTO 360
340     IF U$ = "Y" GOSUB 1900
350     PR# 0
360     PRINT : PRINT : INPUT "REPEAT PROGRAM FOR ANOTHER ALTITUDE";T$
370     IFT$ = "Y" GOTO 20
380     IF T$ = "N" GOTO 395
390     GOTO 360
395     HOME : END
400     PRINT : PRINT "INPUT APPARENT"
410     PRINT "AND GROUND RADIANCE DATA :"
420     FOR I = 0 TO N - 1
430     PRINT I: PRINT "L(APP), L(GRD)"
440     PRINT : INPUT Y(I),X(I)
450     NEXT I
460     HOME : PRINT : PRINT "L(APP)         L(GRD)"
470     PRINT
480     FOR I = 0 TO N - 1
490     PRINTY(I); TAB( 16)X(I)
500     NEXT I
510     PRINT : INPUT "DATA OK?";V$
520     IF V$ = "N" GOTO 40
530     HOME : FLASH : PRINT "LINEAR REGRESSION OF L(APP) VS L(GRD)"
540     PRINT "IN PROGRESS": NORMAL
550     GOSUB 3500
560     HOME : GOSUB 760
570     PRINT : PRINT : INPUT "HARD COPY OF DATA?";C$
575     IF C$ = "N" GOTO 360
580     IF C$ = "Y" THEN  GOSUB 755
585     PR# 0
590     GOTO 360
755     PR# 1
760     PRINT : PRINT : PRINT "DATA SUMMARY"
770     PRINT "------------"
775     PRINT : PRINT "ALTITUDE : ";E;"": PRINT
780     PRINT : PRINT"L(APP)            L(GRD)"
785     PRING "------------------------"
786     PRINT
790     FOR I = 0 TO N - 1
800     PRINT Y(I); TAB( 16)X(I)
810     NEXT I
820     GOSUB 2060
825     RETURN
990     REM  SIMPSONS INTEGRATION OF PLANCK'S LAW
995     REM  FOR CONVERSION OF TEMP TO RADIANCE
998     REM  WAVELENGTH INTERVAL
1000   B = 14;E = 8
```

```
1010  W1 = (B - E) / 40
1020  W = E
1030   GOSUB 1850
1040  Y1 = F
1050  W = B
1055   GOSUB 1850
1060  Y2 = F
1070  C = 0
1080  D = 0
1090   REM  LOOP FOR EACH INTERVAL
1200   FOR Z = 1 TO (B - E) / W1 - .5
1210  W = E + Z * W1
1220   GOSUB 1850
1230  Y = F
1240   REM  INTERVAL EVEN OR ODD?
1250  T2 = z / 2:R = INT (T2)
1260   IF T2 = R THEN 1803
1800   REM  SUM ALL ODD INTERVALS
1802  C = C + Y
1804   GOTO 1810
1806   REM  SUM ALL EVEN INTERVALS
1808  D = D + Y
1810   NEXT Z
1812   REM  COMPUTE INTEGRAL
1814  L(I) = W1 / 3 * (Y1 + (C * 4) + D * 2 + Y2)
1816   PRINT "RADIANCE = ";L(I);""
1820   RETURN
1850   REM  DEFINE RADIANCE FUNCTION
1852  K = 37415.1 / 3.14159
1854  M = 14387.9
1856  U = M / (W * T)
1858  F = (K / (W ^ 5)) * (1 / ( EXP (U) - 1)
1860   RETURN
1900   PR# 1: PRINT  CHR$ (9);"80N"
1980   HOME : NORMAL : PRINT : PRINT : PRINT "DATA SUMMARY"
1990   PRINT "------------": PRINT
2000   PRINT "ALTITUDE : ";E;""
2020   PRINT : PRINT "TAPP      L(APP)          T(GRD)          LGRD)"
2025   PRINT "-------------------------------------------------"
2030   FOR I = 0 TO N - 1
2040   PRINT TAPP(I); TAB( 3);Y(I); TAB( 3);TG(I); TAB( 3);X(I)
2050   NEXT I
2060   PRINT : PRINT : PRINT "FITTED EQUATION IS: "
2070   PRINT "   L(ALT) = "; INT (1000 * A + .5) / 1000;"   ";
2080   IF B > = 0 THEN  PRINT "+  ";
2090   PRINT  INT (1000 * B + .5) / 1000"  *  L(GRD)"
2100   PRINT : PRINT : PRINT " STANDARD DEVIATION OF FIT : ";
2110   PRINT  INT (100000 * D + .5) / 100000
2115   PRINT : PRINT "CORRELATION COEFFICIENT : "; INT (100000 *
       R2 + .5) / 100000
2120   PRINT : PRINT " LU = "; INT (10000000 * A + .5) / 10000000;""
```

```
2130    PRINT : PRINT "TAU = "; INT (10000000 * B + .5) / 10000000;""
2140    RETURN
3490    REM  LINEAR REGRESSION,REF: BASIC SCIENTIFIC SUBROUTINES,PG.20
3500   A1 = 0:A2 = 0:B0 = 0:B1 = 0:B2 = 0
3502    FOR M = 0 to N - 1
3503   A1 = A1 + X(M)
3504   A2 = A2 + X(M) * X(M)
3505   B0 =  B0 + Y(M)
3506   B1 = B1 + Y(M) * X(M)
3507   B2 = B2 + Y(M) * Y(M)
3508    NEXT M
3509   R2 = (N * B1 - A1 * B0) /  SQR ((N * A2 - A1 ^ 2) * (N * B2 -
        B0 ^ 2))
3510   A1 = A1 / N
3511   A2 = A2 / N
3512   B0 = B0 / N
3513   B1 = B1 / N
3514   D = A1 * A1 - A2
3515   A = A1 * B1 - A2 * B0
3516   A = A / D
3517   B = A1 * B0 - B1
3518   B = B / D
3519    REM  STANDARD DEVIATION
3521   D = 0
3522    FOR M = 0 TO N - 1
3523   D1 = Y(M) - A - B * X(M(
3524   D = D + D1 * D1
3525    NEXT M
3526   D =  SQR (D / (N - 2))
3600    RETURN

]
```

```
2       REM  ************************************************************
5       REM  ********** ANGULAR ATMOSPHERIC CALIBRATION **********
6       REM  ************************************************************
7       REM  THIS PROGRAM CALCULATES THE
8       REM  ATMOSPHERIC TAU AND RADIANCE
9       REM  BY THE 'ANGULAR' CALIBRATION TECHNIQUE; REFERENCE: FIGURE 10
10      REM  ****************************************************************************
20      DIM DV(90),DA(90),VV(90),VA(90),TV(90),TA(90),LV(90),LA(90),
        TH(90)
22      DIM L(90),PA(90),TW(90),OW(90)
25      DIM MA(90),PV(90),BA(90),BV(90),TB(90),BT(90),LB(90),PBO(90),
        WA(90)
30      DIM WT(90),EM(90),R(90),T(101),VR(90),AR(90)
50      DIM D(90),DT(90),DBB(90),V(90),VBB(90)
52      DIM X(100,Y(100,WN(90),A(90),W(90),Z(90)
53      DIM RA(100)
55      REM  DATA: TBB, GAIN
60      DATA  22.15,2.434
70      READ TBB,G
80     D$ = CHR$ (4)
200     HOME
205     INVERSE
210     INPUT "INPUT WEDGE FROM <D>ISC or <K>EYBOARD?";W$
220     IF W$ = "K" THEN  GOSUB 9000
230     IF W$ = "D" THEN  GOTO 238
235     IF W$ <  > "D" THEN  GOTO 210
238     FLASH : PRINT : PRINT "YOU MUST WORK WITH ONLY"
239     PRINt "ONE V-D CURVE AT A TIME!": INVERSE
240     PRINT : PRINT "TBB, GAIN SET CORRECTLY? : "
242     NORMAL : PRINT "TBB = ";TBB;" :GAIN = "G;"": INVERSE : GOSUB
        7900
249     PRINT "==================="
250     NORMAL : PRINT "ANGULAR CALIBRATION": INVERSE
252     PRINT "==================="
300     PRINT : INPUT "WHAT ALTITUTDE ARE YOU WORKING AT?";H
320     PRINT : PRINT "HOW MANY TARGETS"
330     INPUT "FOR ANALYSIS";N
335     PRINT : FLASH : PRINT "VERT. & ANGLE DENSITY DATA"
337     PRINT "MUST BE FUNCTION OF CONSTANT ANGLE"
339     PRINT "FOR CALIBRATION PURPOSES!!!!": INVERSE
340     PRINT : INPUT "CALIBRATION ANGLE = ";AH
341     REM  CONVERT ANGLE TO RADIATION MEASURE
342    TH = 3.14159 * AH / 180
350     PRINT : PRINT "INPUT VERT., ANGLE AND B.B. DENSITY DATA : "
360     FOR I = 0 TO N - 1
370     PRINT I: PRINT "DV,  DA,  DBB"
380     INPUT DV(I),DA(I),DBB(I)
385     NEXT I
386     NORMAL
387     HOME : PRINT "DV","DA","DBB"
389     PRINT
```

```
390    FOR I = 0 TO N - 1
392    PRINT DV(I),DA(I),DBB(I)
394    NEXT I
395    PRINT : INPUT "DATA OK?";T$
400    IF T$ = "N" GOTO 340
410    HOME
420    FLASH : PRINT : PRINT : PRINT "ANALYSIS IN PROGRESS": NORMAL
430    FOR I = 0 TO N - 1
432   A = DBB(I)
434    GOSUB 5000
436   VBB(I) = B
440   A = DV(I)
450    GOSUB 5000
460   VV(I) = B
470   A = DA(I)
480    GOSUB 5000
490   VA(I) = B
495    REM  TV(I) & TA(I) ARE APPARENT TEMPS
500   TV(I) = ((VV(I) - VBB(I)) * G) + 273.16 + TBB
510   TA(I) = ((VA(I) - VBB)(I)) ( G) + TBB + 273.16
520    NEXT I
530    FOR I = 0 TO N - 1
540   T = TV(I)
550    GOSUB 765
560   LV(I) = L(I)
565   X(I) = LV(I)
570   T = TA(I)
580    GOSUB 765
590   LA(I) = L(I)
595   TV(I) = INT (TV(I) * 100 + .5) / 100
596   Y(I) = LA(I)
597   TA(I) = INT (TA(I) * 100 + .5) / 100
598   TH(I) = TH
600    NEXT I
605    GOSUB 9500
608   Z = (1 /  COS (TH)) - 1
610   TU = B ^ (1 / Z)
611    REM  MACLEOD's COEFF: WU=A/((1/COS(TH))-B)
612    REM  SCHOTT's COEFF AT LINE 613
613   WU = A / (((1 /  COS (TH)) - 1) * B)
615    PRINT  CHR$ (7)
616    GOSUB 10000
618    PRINT  CHR$ (7)
620    GOTO 2000
712    REM  ------------------------------
714    REM SCHOTT'S COEFF IN USE
716    REM  ------------------------------
750    REM  RADIANCE CALCULATION BY INTEGRATING PLANCK'S B.B. LAW.
       REF:SLATER,PG.37
760    REM  WAVELENGTH INTERVAL
765    NOTRACE :B = 14:E = 8
```

```
766   W1 = (B - E) / 40
768   W = E
770    GOSUB 850
772   Y1 = F
774   W = B
776    GOSUB 850
778   Y2 = F
780   C = 0
782   D = 0
784    REM  LOOP FOR EACH INTERVAL
786    FOR Z = 1 TO (B - E) / W1 - .5
788   W = E + Z * W1
790    GOSUB 850
792   Y = F
794    REM  INTERVAL EVEN OR ODD?
796   T2 = Z / 2:R =  INT (T2)
798    IF T2 = R THEN 808
800    REM  SUM ALL ODD INTERVALS
802   C = C + Y
804    GOTO 810
806    REM  SUM ALL EVEN INTERVALS
808   D = D + Y
810    NEXT Z
812    REM  COMPUTE INTEGRAL
814   L(I) = W1 / 3 * (Y1 + (C * 4) + D * 2 + Y2)
820    RETURN
850    REM  DEFINE RADIANCE FUNCTION
852   K = 37415.1 / 3.14159
854   M = 14387.9
856   U = M / (W * T)
858   F = (K / (W ^ 5)) * (1 / ( EXP (U) - 1))
860    RETURN
1000   INPUT "DO YOU WISH TO REPEAT THE STUDY?";Q$
1010   IF Q$ = "Y" THEN  GOTO 200
1020   IF Q$ = "N" THEN  GOTO 1100
1025   GOTO 1000
1100   PRINT "YOU ARE ABOUT TO EXIT 'ANGULAR CALIB'"
1110   INPUT "DO YOU WISH TO EXIT? (Y/N)";S$
1120   IF S$ = "N" THEN GOTO 1000
1130   FLASH : HOME : NORMAL : PRINT  CHR$ (7): END
1900   REM  CALCULATION OF TAU, LU, WO, AND TAPP
1910   REM  SLOPE(TAU) = B, INTERCEPT(WA TERM) = A, ANGLE = TH
2000   PRINT : PRINT "END OF CALIBRATION"
2065   INPUT "DO YOU WISH A HARD COPY?";B$
2070   IF B$ = "N" GOTO 2088
2075   IF B$ = "Y" GOTO 2085
2080   GOTO 2000
2085   GOSUB 2999: REM   GOSUB 11000
2087   PR# 0
2088   FLASH : PRINT : INPUT "CONTINUE WITH ANALYSIS?";T$
2089   IF T$ = "N" GOTO 200
```

```
2090    IF T$ = "Y" GOTO 2093
2091    GOTO 2088
2093    PRINT : INPUT "CALCULATE T(APP)'S USING CALIB'N DATA?";D$
2094    FLASH : PRINT : PRINT : "ANALYSIS PROGRAM HAS NOT BEEN VERIFIED
        PAST THIS POINT" : NORMAL
2095    IF D$ = "N" GOTO 200
2100    IF D$ = "Y" GOTO 2112
2105    GOTO 2090
2110    REM LA(I),THETA ALREADY = LA(I), TH(I)
2112    GOSUB 4700
2114    FOR I = 0 TO N - 1
2115    GOSUB 4492
2120   PA(I) = T
2122   QA(I) = WT(I)
2125   MA(I) = LA(I)
2130   LA(I) = LV(I)
2132   TH(I) = 0
2135    GOSUB 4492
2140   PV(I) = T
2142   QV(I) = WT(I)
2145    NEXT I
2150    GOSUB 3240
2152    PRINT  CHR$ (&)
2155    PRINT : INPUT "HARD COPY?";F$
2160    IF F$ = "N" GOTO 2500
2165    IF F$ = "Y" GOTO 2175
2170    GOTO 2155
2175     PR# 1: GOSUB 3200
2180    PR# 0: GOTO 2500
2500    PRINT : INPUT "CALCULATE T(APP)'S USING NEW DATA?";E$
2505    IF E$ = "N" GOTO 1000
2510    IF E$ = "Y" GOTO 2540
2515    GOTO 2500
2540    PRINT : INPUT "HOW MANY TARGET POINTS";M
2545    PRINT : PRINT "INPUT NEW DENSITY AND NADIR OFFSET (MM)"
2550    FOR I = 0 TO M - 1
2555    PRINT I: PRINT "DEN, OFFSET"
2560    INPUT BA(I),Z(I)
2562   TH(I) = ATN ((Z(I) * 3464) / (H * 70)): REM  TH=ATN(z(MM)*SCALE/H)
2565    NEXT I
2570    INPUT "DATA OK?";F$
2575    IF F$ = "N" GOTO 2545
2580    IF F$ = "Y" GOTO 2590
2585    GOTO 2570
2590    REM  INTERPOLATE ON V-D & CALC. TEMP
2595    FOR I = 0 TO M - 1
2600   A = BA(I)
2605    GOSUB 5000
2610   BV(I) = B
2615   TB(I) = (G * (BV(I) - VBB(I)) + TBB) + 273.15
2620    NEXT I
```

```
2630    FOR I = 0 TO N - 1
2635    T = BT(I)
2640    GOSUB 765
2645    LB(I) = L(I)
2650    LA(I) = LB(I)
2655    NEXT I
2660    FOR I = 0 TO M - 1
2665    GOSUB 4492
2668    PB(I) = T(I)
2670    NEXT I
2675    GOSUB 2800
2680    PRINT : PRINT "HARD COPY?";G$
2685    IF G$ = "N" GOTO 1000
2690    IF G$ = "Y" GOTO 2697
2695    GOTO 2680
2697    PR# 1: GOSUB 2800
2698    GOTO 2500
2800    PRINT : PRINT : PRINT "T(APP) NEW DATA SUMMARY"
2805    PRINT "----------------------------------": PRINT
2810    PRINT "#","ANGLE","DEN,"TEMP","RADIANCE","T(APP)"
2820    FOR I = 0 TO M - 1
2825    PRINT I,TH(I),BA(I),TB(I),LB(I),PB*I)
2830    NEXT I
2835    PRINT : PRINT : RETURN
2998    REM  CALIBRATION DATA DISPLAY
2999    PR# 1: PRINT  CHR$ (9);"80N"
3000    PRINT "ANGULAR CALIBRATION DATA SUMMARY"
3005    PRINT "--------------------------------"
3040    PRINT : PRINT "ALTITUDE : ";H
3042    PRINT "BB DENSITY = ";DBB(1)
3044    PRINT
3045    PRINT "TV     TA     V-RADIANCE     A-RADIANCE     DV    DA"
3046    PRINT "-----------------------------------------------------"
3050    FOR I = 0 TO N - 1
3060    PRINT TV(I); TAB( 2);TA(I); TAB( 2);LV(I); TAB( 2);LA(I);
        TAB(2);DV(I); TAB( 2);DA(I)
3065    NEXT I
3070    PRINT : PRINT "FITTED EQUATION IS : "
3075    PRINT "  LA = "; INT (1000 * A + .5) / 1000;" ";
3080    IF B >  = 0 THEN PRINT "+  ";
3085    PRINT  INT (1000 * B + .5) / 1000"   *  LV"
3086    PRINT : PRINT "SLOPE = ";B
3087    PRINT : PRINT "INTERCEPT = ";A
3088    PRINT : PRINT "THETA = ";TH;"RAD."
3089    PRINT : PRINT "THETA + ";AH;" DEG."
3090    PRINT : PRINT "STANDARD DEVIATION OF FIT : "; INT (100000 *
        D + .5) / 100000
3094    PRINT : PRINT "CORRELATION COEFFICIENT : "; INT (100000 * R2 +
        .5) / 100000
3095    PRINT : PRINT "TAU(H,0) = ";TU
3100    PRINT: PRINT "WA(H,0) = "WU
```

```
3105    RETURN
3200    PRINT : PRINT : PRINT
3240    PRINT : PRINT "T(GRD) DATA SUMMARY"
3242    PRINT "------------------"
3250    PRINT "#","RAD(APP)","T(APP)","T(GRD)","RAD(GRD)","DA"
3255    PRINT "---------------------------------------------------------
        --------------------------------"
3260    PRINT
3265    FOR I = 0 TO N
3270    PRINT I,MA(I),TA(I),PA(I),QA(I),DA(I)
3275    NEXT I
3278    PRINT : PRINT
3285    PRINT "#","RAD(APP)","T(APP)","T(GRD)","RAD(GRD)","DV"
3290    PRINT "---------------------------------------------------------
        --------------------------------"
3295    PRINT
3300    FOR I = 0 TO N
3305    PRINT I,LA(I),TV(I),PV(I),QV(I),DV(I)
3310    NEXT I 3315    RETURN
4490    REM  TAPP DETERMINATION BY REVERSE PLANCK EQUATION
4492    REM  MACLEOD'S COEFF. IN USE ONLY
4493    NORMAL
4494   WA(I) = WU ( TU ^ ((1 /  COS (TH(I))) - 1)) /  COS (TH(I))
4496   TW(I) = TU ^ (1 /  COS (TH(I)))
4500   WO(I) = (LA(I) - WA(I)) / TW(I)
4510   WT(I) = WO(I): REM  WT(I) = (WO(          I) - WS * R(I)) /
        EM(I)
4515    PRINT "WT = ";WT(I)
4520    REM    ITERATIVE SOLUTION TO REVERSE PLANCK EQUATION
4530    FOR K = 0 TO 69
4540    IF RA(K) > WT(I) GOTO 4568
4550    NEXT K
4560   Y(1) = T(K):Y(0) = T(K - 1)
4565   X(1) = RA(K):X(0) = RA(K - 1)
4570    PRINT Y(1),Y(0),X(1),X(0)
4580    GOSUB 8500
4590   B(I) = BC
4600   ANT(I) = A
4610   T = (B(I) * WT(I)) + ANT(I)
4620    PR# 0: RETURN
4700   D$ = CHR$ (4)
4704   N$ = "TRAD"
4710    PRINT     D$;"OPEN";N$: PRINT D$;"READ";N$
4720    FOR K = 0 TO 69
4730    INPUT RA(K)
4736    INPUT (T(K)
4737    PRINT T(K)
4740    NEXT K
4750    PRINT D$;"CLOSE";N$
4760    PRINT "RADIANCE TABLE RETRIEVED"
4762    RETURN
```

```
5000   GOTO 12000
5005   REM   CURVALINEAR INTERPOLATION
5010  P = 7: REM     NO. OF WEDGE STEPS
5020   REM  ENTER 'X' COORD OF PT TO BE INTERPOLATED
5050   B = 0
5055   REM  LAGRANGE INTERPOLATION
5060   FOR J = 1 TO P
5070  T = 1
5080   FOR K = 1 TO P
5090   IF K = J THEN 6010
6000  T = T * (A - X(K)) / (X/(J) - X(K))
6010   NEXT K
6020   B = B + T * Y(J)
6030   NEXT J
6040   RETURN
7000   REM  STEP WEDGE DATA FILE SAVE
7004   PRINT : PRINT "FILE NAME MUST BE"
7005   PRINT "OF FORM: WN'I'"
7006   PRINT "WHERE 'I" = DATA SET NO."
7007   PRINT "IE. WN1, WN2, ETC."
7008   PRINT
7010   INPUT "INPUT FILE NAME: ";N$
7020   PRINT D$;"OPEN";N$: PRINT D$;"DELETE";N$: PRINT D$;"OPEN";N$:
       PRINT D$;"WRITE";N$
7040   FOR I = 1 TO 17
7050   PRINT D(I)
7060   NEXT I
7080   PRINT D$;"CLOSE";N$
7085   PRINT  CHR$ 7): PRINT "WEDGE DATA SAVED"
7090   RETURN
7900   REM   AUTO V-D DATA RETRIEVAL
7920   PRINT "TYPE IN WEDGE 'FILENAME'"
8000   REM  STEP WEDGE DATA FILE RETRIEVAL
810    PRINT : INPUT "FILE NAME: ";N$
8020   PRINT D4;"OPEN";N$: PRINT D$;"READ";N$
8030   FOR I = 1 TO |7
8040   INPUT D(I)
8042  X(I) = D(I)
8044  Y(I) = I - 4
8046   PRINT Y(I),X(I)
8050   NEXT I
8060   PRINT D$;"CLOSE";N$
8070   PRINT "";N$;" DATA RETRIEVED"
8080   PRINT : RETURN
8500   REM  LINEAR INTERPOLATION FOR RADIANCE CALCULATION
8510  A1 = 0:A2 = 0:B0 = 0:B1 = 0:B2 = 0:A = 0:BC = 0:D = 0
8512   FOR M = 0 TO 1
8514  A1 = A1 + X(M)
8516  A2 = A2 + X(M) ^ 2
8518  B0 = B0 + Y(M)
8520  B1 = B1 + Y(M) * X(M)
```

```
8524    NEXT M
8526   A1 = A1 / 2
8528   A2 = A2 / 2
8530   B0 = B0 / 2
8532   B1 = B1 / 2
8534   D = A1 * A1 - A2
8536   A = A1 * A1 - A2
8536   A = A1 * B1 - A2 * B0
8538   A = A / D
8540   BC = A1 * B0 - B1
8542   BC = BC / D
8544    RETURN
9000    REM  KEYBOARD I/P OF WEDGE DATA
9010    PRINT"I/P WEDGE DENSITY DATA": PRINT : PRINT
9020    FOR I = 1 TO |7
9030    PRINT "D(";I - 1;") = "
9035    INPUT D(I)
9040    NEXT I
9050    PRINT : PRINT
90609   PRINT "WEDGE DATA TO BE SAVED TO DISC": GOSUB 7000
9080    PRINT : INPUT "I/P ANOTHER WEDGE DATA SET?";B$
9090    IF B$ = "Y" THEN  GOTO 9010
9100    PRINT : GOTO 238
9499    REM  LINEAR REGRESSION
9500   A1 = 0:A2 = 0:B0 = 0:B1 = 0:B2 = 0:A = 0:B = 0:D = 0
9502    FOR M = 0 TO N - 1
9503   A1 = A1 + X(M)
9504   A2 = A2 + X(M) ^ 2
9505   B0 = B0 + Y(M)
9506   B1 = B1 + Y(M) * X(M)
9507   B2 = B2 + Y(M) ^ 2
9508    NEXT M
9509    R2 = (N *B1 - A1 * B0) /  SQR ((N * A2 - A1 ^ 2) * (N * B2 - B0
        ^ 2))
9510   A1 = A1 / N
9511   A2 = A2 / N
9512   B0 = B0 / N
9513   B1 = B1 / N
9514   D = A1 * A1 - A2
9515   A = A1 * B1 - A2 * B0
9516   A = A / D
9517   B = A1 * B0 - B1
9518   B = B / D
9519    If N = 2 GOTO 9600: REM  STD DEV'N
9521   D = 8
9522    FOR M = 0 TO N - 1
9523   D1 = Y(M) - A - B * X(M)
9524   D = D + D1 * D1
9525    NEXT M
9528   D =  SQR (D / (N - 2))
9600    RETURN
```

```
10000  PRINT "CALIBRATION DATA SUMMARY"
10005  PRINT "------------------------"
10010  PRINT : PRINT "ALTITUTDE : ";H
10015  PRINT "TA        LTA      V-RAD     A-RAD    DV    DA"
10020  PRINT "----------------------------------------"
10025  FQR I = 0 TO N - 1
10030 VR(I) = INT (LV(I) * 100000 + .5) / 100000
10035 AR(I) = INT (LA(I) * 100000 + .5) / 100000
10040  PRNT TV(I); TAB( 7)TA(I); TAB( 15)VR(I); TAB( 24)AR(I);
       TAB( 32)DV(I); TAB( 37)DA(I)
10045  NEXT I
10050  PRINT "CORRELATION COEFFICIENT : "; INT (100000 * R2 + .5) /
       100000
10055  PRINT"TAU(H,0) = ";TU
10060  PRINT"WU(H,0)  = ";WU
10065  RETURN
11000  PR# 1
11005  PRINT "A.CALIB. DATA"
11010  PRINT "--------------"
11020  PRINT "TV            TA            V-RAD           A-RAD           VV
       VA           DV          DA"
11030  PRINT"------------------------------------------------------------
       ----------------------------------------"
11040  FOR I = 0 TO N - 1
11050  PRINT TV(I); TAB( 4)TA(I); TAB( 4)LV(I); TAB( 4)LA(I);
       TAB( 4)VV( I); TAB( 4)VA(I); TAB( 4)DV(I); TAB( 4)DA(I)
11060  NEXT I
11061  PRINT "DBB                    VBB"
11062  FOR I = 0 TO N - 1
11064  PRINT DBB(I),VBB(I)
11066  NEXT I
11070  PRINT "V                    DEN"
11072  FOR I = 0 TO 6
11074  PRINT I,D(I)
11076  NEXT I
11080  PRINT "GAIN = ";G
11085  PRINT "TBB = ";TBB
11100  PR# 0
11110  RETURN
12000  REM  LINEAR INTERPOLATION
12005 P = 17
12010  FOR J = 1 TO P
12015  IF X(J) > A GOTO 12025
12017  IF X(J) = A (GOTO 12035
12020  NEXT J
12025  B = Y(J - 1) + (Y(J) - Y(J - 1)) / (X(J) - X(J - 1)) * A - X(J -
       1))
12030  RETURN
12035 B = Y(J)
12040  GOTO 12030

]
```

```
5       REM ----------------------------------------------------------------
10      REM **************** LOWTRAN SPECTRAL CORRECTION ***************
20      REM ----------------------------------------------------------------
30      REM THIS PROGRAM CORRECTS A GROUND RADIANCE SIGNATURE
32      REM ESTABLISHED USING LOWTRAN ATMOSPHERIC CALIBRATION DATA
34      REM FOR THE SPECTRAL RESPONSE FUNCTION OF THE I.R. LINE SCANNER.
36      REM REF : EQUATION (24)
40      REM ----------------------------------------------------------------
50      DIM WL(50),L(50),RP(50),LX(50),RX(50),RT(50)
62      HOME
65      INVERSE
70      PRINT "SPECTRAL CORRECTION FOR BLACKBODY"
74      PRINT "RADIANCE SIGNATURE": PRINT : PRINT
80      INPUT "WHAT IS THE BLACKBODY TEMPERATURE";T
90      PRINT : INPUT "HOW MANY DATA POINTS TO DESCRIBE THE SPECTRAL
        BANDWIDTH?";N: PRINT
92      INPUT "LOWTRAN,SPECTRAL DATA FROM <D>ISC OR <K>EYBOARD?";W$
93      IF W$ = "K" GOTO 96
94      IF W$ = "D" GOTO 2000
95      GOTO 92
96      REM
100     PRINT : PRINT "INPUT WAVELENGTH, RESPONSE FACTOR"
110     FOR I = 0 TO N - 1
120     PRINT : PRINT "";I + 1;" WVL....R....RAD"
130     INPUT @L(I),RP(I),L(I)
140     NEXT I
150     HOME : PRINT "WAVELENGTH.........RESPONSE.........RADIANCE"
160     PRINT : NORMAL
170     FOR I = 0 TO N - 1
180     PRINT WL(I),RP(I),L(I)
185     RT(I) = RP(I)
190     NEXT I
200     PRINT : INPUT "DATA OK? (Y/N)";K$
210     IF K$ = "Y" GOTO 235
220     IF K$ = "N" GOTO 100
230     GOTO 200
235     PRINT : INVERSE
240     PRINT "DATA TO BE SAVED TO DISC": GOSUB 7000
248     HOME : PRINT "SCANNER BLACKBODY SPECTRAL"
250     PRINT "CORRECTION CALCULATION IN PROGRESS"
251     NORMAL
252     RD = 0
254     AREA = 0
255     FOR I = 0 TO N - 1
258     RT(I) = RP(I)
285     PRINT "INTERVAL ";I;" RADIANCE = ";L(I)
287     RX(I) = (RP(I) + RP(I +1)) / 2
288     IF I = 0 THEN RP(I) = RX(I)
289     IF I = N - 1 THEN RP(I) = RX(I)
290     LX(I) = L(I) * RX(I)
330     RD = LX(I) + RD
```

```
370     AREA = RX(I) * (WL(I + 1) - WL(I)) + AREA
380      NEXT I
390     LOW = (RD / AREA) * (WL(N - 1) - WL(0))
395      PRINT  CHR$ (7)
400      GOSUB 500
405      PRINT  CHR$ (7)
410      INPUT "HARD COPY? (Y/N)";J$
420      IF J$ = "Y" GOTO 440
430      IF J$ = "N" GOTO 1000
435      GOTO 410
440      GOSUB 499
450      GOTO 1000
499      PR# 1: PRINT  CHR$ (9);"80N"
500      PRINT : PRINT : PRINT "WAVELENGTH......RESPONSE........RADIANCE
         ........RAD*RESPONSE....RESPONSE"
510      PRINT
520      FOR I = 0 TO N - 1
530      PRINT WL(I),RT(I),L(I),LX(I),RP(I)
540      NEXT I
550      PRINT : PRINT "SPECTRAL RESPONSE INTEGRAL = ";AREA: PRINT :
         PRINT " GRD. SPECTRALLY CORRECTED RADIANCE = ";RD
560      PRINT : PRINT "SCANNER GRD. SPECTRALLY CORRECTED RADIANCE =
         ";LOW
565      PRINT : PRINT "GRD. TEMPERATURE = ";T
568      PRINT "**********************************************************
         ************************"
570      PR# 0: RETURN
1000     INPUT "DO YOU WISH TO REPEAT THE STUDY?";Q$
1010     IF Q$ = "Y" THEN  GOTO 70
1020     IF Q$ = "N" THEN  GOTO 1100
1025     GOTO 1000
1100     PRINT "YOU ARE ABOUT TO EXIT"
1110     INPUT "DO YOU WISH TO EXIT? (Y/N)";S$
1120     IF S$ = "N" THEN  GOTO 1000
1130     FLASH : HOME : NORMAL : PRINT  CHR$ (7): END
2000     REM  DATA RETRIEVAL
2005    D$ =  CHR$ (4)
2008     PRINT : PRINT "DATA FILENAME TO BE OF FORM 'LOW'I''": PRINT
2009     PRINT : INVERSE
2010     PRINT : INPUT "FILE NAME? : ";N$
2020     PRINT D$;"OPEN";N$: PRINT D$;"READ";N$
2030     FOR I = 0 TO N - 1
2040     INPUT WL(I)
2042     INPUT RP(I)
2044     INPUT L(I)
2050     PRINT WL(I),RP(I),L(I)
2060     NEXT I
2070     PRINT D$;"CLOSE";N$
2080     PRINT "";N$;" DATA RETRIEVED"
2090     PRINT : GOTO 248
7000     REM  DATA SAVE TO DISC
```

```
7005   D$ = CHR$ (4)
7008    PRINT "FILENAME MUST BE OF FORM 'LOW'I''": PRINT
7010    INPUT "INPUT FILE NAME: ";N$
7020    PRINT D$;"OPEN";N$: PRINT D$;"DELETE";N$: PRINT D$;"OPEN";N$:
        PRINT D$;"WRITE";N$
7030    FOR I = 0 TO N - 1
7050    PRINT WL(I)
7052    PRINT RP(I)
7054    PRINT L(I)
7060    NEXT I
7080    PRINT D$;"CLOSE";N$
7090    PRINT "DATA SAVED"
7100    RETURN

]
```

```
5       REM  ****************************************************************
10      REM  ********** BLACK*BODY SPECTRAL CORRECTION *****************
20      REM  ****************************************************************
30      REM  THIS PROGRAM CORRECTS A BLACKBODY RADIANCE SIGNATURE
32      REM  ESTABLISHED USING LOWTRAN ATMOSPHERIC CALIBRATION DATA
34      REM  FOR THE SPECTRAL RESPONSE FUNCTION OF THE I.R. LINE SCANNER
36      REM  REFERENCE: EQUATION 24
************************************************************************
50      DIM WL(50),L(50),RP(50),LX(50),RX(50)
62      HOME
65      INVERSE
70      PRINT "SPECTRAL CORRECTION FOR BLACKBODY"
74      PRINT "RADIANCE SIGNATURE": PRINT : PRINT
80      INPUT "WHAT IS THE BLACKBODY TEMPERATURE";T
90      PRINT : INPUT "HOW MANY DATA POINTS TO DESCRIBE THE SPECTRAL
        BANDWIDTH?";N: PRINT
100     PRINT : PRINT "INPUT WAVELENGTH, RESPONSE FACTOR"
110     FOR I = 0 TO N - 1
120     PRINT : PRINT "";I;" WVL....R"
130     INPUT WL(I),RP(I)
140     NEXT I
150     HOME : PRINT "WAVELENGTH..........RESPONSE"
160     PRINT : NORMAL
170     FOR I = 0 TO N - 1
180     PRINT WL(I),RP(I)
190     NEXT I
200     PRINT : INPUT "DATA OK? (Y/N)";K$
210     IF K$ = "Y" GOTO 240
220     IF K$ = "N" GOTO 100
230     GOTO 200
240     HOME : PRINT "SCANNER BLACKBODY SPECTRAL"
250     PRINT "CORRECTION CALCULATION IN PROGRESS"
255     FOR I = 0 TO N - 2
256     REM  PR#1
260    E = WL(I)
270    B = WL(I + 1)
275     PRINT E,B
280     GOSUB 765
285     PRINT "INTERVAL ";I;" RADIANCE = ";L(I)
287    RX(I) = (RP(I) + RP(I + 1)) / 2
290    LX(I) = L(I) * RX(I)
300     NEXT I
305     PR# 0
310    RD = 0
320     FOR I = 0 TO N - 2
330    RD = LX(I) + RD
340     NEXT I
350    AREA = 0
360     FOR I = 0 TO N - 2
370    AREA = RX(I) * (WL(I + 1) - WL(I)) + AREA
380     NEXT I
```

```
390    LBB = (RD / AREA) * (WL(N - 1) - WL(0))
395     PRINT  CHR$ (7)
400     GOSUB 500
405     PRINT  CHR$ (7)
410     INPUT "HARD COPY? (Y/N)";J$
420     IF J$ = "Y" GOTO 440
430     IF J$ = "N" GOTO 1000
435     GOTO 410
440     GOSUB 499
450     GOTO 1000
499     PR# 1: PRINT  CHR$ (9);"80N"
500     PRINT : PRINT : PRINT "WAVELENGTH......RESPONSE........RADIANCE
        ........RAD*RESPONSE....RESPONSE"
510     PRINT
520     FOR I = 0 TO N - 1
530     PRINT WL(I),RP(I),L(I),LX(I),RX(I)
540     NEXT I
550     PRINT : PRINT "SPECTRAL RESPONSE INTEGRAL = ";AREA: PRINT :
        PRINT "B.B. SPECTRALLY CORRECTED RADIANCE = ";RD:
560     PRINT : PRINT "SCANNER B.B. SPECTRALLY CORRECTED RADIANCE =
        ";LBB
565     PRINT : PRINT "B.B. TEMPERATURE = ";T
568     PRINT "********************************************************
        ***********************"
570     PR# 0: RETURN
750     REM  RADIANCE CALCULATION BY INTEGRATING PLANCK'S B.B. LAW.
        REF:SLATER,PG.37
760     REM  WAVELENGTH INTERVAL
765     REM  E(MIN)=8, B(MAX)=14
766    W1 = (B - E) / 40
768    W = E
770     GOSUB 850
772    Y1 = F
774    W = B
776     GOSUB 850
778    Y2 = F
780    C = 0
782    D = 0
784     REM  LOOP FOR EACH INTERVAL
786     FOR Z = 1 TO (B - E) / W1 - .5
788    W = E + Z * W1
790     GOSUB 850
792     Y = F
794     REM  INTERVAL EVEN OR ODD?
796    T2 = Z / 2:R = INT (T2)
798     IF T2 = R THEN 808
800     REM  SUM ALL ODD INTERVALS
802    C = C + Y
804     GOTO 810
806     REM  SUM ALL EVEN INTERVALS
808    D = D + Y
```

```
810     NEXT Z
812     REM  COMPUTE INTEGRAL
814    L(I) = W1 / 3 * (Y1 + (C * 4) + D * 2 + Y2)
820     RETURN
850     REM  DEFINE RADIANCE FUNCTION
852    K = 37415.1 / 3.14159
854    M = 14387.9
856    U = M / (W * T)
858    F = (K / (W ^ 5)) * (1 / ( EXP (U) - 1))
860     RETURN
1000    INPUT "DO YOU WISH TO REPEAT THE STUDY?";Q$
1010    IF Q$ = "Y" THEN  GOTO 70
1020    IF Q$ = "N" THEN  GOTO 1100
1025    GOTO 1000
1100    PRINT "YOU ARE ABOUT TO EXIT"
1110    INPUT "DO YOU WISH TO EXIT? (Y/N)";S$
1120    IF S$ = "N" THEN  GOTO 1000
1130    FLASH : HOME : NORMAL : PRINT  CHR$ (7): END

]
```

```
1       REM  ---------------------------------------------------------
2       REM  ------------ GROUND-TEMPERATURE CALCULATION -------------
3       REM  ---------------------------------------------------------
4       REM  THIS PROGRAM CALCULATES THE GROUND
5       REM  TEMPERATURE USING AS AN INPUT THE ATMOSPHERIC CALIBRATION
7       REM  DATA FROM THE PROFILE, ANGULAR, AND LOWTRAN
8       REM  DETERMINATION TECHNIQUES; REFERENCE: FIGURE 13
9       REM  ---------------------------------------------------------
35      DIM DV(90),DA(90),VV(90),VA(90),TV(90),TA(90),LV(90),LA(90),TH(90)
36      DIM L(90),PA(90),TW(90),WO(90)
40      DIM MA(90),PV(90),BA(90),BV(90),TB(90),BT(90),LB(90),PB(90),WA(90)
45      DIM WT(90),EM(90),R(90),T(101),VR(90),AR(90)
50      DIM D(90),DT(90),DBB(90),V(90),VBB(90)
51      DIM XX(90),YY(90)
52      DIM X(100),Y(100),WN(90),A(90),W(90),Z(90)
53      DIM RA(100),AH(100),B(100),ANT(100),MM(90),RR(90)
55      REM  DATA: TBB, GAIN, SKY RADIANCE, WATER EMISSIVITY
60      DATA  22.15,2.434
65      DATA  0.00148399,.986
66      DATA  295.158,295.707,296.393,298.237,304.118,307.200,308.020,
        311.983,314.092
70      READ TBB,G,L.S,EM
72      FOR I = 0 TO 8
74      READ RR(I)
76      NEXT I
80      D$ = CHR$ (4)
100     GOSUB 4700
200     HOME
205     INVERSE
210     INPUT "INPUT WEDGE FROM <D>ISC OR <K>EYBOARD?";W$
220     IF W$ = "K" THEN  GOSUB 9000
230     IF W$ = "D" THEN  GOTO 210
238     FLASH : PRINT : RPINT "YOU MUST WORK WITH ONLY"
239     PRINT "ONE V-D CURVE AT A TIME!": INVERSE
240     PRINT : PRINT "TBB, GAIN SET CORRECTLY? : "
242     NORMAL : PRINT "TBB = ";TBB;" : GAIN = ";G;"": INVERSE " GOSUB
        7900
249     PRINT "=================="
250     NORMAL : PRINT "GROUND TEMP CALCULATION": INVERSE
252     PRINT "=================="
299     PRINT "ONLY ONE ALTITUDE AT A TIME, PLEASE!!!!!"
300     PRINT : INPUT "WHAT ALTITUTDE ARE YOU WORKING AT?";H
320     PRINT : PRINT "HOW MANY TARGETS"
330     INPUT "FOR ANALYSIS";N
340     PRINT "WHAT IS ATMOSPHERE TAU(0), LU(0)?"
345     INPUT TU,LU
350     PRINT : PRINT "INPUT TARGET AND B.B. DENSITY, AND VIEW ANGLE"
360     FOR I = 0 TO N - 1
370     PRINT I: PRINT "DEN,  DBB,  VIEW ANGLE"
380     INPUT DV(I),DBB(I),AH(I)
385     NEXT I
```

```
386    NORMAL
387    HOME : PRINT "DEN","DBB","ANGLE"
389    PRINT
390    FOR I = 0 TO N - 1
392    PRINT DV(I),DBB(I),AH(I)
394    NEXT I
395    PRINT : INPUT "DATA OK?;T$
400    IF LT$ = "N" GOTO 340
410    HOME
420    FLASH : PRINT : PRINT : PRINT "ANALYSIS IN PROGRESS": NORMAL
430    FOR I = 0 TO N - 1
432   A = DBB(I)
434    GOSUB 5000
436   VBB(I) = BV
440   A = DV(I)
450    GOSUB 5000
460   VV(I) = BV
495    REM    TV(I) IS AN APPARENT TEMPERATURE
500   TV(I) = ((VV(I) - VBB(I)) * G) + 273.16 + TBB
520    NEXT I
530    FOR I = 0 TO N - 1
535   T = 0
540   T = TV(I)
550    GOSUB 765
560   LV(I) = L(I)
600    NEXT I
618    PRINT  CHR$ (7)
620    GOTO 2000
750    REM  RADIANCE CALCULATION BY INTEGRATING PLANCK'S B.B. LAW.
       REF:SLATER,PG.37
760    REM  WAVELENGTH INTERVAL
765    NOTRACE :B = 14:E = 8
766   W1 = (B - E) / 40
768   W = E
770    GOSUB 850
772   Y1 = F
774   W = B
776    GOSUB 850
778   Y2 = F
780   C = 0
782   D = 0
784    REM  LOOP FOR EACH INTERVAL
786    FOR Z = 1 TO (B - E) / W1 - .5
788   W = E + Z * W1
790    GOSUB 850
792   Y = F
794    REM  INTERVAL EVEN OR ODD?
796   T2 = Z / 2:R = INT (T2)
798    IF T2 = R THEN 808
800    REM  SUM ALL ODD INTERVALS
802   C = C + Y
```

```
804     GOTO 810
806     REM  SUM ALL EVEN INTERVALS
808    D = D + Y
810     NEXT Z
812     REM  COMPUTE INTEGRAL
814    L(I) = W1 / 3 * (Y1 + (C * 4) + D * 2 + Y2)
820     RETURN
850     REM  DEFINE RADIANCE FUNCTION
852    K = 37415.1 / 3.14159
854    M = 14387.9
856    U = M / (W * T)
858    F = (K / (W ^ 5)) * (1 / ( EXP (U) - 1))
860     RETURN
1000    INPUT "DO YOU WISH TO REPEAT THE STUDY?";Q$
1010    IF Q$ = "Y" THEN  GOTO 200
1020    IF Q$ = "N" THEN  GOTO 1100
1025    GOTO 1000
1100    PRINT "YOU ARE ABOUT TO EXIT 'GRD-TEMP'"
1110    INPUT "DO YOU WISH TO EXIT? (Y/N)";S$
1120    IF S$ = "N" THEN  GOTO 1000
1130    FLASH : HOME : NORMAL : PRINT  CHR$ (7): END
1900    REM  CALCULATION OF TAU, LU, WO, AND TAPP
1910    REM  SLOPE(TAU) = B, INTERCEPT(WA TERM) = A, ANGLE = TH
2000    REM GOSUB 4700
2010    FOR I = 0 TO N - 1
2015    REM    CONVERT ANGLE TO RADIAN measure
2020   TH(I) = 3.14159 * AH(I) / 180
2030   ZP = 1 /  COS (TH(I))
2035   TZ(I) = TU ^ ZP
2040   LZ(I) = LU * (TU ^ (ZP - 1)) * ZP
2115    GOSUB 4493
2120   PV(I) = TT
2145    NEXT I
2146    GOSUB 6000
2148    FOR I = 0 TO N - 1
2150   MM(I) = RR(I) - PV(I)
2151    NEXT I
2152    PRINT  CHR$ (7)
2155    PRINT : INPUT "HARD COPY?:;F$
2160    IF F$ = "N" GOTO 2500
2165    IF F$ = "Y" GOTO 2175
2170    GOTO 2155
2175    PR# 1: PRINT  CHR$ (9);"80N": GOSUB 3200
2180    PR# 0
2500    PRINT : INPUT "CALCULATE T(APP)'S USING NEW DATA?";E$
2505    IF E$ = "N" GOTO 1000
2510    IF E$ = "Y" GOTO 249
2515    GOTO 2500
3200    PRINT : PRINT : PRINT
3240    PRINT : PRINT "T(GRD) DATA SUMMARY"
3242    PRINT "-------------------"
```

```
3278    PRINT : PRINT "ALTITUTDE = ";H: PRINT "TAU(0) = ";TU: PRINT
        "LU(0) = ";LU: PRINT "DBB = ";DBB(0): PRINT
3279    PRINT "EM = ";EM: PRINT "LSKY = ";LS: PRINT "GAIN = ";G: PRINT
        "TBB = ";TBB: PRINT
3280    PRINT "VBB = ";VBB(0): PRINT
3285    PRINT "T(GRD)     RAD(GRD)     DEN   ANGLE     T(APP)
        RAD(APP)    DELTA T"
3290    PRINT "------------------------------------------------------------"
3295    PRINT
3300    FOR I = 0 TO N - 1
3305    PRINT PV(I); TAB( 3);WT(I); TAB( 3);DV(I); TAB( 3);AH(I);
        TAB( 3);TV(I); TAB( 3);LV(I); TAB( 3);MM(I)
3310    NEXT I
3315    RETURN
4490    REM  TAPP DETERMINATION BY REVERSE PLANCK EQUATION
4492    REM  SCHOTT'S COEFF. IN USE FOR COMPUTATIONAL EFFICIENCY
4493    NORMAL
4500   LO(I) = (LV(I) - LZ(I)) / TZ(I)
4505   WT(I) = (LO(I) - (LS * (1 - EM))) / EM
4515    PRINT "WT = ";WT(I)
4520    REM  ITERATIVE SOLUTION TO REVERSE PLANCK EQUATION
4530    FOR K = 0 TO 69
4540    IF RA(K) > WT(I) GOTO 4560
4550    NEXT K
4560   YY(1) = T(K):YY(0) = T(K - 1)
4565   XX(1) = RA(K):XX(0) = RA(K - 1)
4569    REM  PR#1
4570    PRINT YY(1),YY(0),XX(1),XX(0)
4571    PR# 0
4580    GOSUB 8500
4590   B(I) = BC
4600   ANT(I) = A
4610   TT = (B(I) * WT(I)) + ANT(I)
4620    PR# 0: RETURN
4700   D$ = CHR$ (4)
4704   N$ = "TRAD"
4710    PRINT D$;"OPEN";N$: PRINT D$;"READ";N$
4720    FOR K = 0 TO 69
4730    INPUT RA(I)
4736    INPUT T(K)
4737    PRINT T(K),RA(K)
4740    NEXT K
4750    PRINT D$;"CLOSE";N$
4760    PRINT "RADIANCE TABLE RETRIEVED"
4762    RETURN
5000    GOTO 12000
6000    PRINT : PRINT "T(GRD) DATA SUMMARY"
6010    PRINT "-------------------"
6020    PRINT : PRINT "ALTITUDE = ";H: PRINT "TAU(0) = ";TU: PRINT
        "LU(0) = ";LU: PRINT "DBB = ";DBB(0): PRINT
6030    PRINT "T(GRD)","RAD(GRD)","ANGLE"
```

```
6040   PRINT "---------","-----","-------"
6050   PRINT
6060   FOR I = 0 TO N - 1
6070   PRINT PV(I),WT(I),AH(I)
6080   NEXT I
6090   RETURN
7000   REM  STEP WEDGE DATA FILE SAVE
7004   PRINT : PRINT "FILE NAME MUST BE"
7005   PRINT "OF FORM: WN'I'"
7006   PRINT "WHERE 'I' = DATA SET NO."
7007   PRINT "IE. WN1, WN2, ETC."
7008   PRINT
7010   INPUT "INPUT FILE NAME: ";N$
7020   PRINT D$;"OPEN";N$: PRINT D$;"DELETE";N$: PRINT D$;"OPEN";N$:
       PRINT D$;"WRITE";N$
7040   FOR i = 1 TO 17
7050   PRINT D(I)
7060   NEXT I
7080   PRINT D$;"CLOSE";N$
7085   PRINT  CHR$ (7): PRINT "WEDGE DATA SAVED"
7090   RETURN
7900   REM  AUTO V-D DATA RETRIEVAL
7920   PRINT "TYPE IN WEDGE 'FILENAME'"
8000   REM  STEP WEDGE DATA FILE RETRIEVAL
8005   PRINT "VOLTAGE RANGE SET FOR FILES 'WN6' & 'WN9'"
8010   PRINT : INPUT "FILE NAME: ";N$
8020   PRINT D$;"OPEN";N$: PRINT D$;"READ";N$
8030   FOR I = 1 TO 17
8040   INPUT D(I)
8042  X(I) = D(I)
8044  Y(I) = I - 4
8046   PRINT Y(I),X(I)
8050   NEXT I
8060   PRINT D$;"CLOSE";N$
8070   PRINT "";N$;" DATA RETRIEVED"
8080   PRINT : RETURN
8500   REM  LINEAR INTERPOLATION FOR RADIANCE CALCULATION
8510  A1 = 0:A2 = 0:B0 = 0:B1 = 0:B2 = 0:A = 0:BC = 0:D = 0
8512   FOR M = 0 TO 1
8514  A1 = A1 + XX(M)
8516  A2 = A2 + XX(M) ^ 2
8518  B0 = B0 + YY(M)
8520  B1 = B1 + YY(M) * XX(M)
8524   NEXT M
8526  A1 = A1 / 2
8528  A2 = A2 / 2
8530  B0 = B0 / 2
8532  B1 = B1 / 2
8534  D = A1 * A1 - A2
8536  A = A1 * B1 - A2 * B0
8538  A = A / D
```

```
8540  BC = A1 * B0 - B1
8542  BC = BC / D
8544   RETURN
9000   REM  KEYBOARD I/P OF WEDGE DATA
9010   PRINT "I/P WEDGE DENSITY DATA": PRINT : PRINT
9020   FOR I = 1 TO 17
9030   PRINT "D(";I - 1;") = "
9035   INPUT D(I)
9040   NEXT I
9050   PRINT : PRINT
9060   PRINT "WEDGE DATA TO BE SAVED TO DISC": GOSUB 7000
9080   PRINT : INPUT "I/P ANOTHER WEDGE DATA SET?";B$
9090   IF B$ = "Y" THEN  GOTO 9010
9100   PRINT : GOTO 238
12000  REM  LINEAR INTERPOLATION
12005 P = 17
12008 BV = 0
12010  FOR J = 1 TO P
12015  IF X(J) > A GOTO 12025
12017  IF X(J) = A GOTO 12035
12020  NEXT J
12025  BV = Y(J - 1) + (Y(J) - Y(J - 1)) / (X(J) - X(J - 1)) *
       (A - X(J - 1))
12030  RETURN
12035 BV = Y(J)
12040  GOTO 12030

]
```

```
1        REM  *********************************
2        REM  ***** RADIANCE*TEMPERATURE *****
3        REM  ***** CONVERSION ***************
4        REM  THIS PROGRAM CONVERTS
5        REM  RADIANCE TO TEMPERATURE
7        REM  AND VICE-VERSA
9        REM  *********************************
35       DIM DV(90),DA(90),VV(90),VA(90),TV(90),TA(90),LV(90),LA(90),TH(90)
36       DIM L(90),PA(90),TW(90),WD(90)
40       DIM MA(90),PV(90),BA(90),BV(90),TB(90),BT(90),LB(90),PB(90),WA(90)
45       DIM WT(90),;EM(90),R(90),T(101),VR(90),AR(90)
50       DIM D(90),DT(90),DBB(90),V(90),VBB(90)
51       DIM XX(90),YY(90)
52       DIM X(100),Y(100),WN(90),A(90),W(90),Z(90)
53       DIM RA(100),AH(100),B(100),ANT(100),MM(90),RR(90)
100      GOSUB 4700
110      HOME
120      INVERSE
130      FLASH : PRINT : PRINT "RADIANCE/TEMPERATURE"
140      PRINT "CONVERSION": INVERSE
150      PRINT : PRINT "HOW MANY TARGETS"
160      INPUT "FOR ANALYSIS";N
210      INPUT "INPUT <T>EMPERATURE OR <R>ADIANCE VALUES?";W$
220      IF W$ = "R" THEN  GOSUB 1900
230      IF W$ = "T" THEN  GOSUB 1900
235      IF W$ <  > "D" THEN  GOTO 210
350      PRINT : PRINT "INPUT TEMPERATURE"
360      FOR I = 0 TO N - 1
370      PRINT I: PRINT "TEMPERATURE"
380      INPUT TV(I)
385      NEXT I
386      NORMAL
387      HOME : PRINT "TEMPERATURE"
389      PRINT
390      FOR I = 0 TO N - 1
392      PRINT TV(I)
394      NEXT I
395      PRINT : INPUT "DATA OK?";T$
400      IF T$ = "N" GOTO 350
410      HOME
420      FLASH : PRINT : PRINT : PRINT "ANALYSIS IN PROGRESS": NORMAL
530      FOR I = 0 TO N - 1
535     T = 0
540     T = TV(I)
550      GOSUB 765
560     LV(I) = L(I)
600      NEXT I
618      PRINT  CHR$ (7)
620      GOSUB 6000
625      GOTO 2152
```

```
750   REM  RADIANCE CALCULATION BY INTEGRATING PLANCK'S B.B. LAW.
      REF:SLATER,PG.37
760   REM  WAVELENGTH INTERVAL
765   NOTRACE :B = 14:E = 8
766  W1 = (B - E) / 40
768  W = E
770   GOSUB 850
772  Y1 = F
774  W = B
776   GOSUB 850
778  Y2 = F
780  C = 0
782  D = 0
784   REM  LOOP FOR EACH INTERVAL
786   FOR Z = 1 TO (B - E) / W1 - .5
788  W = E + Z * W1
790   GOSUB 850
792  Y = F
794   REM  INTERVAL EVEN OR ODD?
796  T2 = Z / 2:R = INT (T2)
798   IF T2 = R THEN 808
800   REM  SUM ALL ODD INTERVALS
802  C = C + Y
804   GOTO 810
806   REM  SUM ALL EVEN INTERVALS
808  D = D + Y
810   NEXT Z
812   REM  COMPUTE INTEGRAL
814  L(I) = W1 / 3 * (Y1 + (C * 4) + D * 2 + Y2)
820   RETURN
850   REM  DEFINE RADIANCE FUNCTION
852  K = 37415.1 / 3.14159
854  M = 14387.9
856  U = M / (W * T)
858  F = (K / (W ^ 5)) * (1 / ( EXP (U) - 1))
860   RETURN
1000  INPUT "DO YOU WISH TO REPEAT THE STUDY?";Q$
1010  IF Q$ = "Y" THEN  GOTO 110
1020  IF Q$ = "N" THEN  GOTO 1100
1025  GOTO 1000
1100  PRINT "YOU ARE ABOUT TO EXIT"
1110  INPUT "DO YOU WISH TO EXIT? (Y/N)";S$
1120  IF S$ = "N" THEN  GOTO 1000
1130  FLASH : HOME : NORMAL : PRINT  CHR$ (7): END
1900  PRINT : PRINT "INPUT RADIANCE"
1910  FOR I = 0 TO N - 1
1920  PRINT I: PRINT "RADIANCE"
1930  INPUT LV(I)
1940  NEXT I
1950  NORMAL
1960  HOME : PRINT "RADIANCE"
```

```
1970    PRINT
1972    FOR I = 0 TO N - 1
1975    PRINT LV(I)
1978    NEXT I
1980    PRINT : INPUT "DATA OK?";T$
1982    IF T$ = "N" GOTO 1900
1984    HOME
1986    FLASH : PRINT : PRINT : PRINT "ANALYSIS IN PROGRESS": NORMAL
2010    FOR I = 0 TO N - 1
2115    GOSUB 4493
2120   TV(I) = TT
2145    NEXT I
2146    GOSUB 6000
2152    PRINT  CHR$ (7)
2155    PRINT : INPUT "HARD COPY?";F$
2160    IF F$ = "N" GOTO 1000
2165    IF F$ = "Y" GOTO 2175
2170    GOTO 2155
2175    PR# 1: PRINT  CHR$ (9);"80N": GOSUB 6000
2180    PR# 0: GOTO 1000
4493    NORMAL
4520    REM  ITERATIVE SOLUTION TO REVERSE PLANCK EQUATION
4530    FOR K = 0 TO 69
4540    IF RA(K) > LV(I) GOTO 4560
4550    NEXT K
4560   YY(1) = T(I):YY(0) = T(K - 1)
4565   XX(1) = RA(K):XX(0) = RA(K - 1)
4580    GOSUB 8500
4590   B(I) = BC
4600   ANT(I) = A
4610   TT = (B(I) * LV(I)) + ANT(I)
4620    RETURN
4700   D$ =  CHR$ (4)
4704   N$ = "TRAD"
4710    PRINT D$;"OPEB";N$: PRINT D$;"READ":N$
4720    FOR K = 0 TO 69
4730    INPUT RA(K)
4736    INPUT T(K)
4737    PRINT T(K),RA(K)
4740    NEXT K
4750    PRINT D$;"CLOSE";N$
4760    PRINT "RADIANCE TABLE RETRIEVED"
4762    RETURN
5000    GOTO 12000
6000    PRINT : PRINT "RAD/TEMP CONVERSION SUMMARY"
6010    PRINT "------------------"
6030    PRINT "TEMP     RADIANCE"
6040    PRINT "-----------------"
6050    PRINT
6060    FOR I = 0 TO N - 1
6070    PRINT TV(I),LV(I)
```

```
6080    NEXT I
6090    RETURN
8500    REM  LINEAR INTERPOLATION FOR RADIANCE CALCULATION
8510   A1 = 0:A2 = 0:B0 = 0:B1 = 0:B2 = 0:A = 0:BC = 0:D = 0
8512    FOR M = 0 TO 1
8514   A1 = A1 + XX(M)
8516   A2 = A2 + XX(M) ^ 2
8518   B0 = B0 + YY(M)
8520   B1 = B1 + YY(M) * XX(M)
8524    NEXT M
8526   A1 = A1 / 2
8528   A2 = A2 / 2
8530   B0 = B0 / 2
8532   B1 = B1 / 2
8534   D = A1 * A1 - A2
8536   A = A1 * A1 - A2 * B0
8538   A = A / D
8540   BC = A1 * B0 - B1
8542   BC = BC / D
8544    RETURN

]
```

VITA

The author of this study is a member of the Canadian Armed Forces, holding the officer rank of Captain. His professional training has focused on the many-faceted discipline of aerospace engineering.

Captain Byrnes is a native of Kingston, Ontario. He graduated from the St. Catharines Collegiate Institute & Vocational School with an Honours Graduation Certificate and received his baccalaureate in physics sciences from Laurentian University of Sudbury, Ontario, in 1975.

From 1976 to 1980, Captain Byrnes was employed with the Aircraft Maintenance Development Unit, (A.M.D.U.), Trenton as a project engineer, and later manager, of the Structures and Life Support Systems section. He then moved on to Canadian Forces Base Trenton where he was employed in the Aircraft Maintenance Engineering Organization, being responsible for the maintenance of aircraft used by 424 Transport and Rescue Squadron. From Trenton, Captain Byrnes was selected to attend at R.I.T.

Captain Byrnes' next assignment will be at the Aerospace Engineering Test Establishment, at C.F.B. Cold Lake, Alberta, the sister organization of the A.M.D.U. He will be responsible for the engineering and management of the imaging resources of this elite organization.